2021

# Development of isolation and detection methods for the analysis of DNA and bacteria

Marcelino Varona
*Iowa State University*

**Development of isolation and detection methods for the analysis of DNA and bacteria**

by

**Marcelino Varona**
**(Obed M Varona Ortiz)**

A dissertation submitted to the graduate faculty

in partial fulfillment of the requirements for the degree of

DOCTOR OF PHILOSOPHY

Major: Analytical Chemistry

Program of Study Committee:
Jared L. Anderson, Major Professor
Robbyn Anand
Young-Jin Lee
Marit Nilsen-Hamilton
Vincenzo Venditti

The student author, whose presentation of the scholarship herein was approved by the program of study committee, is solely responsible for the content of this dissertation. The Graduate College will ensure this dissertation is globally accessible and will not permit alterations after a degree is conferred.

Iowa State University

Ames, Iowa

2021

# TABLE OF CONTENTS

## ACKNOWLEDGMENTS

I would like to thank my major Professor and advisor, Dr. Jared Anderson, for his support and guidance throughout my time at Iowa State University. He encouraged me to pursue challenging projects and supported my ideas, even when initial trials and experiments were unsuccessful. Throughout my five years, he has provided many opportunities that I would not have imagined were a possibility before graduate school. His mentorship has been a key component in my success so far.

I also would like to acknowledge my previous group members, Drs Kevin Clark, Omprakash Nacham, and Henry Nan. They are all excellent scientists who set an example of how to make the most of my graduate career. Additionally, I want to thank my current group members: Miranda Emaus, Qamar Farooq, Han Chen, Philip Eor, Nabeel Abbasi, Derek Eitzmann, Victoria Zeger, Shu-An Hsie, and Donghyun Ryoo, for the good scientific discussions and fun times in the lab and at conferences.

I am also very grateful for my good friends, Mark and Anna Campbell and Dr. Justin Lawrie. From weekend getaways to see Above and Beyond, to baby G's and Japanese Minow Farmers, their love, support, and friendship were a constant source of encouragement for the past 5 years. I would also like to acknowledge my undergraduate chemistry professors Drs. John and Kristy Jurchen. They encouraged me to pursue graduate studies and I will always be grateful for their influence and support. I am also very grateful for the friends I've made in Ames.

Finally, I would like to thank my family. In particular my sister, Ana Belen, for taking my late night phone calls and always being a voice of encouragement and reason. My parents as well, Brontis and Norma Varona, for their love and support. They have always encouraged me to pursue my dreams and passions.

## ABSTRACT

Nucleic acids are essential biopolymers that have served as diagnostic biomarkers for many applications. Traditional nucleic acid isolation methods typically rely on nucleic acid adsorption onto silica particles and require multiple centrifugation steps, organic solvents and significant user intervention. Additionally, popular detection methods, such as polymerase chain reaction (PCR), suffer from long analysis times and require complex thermal cycling equipment. These drawbacks limit the utility of traditional isolation/detection methods for rapid in-field testing and point-of-care applications. The work presented in this dissertation addresses challenges associated with nucleic acid isolation and detection through the development of solid-phase microextraction (SPME) and isothermal amplification methodologies.

SPME is an alternative sample preparation methodology that circumvents many limitations of conventional methods. A rapid SPME method was developed and optimized to enable the isolation of DNA from mycobacterium smegmatis in artificial sputum samples. For detecting the extracted DNA, a colorimetric isothermal multiple-self-matching initiated amplification (IMSA) assay was designed using hydroxy napthol blue (HNB). A custom buffer was designed to allow direct coupling of the 1 M NaCl SPME desorption solution with the IMSA assay. The custom buffer was successfully applied in multiple studies for the detection of a variety of DNA sequences.

A significant limitation of isothermal amplification methodologies is the lack of sequence-specificity in the detection method. Traditional methods rely on colorimetric indicators that indirectly detect amplification. Molecular beacons (MB) were employed along with HNB to specifically detect loop-mediated isothermal amplification (LAMP) using a transilluminator. The high specificity of the method was demonstrated by discriminating two sequences that varied by a single nucleotide.

To further demonstrate the applicability of MB-LAMP, an assay was designed for the detection of BRAF V600E, a mutation present in 90% of melanomas. Two MBs were employed containing a FAM (wild-type) or HEX (mutant) fluorophore to identify each sequence. A plate reader was employed in order to simply the detection scheme. Additionally, SPME was successfully applied to isolate the mutant sequence from human plasma and enable detection with the MB-LAMP assay.

The specific detection of LAMP was further simplified by employing MBs and a biotinylated primer in a lateral-flow immunoassay format. This approach eliminated the need for additional equipment in the detection step. The versatility of the method was demonstrated through the detection of three independent sequences. Additionally, the high specificity of the method was highlighted through the differentiation of wild type and mutant BRAF V600E. The developed detection scheme was also compatible with SPME and enabled detection from pond water, human plasma, and artificial saliva.

A disadvantage to the previously used SPME extraction phases is the lack of specificity, as the primary interaction with the nucleic acid was anion exchange. To circumvent this, a sequence-specific SPME sorbent was developed in collaboration with Millipore Sigma. A commercially-available polyacrylate SPME fiber was modified with an amine-labeled oligonucleotide complementary to a DNA target using carbodiimide coupling chemistry. Several parameters were optimized including desorption time and the use of Exonuclease III to minimize carryover.

While detection of nucleic acids from pathogens is often sufficient in many cases, certain applications such as food safety require knowledge of the viability of the detected organisms. Traditional methods rely on pre-enrichment cultures that are time consuming to perform, decrease

the sample-to-answer time. Magnetic ionic-liquids have been previously shown to be capable of enriching viable bacteria from a variety of food matrices. In the study presented within this dissertation, the physiological effects of magnetic ionic liquids on a variety of bacteria were evaluated. *Salmonella* and *E. coli* O157:H7 that were captured by magnetic ionic liquids were plated on selective and non-selective agars to evaluate whether or not cellular injury occurred. Additionally, the ability for magnetic ionic liquids to capture a wide range of Gram-negative bacteria was also evaluated.

# CHAPTER 1. GENERAL INTRODUCTION

Sections adapted and reprinted with permission from ACS Omega 2021, *6*, 3463-3469



Marcelino Varona, and Jared L. Anderson

## Nucleic Acid Extraction

Nucleic acid (NA) analysis is routinely performed in a variety of different fields including disease diagnostics, forensics, and genomics. Due to the powerful nature of methods such as quantitative polymerase chain reaction (qPCR) and Next Generation Sequencing, highly specific information can be obtained regarding nucleic acid samples. One common requirement of the majority of analysis techniques employed is the need for pure input NA in order to perform optimally. This requires methods capable of efficiently isolating pure NA material from complex biological samples while minimizing co-extraction of matrix components that can inhibit downstream detection.[1]

Traditional NA purification methods can be broadly categorized into two categories, liquid-liquid extraction (LLE) and solid-phase extraction (SPE).[2,3] LLE relies on the removal of non-NA cellular components by an organic phase, typically phenol-chloroform, and partitioning of the nucleic acid into the aqueous phase. However, the large volumes of organic solvents used, caustic nature of the solvents, and multiple centrifugation steps represent several drawbacks to this method. SPE circumvents some of the limitations posed by LLE and typically relies on NA binding onto silica sorbents or cationic resins. Two popular formats for NA SPE include spin columns and coated magnetic particles. While SPE does reduce the amount of organic solvents used, ethanol and multiple centrifugation steps are also required, limiting its use for rapid analysis.

**Solid-Phase Microextraction for Nucleic Acid Analysis**

Solid-phase microextraction (SPME) was developed by Pawliszyn and co-workers as an alternative sample-preparation technique.[4] The technique relies on the partitioning or adsorption of analytes onto a thin-film of sorbent immobilized on a solid support. As shown in Figure 1, two main-modes can be employed to isolate analytes. These include headspace, where the fiber is placed in the headspace of the sample, and direct immersion, where the sorbent is placed directly into a solution containing the analytes of interest. Traditionally, analytes are subsequently analyzed by a chromatographic technique such as Gas or Liquid Chromatography.

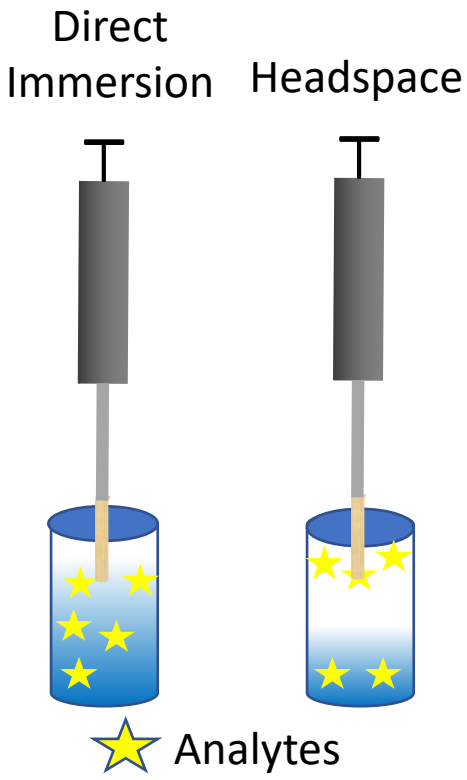


**Figure 1.** Representative schematic of SPME modes

While several commercially available sorbents exist, none of them possess selectivity toward NAs. Polymeric ionic liquids (PILs) represent an alternative class of compounds for the development of SPME phases with unique collectivities. These phases are composed of ionic

liquid (IL) monomers and crosslinkers that possess polymerizable groups within their cation and/or anion structure. PILs have previously been used to isolate various analytes including acrylamide and organic pollutants.[5,6]

Omprakash et al. pioneered the development of PIL-SPME sorbents for the analysis of DNA and RNA.[7,8] Several polymer compositions were systematically investigated to determine the monomer/crosslinker combination that yielded the highest extraction of DNA. Additionally, anion exchange was identified as the primary mechanism through which PILs interact with the NA. Subsequent work was performed in order to investigate PILs for the extraction of mRNA. A significant advantage to both methods was the ability to detect the extracted nucleic acid using traditional biomolecular techniques such as quantitative polymerase chain reaction (qPCR) and reverse transcription quantitative polymerase chain reaction (RT-qPCR).

**Nucleic Acid Detection**

NAs play a prominent role as biomarkers for a wide range of diseases. Since its development, polymerase chain reaction (PCR) has been broadly applied for NA diagnostics and has become the gold standard for many applications. PCR leverages the unique Watson-Crick base pairing of NAs to amplify specific sequences through multiple heating and cooling cycles. To further increase PCR specificity, fluorescent probes including TaqMan and molecular beacons are often used to discriminate single nucleotide differences within an amplified sequence. This has allowed for the development of assays capable of discriminating single-nucleotide polymorphisms (SNPs) for certain diagnostics such as cancer[9] and multi-drug resistant tuberculosis (MDR-TB).[10]

While PCR is considered the gold standard for many diagnostic tests, there remain formidable drawbacks that prevent its use in resource-limited settings and peripheral laboratories. Significant hinderances include the need for sophisticated thermal-cycling equipment and imaging modules for real-time detection. In addition, some PCR methods require extended incubation

periods (<1 h) and can suffer inhibition from molecules present in biological matrices.[1] These limitations increase the difficulty of developing PCR-based diagnostics that can be performed in non-laboratory settings.

## Loop-Mediated Isothermal Amplification

Isothermal amplification techniques have been developed and applied for NA detection in order to circumvent the aforementioned drawbacks. These techniques include, but are not limited to, recombinase polymerase amplification (RPA),[11] rolling circle-amplification (RCA),[12] and loop-mediated isothermal amplification (LAMP).[13] The isothermal nature of these methods eliminate the need for complex thermal cycling equipment and high temperatures. In addition, several colorimetric detection methods have been developed to allow for easy visualization and identification of positive samples.[14,15]

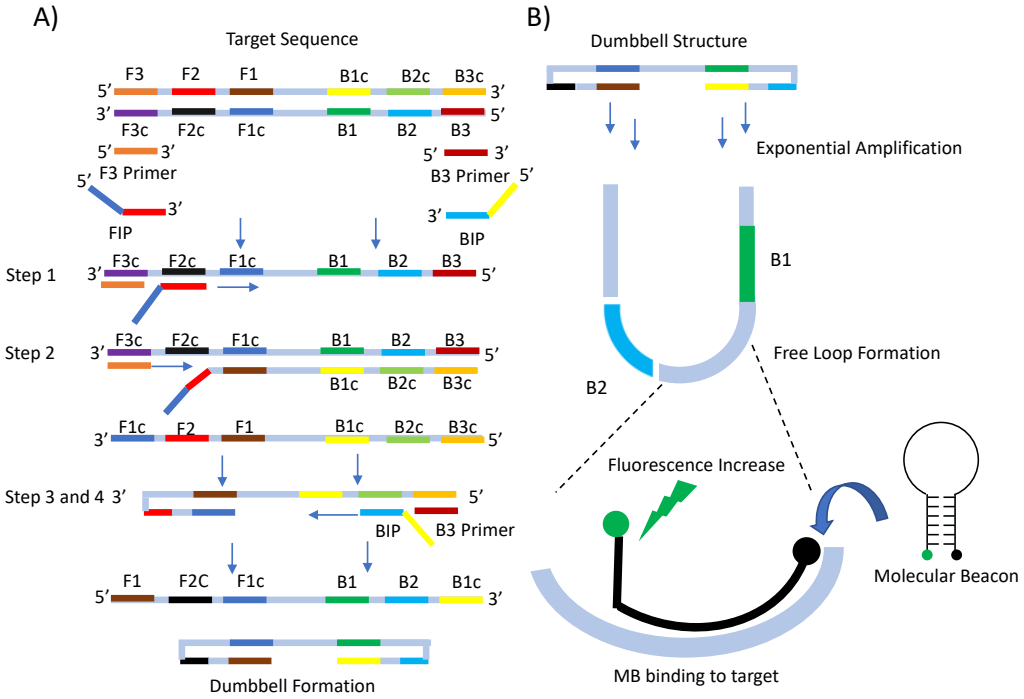


**Figure 2.** A) General LAMP amplification schematic. B) Illustration of mechanism of MB-based specific detection of LAMP. Adapted with permission from ref. 29. Copyright 2019 American Chemical Society

LAMP has been the most popular and widely implemented isothermal amplification technique. It relies on 4-6 primers and a DNA polymerase possessing strong strand displacement activity to amplify the target NA sequence. A general amplification schematic is shown in figure 2A. These characteristics have allowed LAMP to achieve equal or lower detection limits to PCR for certain targets.[16] However, due to the length of the primers and the concentration that is often required, LAMP suffers from non-specific amplification arising from the formation of primer-dimers.[17]

Traditional detection methods for LAMP include turbidimetry and the use of dyes to identify when amplification has occurred. Popular dyes include metal indicators such as hydroxy naphthol blue (HNB)[14] and calcein,[18] which change color as the $Mg^{2+}$ concentration decreases during the progression of the amplification reaction. Other dyes, such as SYBR Green I,[19] exhibit increased fluorescence in the presence of double-stranded DNA that is generated during amplification. These traditional methods are unable to differentiate between amplification of the desired sequence and spurious amplification occurring from primer-dimers. Careful primer design and reaction optimization can be used to minimize non-specific amplification and avoid false positive reactions. However, these strategies are unable to provide sufficient specificity when attempting to achieve single-nucleotide differentiation in sequences. Differentiating these types of sequences is highly desirable as they can be an indicator of disease. Therefore, tools capable of rapidly and accurately identifying these sequences are highly desired.

## Probe-based Approaches for SNP Detection

Probe-based approaches typically involve the modification of LAMP primers with fluorophore/quencher pairs to provide a sequence-specific signal. Higgins et al. developed a method which utilized a modified loop-primer probe and endonuclease IV for SNP detection.[20] The probe consisted of the following three components: a 5' quencher, an abasic site, and an internal fluorophore. This approach exploits the enhanced endonuclease activity when a double-stranded abasic site is present. When the mutant sequence was present, the endonuclease cleaved the abasic site and allowed for the fluorophore to be displaced by the polymerase, leading to an increase in observed fluorescence. If the wild-type sequence was present, endonuclease activity was significantly reduced and little to no fluorescence signal could be detected. The approach was successfully applied for the single-plex and multiplex detection of different targets. Multiplexed detection could occur by choosing different fluorophores in the modified loop-primer. This approach improves upon TEC-LAMP which utilizes *Tth* endonuclease IV as the enzyme, as it was unable to differentiate between SNPs using similar probes.

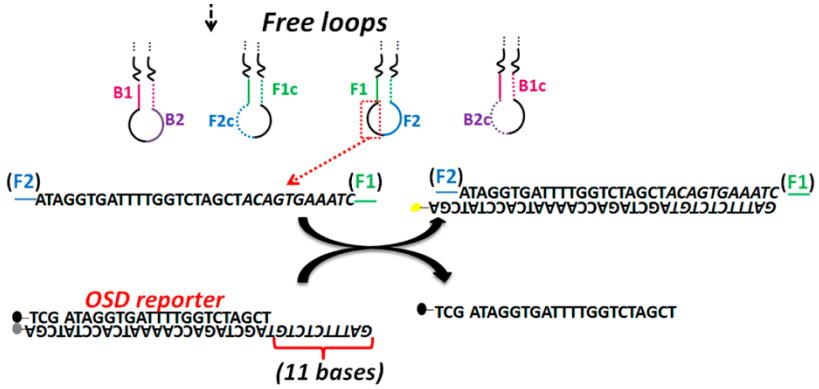


**Figure 3.** Schematic representing the specific detection of LAMP using OSD reporter probes. Adapted with permission from ref. 26 Copyright 2015 American Chemical Society

Another probe-based approach that has been developed involves the use of strand-displacement probes to achieve discrimination between perfectly matched sequences and SNPs.[21]

These probes were designed to target the single-stranded loop regions between the F1/F2 and B1/B2 regions of the LAMP target. A representative schematic of the approach is shown in Figure 3. Strand-displacement probes were composed of two components: reporter F and reporter Q. Reporter F was complementary to the target and is 3' or 5' modified with a fluorophore. Reporter Q hybridizes with reporter F, contains a corresponding quencher, and is generally shorter than reporter F by 10 nucleotides. In the presence of the target sequence, reporter F will bind to the target leading to the displacement of reporter Q, resulting in an increase in the fluorescence detected. The length of reporter F is critical in allowing rapid strand-exchange to occur under LAMP conditions. The SNP-detection capabilities of the method was tested with BRAF V600E, a mutation present in 90% of melanomas. Significantly higher fluorescence could be observed when reporter F was complementary to the target sequence. Discrimination was most successful at a temperature of 60 °C, as higher temperatures potentially reduced the stability of the reporter F and Q duplex. The method was shown to successfully detect down to 5% of the mutant allele in the presence of 95% wild-type sequence.

The aforementioned approach was subsequently modified by Du et al. for the detection of the same target using low cost, commercially-available lateral-flow immunoassay strips (pregnancy tests).[22] A modified reporter was conjugated with human chorionic gonadotropin (hCG), which could be detected by the pregnancy strips. Two different approaches were employed, as shown in Figure 4. It was found that the large LAMP amplicons were unable to migrate through the lateral flow device. Therefore, in one approach, a LAMP positive reaction was indicated by a negative test strip as the hCG modified reporter was bound to the amplicon and unable to migrate through the lateral-flow device. Conversely, amplification of the mismatched sequence yielded a positive signal in the test-band, as the reporter was not incorporated into the amplicon. Another

approach was developed to yield a positive test strip result in the presence of the target nucleic acid and relied on a three-way junction reporter that contained a sequence complementary to the target bound to a magnetic bead and a hCG modified sequence. In the presence of the complementary sequence, the magnetic bead-labeled primer hybridized with the target and enabled release of the hCG-labeled sequence. Upon magnetic separation, the hCG-labeled sequence could be detected on the lateral-flow device. One disadvantage of strand-displacement probes is the required pre-annealing step to make the probe. This adds an additional step to the process, which increases assay complexity.

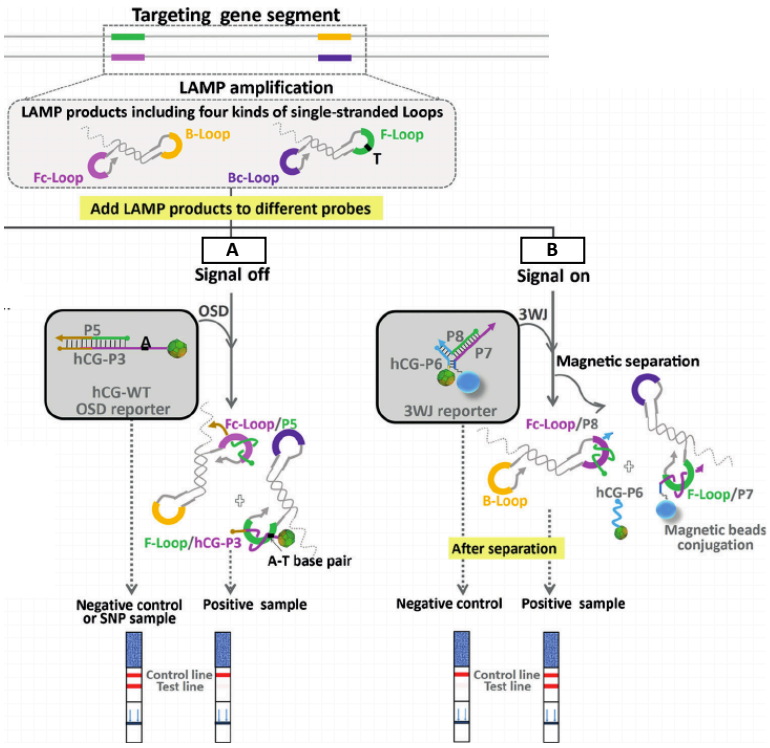


**Figure 4.** Overview of strand-displacement approaches to achieve detection of BRAF V600E on commercially-available pregnancy test strips. A) hCG-modified probe binds to the LAMP amplicon leading to a negative signal on the test strip. B) A three way junction is used that displaces an hCG modified oligonucleotide during LAMP to yield a positive test strip when the target is detected. Adapted with permission from ref. 27. Copyright 2016 Wiley-VCH.

Recently, molecular beacons (MBs) have been demonstrated to impart sequence-specificity to LAMP detection.[23] MBs are dually-labeled with a fluorophore-quencher pair that possess a hairpin structure that remains closed until a target sequence is present. Upon hybridization with the target, the probe 'opens up' and leads to an increase in fluorescence. In absence of the target, the hairpin structure remains closed resulting in minimal fluorescence. These probes have previously been shown to successfully detect SNPs using qPCR and show great promise in LAMP assays.

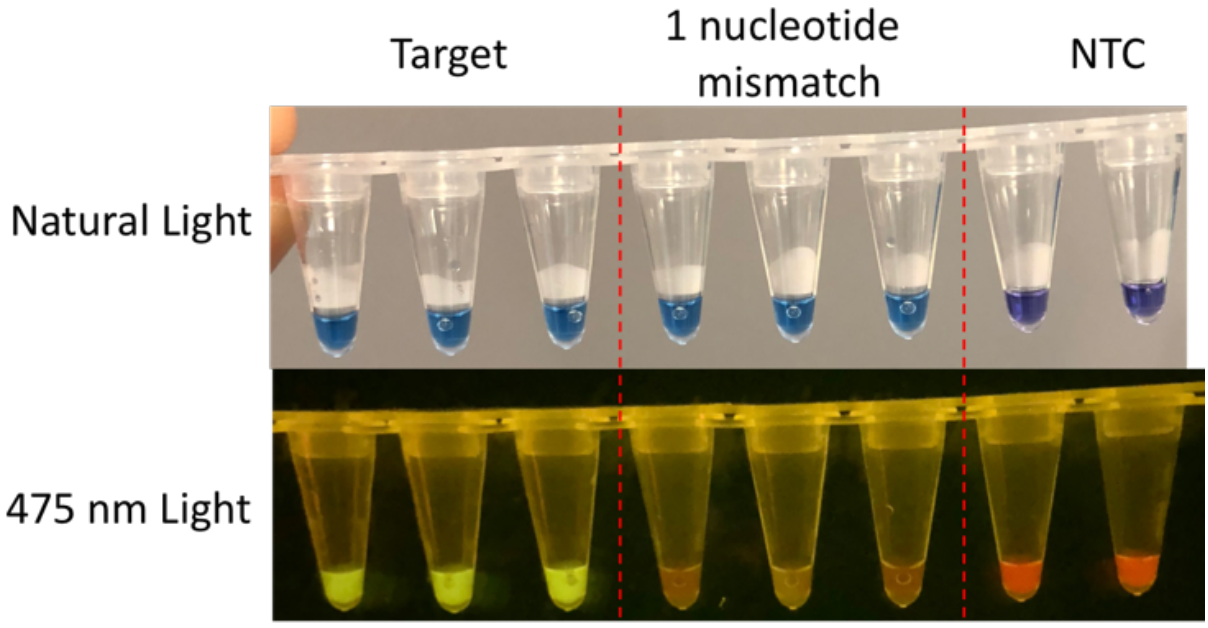


**Figure 5.** MB-LAMP reactions containing HNB for the target and single-nucleotide mismatch, as viewed by natural light and under 475 nm irradiation. Adapted with permission from ref. 29. Copyright 2019 American Chemical Society

Varona et al. demonstrated the successful visual detection of a SNP by the combined use of a MB and HNB, a traditional non-specific indicator of amplification.[24] The strategy involved the use of a transilluminator for the visual identification of positive reactions. Figure 5 shows a representative image of the results. When a negative reaction occurred, strong red fluorescence could be observed due to the presence of HNB. Strong green fluorescence was observed in the

presence of the perfect complement while the SNP sequence resulted in significantly decreased green fluorescence. Several parameters were optimized in order to achieve the greatest visual differentiation. The reaction temperature was found to be important to consider as it allows for greater destabilization between the MB and the mismatched sequence. HNB concentration was also varied in order to achieve a clear and distinct signal from the negative samples. A 1% mutation abundance could be visually differentiated with this method.

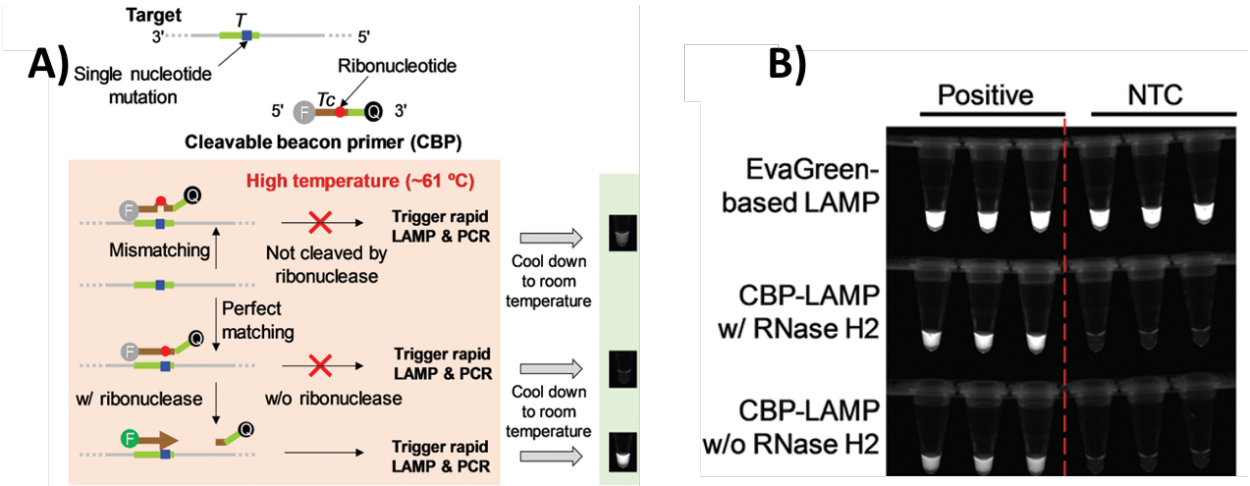


Figure 6. A) Schematic describing the utilization of cleavable beacon primer (CBP) and a ribonuclease for SNP detection. B) Images comparing the fluorescence from reaction containers containing EvaGreen or the CBP with or without RNase H2. Adapted with permission from ref. 31. Copyright 2019 Royal Society of Chemistry

In a subsequent study, an assay was designed for the detection of BRAF V600E with MB-LAMP.[25] Two distinct MBs possessing two fluorophores (FAM and HEX) that were complementary to either the wild-type (FAM) or mutant (HEX) alleles were designed. Endpoint detection was performed with a plate reader, negating the need for real-time fluorescence measurements and allowing for detection of 5% mutation abundance using this assay. In addition, the method could be coupled with polymeric ionic liquid-based solid-phase microextraction for the isolation of DNA from human plasma in clinically-relevant concentrations, demonstrating its potential in clinical applications. The biggest challenge associated with MB-LAMP assay implementation is the MB design. Loop-primers must be carefully chosen to maximize the stability

of the MB-to the target while destabilizing the mismatched sequence. In addition, careful optimization of the stem must be made to achieve optimal results.Ding et al. developed an interesting strategy with a MB-like probe containing an RNA nucleotide in the SNP location as well as incorporating the use of RNase H2.[26] In this approach, the hairpin structure of the MB was eliminated and the probe became linearized during the amplification process (61 °C). If the complementary (mutant) sequence was present, the RNase H2 cleaves the RNA nucleotide, allowing for separation of the fluorophore-quencher pair and accelerated amplification. Upon completion of the reaction and cooling to room temperature, high fluorescence could be observed due to cleaving of the MB by the RNase. However, when the mismatch (wild-type) was present and the RNase was unable to hydrolyze the probe, the MB remained intact and formed the hairpin structure upon cooling. A significant decrease in the observed fluorescence can be observed when reactions containing the wild-type sequence were performed. A schematic of the method and visual appearance of the reaction containers is shown in Figure 6. The developed approach was applied for the detection of a KRAS mutation with successful detection being achieved utilizing real-time fluorescence detection and visually with a transilluminator. Ten (10) copies per reaction could be positively identified and a mutation abundance as low as 0.01% was successfully detected with both methods. Detection was achieved from pure plasmid DNA as well as genomic DNA from KRAS mutant type cells (LS 174T cell).

Tani et al. previously developed a universal probe called the QProbe for the detection of SNPs following PCR amplification using melt-curve analysis.[27] This method was later applied for SNP detection in LAMP by Ayukawa et al.[28] The QProbe is a short, 3’ fluorophore-labeled LNA oligonucleotide. The complementary sequence of the QProbe is added onto a short sequence that is complementary to the desired target. A key aspect of the target sequence is the need for a guanine

base at the 5' end. When these conditions are satisfied, the target and its complement hybridize, which brings the QProbe sequence in close proximity to the guanine base, leading to a quenching of fluorescence. After amplification, a melt-curve is performed and the derivative of the fluorescence calculated. Mismatches in the target sequence will lead to decreased duplex stability and lower melting temperatures. A significant drawback to this method using LAMP is the need for real-time fluorescence monitoring as well as precise thermal cycling equipment.

A similar strategy employed by Komura et al. also relied on differential annealing curves to differentiate between SNPs.[29] In this approach, two separate probes were designed and each contained either a fluorophore or quencher of a quencher pair. These probes were designed to bind in close proximity to each other within the amplicon, allowing quenching when both probes bound their respective targets. The quencher probe was designed to contain the SNP region. Following LAMP, the annealing temperature could be determined by monitoring the fluorescence; as the temperature decreased, the quencher probe was able to bind its complementary target at higher temperatures than the mismatch, resulting in significant difference in the annealing temperature and allowing for the differentiation of SNPs.

**Detection of Viable Bacterial Pathogens**

While PCR and LAMP are well suited for the rapid and specific detection of nucleic acids derived from bacterial pathogens, they are unable to determine the viability of the detected organisms. Enrichment cultures represent the most common and inexpensive way to increase the levels of bacteria to detectable levels.[30] This technique relies on the incubation of samples within selective media in order to promote the growth of the target pathogen while minimizing the growth of other nonpathogenic organisms. While enrichment cultures can be selective towards specific bacteria, they can suffer from long incubation times due to the variability in proliferation rates of

different bacteria. This makes rapid detection of microorganisms a challenge with these traditional techniques.

In order to bacteria faster and more efficiently, physical enrichment can be performed. This can be done with magnetic particles functionalized with antibodies that can recognize the target bacteria and be subsequently separated when an external magnetic field is applied.[31] However, the development of antibodies is expensive and their use in complex food samples can decrease their stability and efficacy. Additionally, magnetic particles are prone to aggregation and settling which drastically reduces their effectiveness.

Magnetic ionic liquids (MILs) have previously been demonstrated for the capture of viable bacteria for subsequent detection with plating and biomolecular techniques such as PCR and RPA.[32,33] MILs are a subclass of ILs that possess a paramagnetic metal within their chemical structure, allowing them to be manipulated by an external magnetic field. Similar to ILs, MILs are highly tunable and their structure can be modulated to obtain a variety of physicochemical properties. In particular, high hydrophobicity MILs can be designed that can perform as extraction solvents in aqueous samples.[34,35] Their hydrophobicity allows them to be easily dispersed into fine microdroplets in aqueous solutions. These microdroplets possess high surface area which allows them to efficiently capture bacteria.

## Organization of Dissertation

**Chapter 1** describes the development of a rapid solid-phase microextraction (SPME) method to isolate DNA from Mycobacterium smegmatis. The extracted nucleic acid was subsequently detected using isothermal multiple-self-matching initiated amplification with hydroxy naphthol blue (HNB). Additionally, a custom buffer was designed to enable direct interfacing of the 1 M SPME desorption solution with the isothermal amplification method. Extraction and detection of Mycobacterial DNA was demonstrated from artificial sputum samples.

**Chapter 2** describes the development of a loop-mediated isothermal amplification (LAMP) assay to detect single-nucleotide polymorphisms. A FAM labeled molecular beacon (MB) is used along with HNB to enable visual detection. Several different parameters, including reaction temperature and HNB concentration, were optimized to provide unambiguous detection of the target sequence. The developed method is able to detect the mutated sequence when present in 5% abundance when compared to the wild-type sequence.

**Chapter 3** describes the development of an MB-LAMP assay for the detection of BRAF V600E, a mutation present in 90% of melanomas. The MB structure was carefully optimized to provide differentiation between the mutant and wild-type sequence. Reaction temperature, molecular beacon concentration, and the use of betaine were optimized. In order to simplify the detection method, a plate reader was used for end-point measurements. Additionally, SPME was employed to isolate the mutant sequence from human plasma samples.

**Chapter 4** expands the detection platforms for MB-LAMP detection. Sequence-specific detection is achieved on commercially-available lateral flow immunoassay strips through the use of a FAM-labeled molecular beacon and a biotinylated loop-primers. The assay was shown to be compatible with three different DNA sequences. High specificity could be achieved and was demonstrated through the differentiation of the BRAF V600E mutant from the wild-type sequence. Additionally, 3D printing was employed to develop an enclosed system to minimize the potential for contamination.

**Chapter 5** demonstrates the development of a sequence-specific DNA extraction SPME phase through the modification of commercially available SPME fibers and carbodiimide chemistry. An oligonucleotide complementary to the target sequence was immobilized onto the SPME fiber and subsequently used to isolate the target sequence. Parameters including stir-rate,

desorption time, and coupling conditions were investigated and optimized. The developed method was successfully shown to isolate the target sequence from aqueous samples.

**Chapter 6** explored the physiological effects of magnetic ionic liquids (MIL) on gram negative bacteria and expands the applicability of MIL-based capture of microorganisms. Potential cytotoxic effects of MILs on Salmonella and E. coli O157:H7 were probed through plating exposed bacteria on selective and no-selective agar. Additionally, the cytotoxic effects of a Dy (III) based MIL were systematically evaluated to identify the MIL component responsible for the observed effects. The broad applicability for the isolation of Gram-negative bacteria was also shown through the capture of seven enterobacterial strains.

## References

(1) Demeke, T.; Jenkins, G. R. *Anal. Bioanal. Chem.* **2010**, *396*, 1977–1990.

(2) Chomczynski, P.; Sacchi, N. *Nat. Protoc.* **2006**, *1*, 581–585.

(3) Boom, R.; Sol, C. J. A.; Salimans, M. M. M.; Jancen, C. L.; Wertheim-van-Dillen, P. M. E.; J, V. der N. *J Clin Microbiol* **1990**, *28*, 495–503.

(4) Arthur, C. L.; Pawliszyn, J. *Anal. Chem.* **1990**, *62*, 2145–2148.

(5) Cagliero, C.; Ho, T. D.; Zhang, C.; Bicchi, C.; Anderson, J. L. *J. Chromatogr. A* **2016**, *1449*, 2–7.

(6) Pacheco-Fernández, I.; Najafi, A.; Pino, V.; Anderson, J. L.; Ayala, J. H.; Afonso, A. M. *Talanta* **2016**, *158*, 125–133.

(7) Nacham, O.; Clark, K. D.; Varona, M.; Anderson, J. L. *Anal. Chem.* **2017**, *89*, 10661–10666.

(8) Nacham, O.; Clark, K. D.; Anderson, J. L. *Anal. Chem.* **2016**, *88*, 7813–7820.

(9) Pratt, E. D.; Cowan, R. W.; Manning, S. L.; Qiao, E.; Cameron, H.; Schradle, K.; Simeone, D. M.; Zhen, D. B. *Anal. Chem.* **2019**, *91*, 7516–7523.

(10) Pandey, P.; Pant, N. D.; Rijal, K. R.; Shrestha, B.; Kattel, S.; Banjara, M. R.; Maharjan, B.; Rajendra, K. C. *PLoS One* **2017**, *12*.

(11) Piepenburg, O.; Williams, C. H.; Stemple, D. L.; Armes, N. A. *PLoS Biol.* **2006**, *4*, e204.

(12) Ali, M. M.; Li, F.; Zhang, Z.; Zhang, K.; Kang, D.-K.; Ankrum, J. A.; Le, X. C.; Zhao, W. *Chem. Soc. Rev.* **2014**, *43*, 3324–3341.

(13) Notomi, T.; Okayama, H.; Masubuchi, H.; Yonekawa, T.; Watanabe, K.; Amino, N.; Hase, T. *Nucleic Acids Res.* **2000**, *28*, E63.

(14) Goto, M.; Honda, E.; Ogura, A.; Nomoto, A.; Hanaki, K. I. *Biotechniques* **2009**, *46*, 167–172.

(15) Ding, X.; Wu, W.; Zhu, Q.; Zhang, T.; Jin, W.; Mu, Y. *Anal. Chem.* **2015**, *87*, 10306–10314.

(16) Khan, M.; Wang, R.; Li, B.; Liu, P.; Weng, Q.; Chen, Q. *Front. Microbiol.* **2018**, *9*, 2089.

(17) Rolando, J. C.; Jue, E.; Barlow, J. T.; Ismagilov, R. F. *Nucleic Acids Res.* **2020**, *48*, e42–e42.

(18) Xu, G.; Zhao, H.; Cooper, J. M.; Reboud, J. *Chem. Commun.* **2016**, *52*, 12187–12190.

(19) Njiru, Z. K.; Mikosza, A. S. J.; Armstrong, T.; Enyaru, J. C.; Ndung'u, J. M.; Thompson, A. R. C. *PLoS Negl. Trop. Dis.* **2008**, *2*, e147.

(20) Higgins, O.; Smith, T. J. *J. Mol. Diagnostics* **2020**, *22*, 640–651.

(21) Jiang, Y. S.; Bhadra, S.; Li, B.; Wu, Y. R.; Milligan, J. N.; Ellington, A. D. *Anal. Chem.* **2015**, *87*, 3314–3320.

(22) Du, Y.; Pothukuchy, A.; Gollihar, J. D.; Nourani, A.; Li, B.; Ellington, A. D. *Angew. Chemie - Int. Ed.* **2017**, *56*, 992–996.

(23) Liu, W.; Huang, S.; Liu, N.; Dong, D.; Yang, Z.; Tang, Y.; Ma, W.; He, X.; Ao, D.; Xu, Y.; Zou, D.; Huang, L. *Sci. Rep.* **2017**, *7*, 40125.

(24) Varona, M.; Anderson, J. L. *Anal. Chem.* **2019**, *91*, 6991–6995.

(25) Varona, M.; Eitzmann, D. R.; Pagariya, D.; Anand, R. K.; Anderson, J. L. *Anal. Chem.* **2020**, *92*, 3346–3353.

(26) Ding, X.; Yin, K.; Chen, J.; Wang, K.; Liu, C. *Chem. Commun.* **2019**, *55*, 12623–12626.

(27) Tani, H.; Miyata, R.; Ichikawa, K.; Morishita, S.; Kurata, S.; Nakamura, K.; Tsuneda, S.; Sekiguchi, Y.; Noda, N. *Anal. Chem.* **2009**, *81*, 5678–5685.

(28) Ayukawa, Y.; Hanyuda, S.; Fujita, N.; Komatsu, K.; Arie, T. *Sci. Rep.* **2017**, *7*, 1–9.

(29) Komura, R.; Kawakami, T.; Nakajima, K.; Suzuki, H.; Nakashima, C. *J. Gen. Plant Pathol.* **2018**, *84*, 247–253.

# CHAPTER 2. SOLID-PHASE MICROEXTRACTION OF DNA FROM MYCOBACTERIA IN ARTIFICIAL SPUTUM SAMPLES TO ENABLE VISUAL DETECTION USING ISOTHERMAL AMPLIFICATION

Reprinted with permission from *Analytical Chemistry* 2018, 90, 11, 6922-6928



Marcelino Varona, Xiong Ding, Kevin D. Clark, and Jared L. Anderson

## Abstract

Point-of-care (POC) technologies for the detection of pathogens in clinical samples are highly valued due to their speed, ease of use, and cost-effectiveness. Furthermore, they are ideally suited for resource-limited settings where expensive and sophisticated laboratory equipment may not be readily available. In this study, a rapid method based on solid-phase microextraction (SPME) of mycobacterial DNA with subsequent isothermal amplification and visual detection was developed. Direct coupling of the SPME desorption solution (1 M NaCl) to the isothermal reaction system was achieved to circumvent dilution steps and improve detection limits. Using this method, DNA was preconcentrated from lysed mycobacteria in just 2 min, subjected to isothermal multiple-self-matching-initiated amplification (IMSA), and the amplicons were detected visually. With a total analysis times of less than 2 h, the optimized method was capable of extracting and visually detecting mycobacterial DNA from artificial sputum samples containing clinically relevant concentrations of mycobacteria (107 colony forming units/mL), demonstrating its potential for future POC applications.

## Introduction

The rapid and sensitive detection of pathogens in clinical samples is important for prompt diagnosis and administration of the most effective treatment.[1] Traditional microbiological methods for pathogen identification include selective culture, immunoassays,[2,3] and nucleic acid

amplification-based methods.[4,5] While culture-based methods are often considered the gold standard owing to their high degree of accuracy, they are incompatible with point-of-care (POC) applications due to the extensive time that is often required for cultures to proliferate (e.g., 2 weeks for Mycobacterium tuberculosis*)*.[1,6] POC methods for the detection of pathogens are highly valuable as they provide rapid results and can be used without extensive training.[7] Although immunoassays are a promising alternative to culture-based approaches, the development of pathogen-specific antibodies is a time consuming (up to 3 months)[8] and expensive process. Nucleic acid amplification-based methods are less expensive alternatives that still maintain high sensitivity and specificity for their targets, making them ideally suited for POC applications.

Popular techniques that exploit the rich information in nucleic acids through the amplification of pathogen specific sequences include polymerase chain reaction (PCR)[9] and real-time quantitative PCR (qPCR).[10] Recently developed isothermal nucleic acid amplification (INAA) techniques such as loop mediated isothermal amplification (LAMP),[11] isothermal multiple-self-matching-initiated amplification (IMSA),[12] and recombinase polymerase amplification (RPA)[13] show incredible promise for POC applications due to their lack of dependence on sophisticated thermal cycling equipment and their compatibility with visual detection methods. However, one core challenge shared by these methods is the need to isolate highly pure nucleic acid samples that are devoid of polymerase inhibitors in order to achieve optimal performance.[14] This need is emphasized when DNA must be isolated from complex sample matrices such as blood or sputum that contain a variety of components that hinder enzymatic amplification. Therefore, sample preparation methods that can rapidly extract and purify nucleic acids from interfering agents and be subsequently interfaced with existing nucleic acid amplification technologies are highly desirable for POC applications.

Conventional methods for nucleic acid purification include phenol-chloroform liquid-liquid extraction (LLE)[15] and silica-based solid phase extraction (SPE).[16] LLE is a time-consuming process that relies on the partitioning of nucleic acids between two immiscible phases. However, the requisite multiple centrifugation steps and the use of organic solvents make this technique unsuitable for POC applications. Silica-based SPE is another commonly used method for the extraction and purification of nucleic acids and relies on the reversible binding of the nucleic acid to the sorbent phase. Using a chaotropic salt such as guanidine hydrochloride, the nucleic acid is dehydrated and subsequently adsorbed onto silica.[17] Following multiple washing steps to remove unwanted compounds such as proteins and lipids, the nucleic acid is eluted with a low-ionic strength solution. This technique is faster and uses less organic solvents than LLE. However, SPE requires significant user intervention, multiple centrifugation steps, and its reuse is not recommended making it incompatible with POC diagnostics.

Solid-phase microextraction (SPME), developed by Pawliszyn and co-workers in 1990,[18] circumvents many of the aforementioned issues associated with both LLE and SPE. SPME involves the immobilization of a thin sorbent layer on a solid support and has been exploited in the extraction of a wide range of compounds including acrylamide in coffee,[19] antifungal medication in plasma,[20] and metabolites *in vivo*.[21] This solvent-less technique does not require centrifugation and overcomes many shortcomings of traditional LLE and SPE approaches.

Recently, our group[22,23] and others[24] have explored the use of polymeric ionic liquids (PILs) as selective phases for the extraction of nucleic acids. PILs are a subclass of ionic liquids that contain polymerizable moieties in the cation and/or anion structures. Our group first applied PILs as SPME coatings for the extraction of nucleic acids from aqueous samples by co-polymerizing the PIL monomer and crosslinker with the fiber support, thereby creating a robust

and selective extraction phase. Electrostatic interactions of the cationic imidazolium moiety of the PIL with the negatively charged phosphate groups of nucleic acids and ion exchange were identified as the two main forces driving the extraction of nucleic acids by the PIL.[22,23] These methods showed that PILs were suitable for the extraction of nucleic acids from aqueous samples. The reusability, robustness, and effectiveness of PIL-SPME make it an attractive sample preparation tool for the purification of nucleic acids in POC applications.

There currently exists one World Health Organization (WHO) endorsed method for the detection of Mycobacterium tuberculosis from sputum samples at the POC. This utilizes PCR and molecular beacon probes to detect tuberculosis and test for drug resistance.[25] Although this method has been used extensively for the detection of mycobacteria from infected patients, the need for an uninterrupted power supply, low ambient temperatures (< 30 °C), and annual calibration demonstrate a need for more robust methods for the detection of mycobacteria in resource limited settings.[26,27]

In this study, a rapid and sensitive method was developed for the isolation and visual detection of genomic DNA from mycobacteria inoculated in artificial sputum media (ASM) by PIL-SPME coupled with IMSA. This is the first reported use of IMSA for the amplification of mycobacterial genomic DNA. By using vortex agitation instead of stirring, the optimized method provided a 15-fold shorter extraction time compared to a previously reported DNA extraction method using PIL-SPME.[22] Furthermore, an IMSA reaction using hydroxynaphtohol blue (HNB) for visual detection was optimized and directly coupled to PIL-SPME in an approach that circumvents dilution of the desorption solution to maximize sensitivity. We demonstrate the potential applicability of the method at the POC by extracting genomic DNA from Mycobacterium smegmatis spiked in artificial sputum media (ASM). The concentration of M. smegmatis was

selected to simulate clinically relevant concentrations of mycobacteria in the sputum of individuals with active infections ($10^7$ cfu $mL^{-1}$).[28] The method is capable of extracting, amplifying, and subsequently visually detecting mycobacterial DNA in less than 2 h. Other commonly used sample preparation methods for the extraction of mycobacterial DNA were compared with the PIL-SPME method and found to be slower while also requiring multiple centrifugation steps that are typically incompatible for POC applications.

## Experimental

### Preparation of DNA

A modified 3.9 kbp plasmid from Eurofin Genomics (Louisville, KY, USA) containing a 280 bp insert was amplified by PCR using the following primers: 5' – GGA TGT GTC TGC GGC GTT TT –3' and 5' – GAG GCC CAC TCC CAT AGG TT – 3'. Following amplification, agarose gel electrophoresis was performed using a Bethesda Research Laboratories (Gaithersburg, MD, USA) Horizontal System Gel Electrophoresis H4 chamber with a Neo/Sci (Rochester, NY, USA) dual output power supply. The amplicon band was excised from the gel and purified using a QIAquick Gel Extraction kit (Qiagen, Hilden, Germany) according to the manufacturer's instructions. To quantify the amount of DNA recovered, a NanoDrop 2000c spectrophotometer (Thermo Scientific, Waltham, MA, USA) was used. A standard solution of 1 ng µL-1 (3.48×109 copies) was then serially diluted and the dilutions stored at -20.0 °C. For the extraction of DNA from Mycobacterium smegmatis MC2 155 (ATCC, Manassas, VA, USA), a QiaAmp DNA Mini kit was used according to the manufacturer's instructions. The recovered DNA was quantified with a Nanodrop spectrophotometer. A standard solution of 1.3 ng µL-1 was serially diluted (130 pg µL-1 - 0.13 pg µL-1) and stored in -20.0 °C.

**qPCR Assays and conditions**

Quantification of DNA during the method development process was performed using real-time quantitative polymerase chain reaction (qPCR) on a CFX96 Touch Real-Time PCR Detection System from Bio-Rad Laboratories (Hercules, CA). The following amplification conditions were used: an initial denaturation step of 3 min at 95.0 °C, followed by 40 cycles of 10 s at 95.0 °C and 30 s at 58.0 °C. All reactions were performed in triplicate. The following volumes of reagents were used for each reaction: 1 µL of DNA template solution, 10 µL (2X) SsoAdvanced Universal SYBR Green Supermix (Bio-Rad laboratories), 8.2 µL of deionized water, and 0.8 µL of 10 µM forward and reverse primers (Integrated DNA Technologies, Coralville, IA, USA). To quantify the amount of DNA extracted by the SPME fibers, an external five-point calibration curve was prepared (10-fold dilutions, 1 to 1×10-4 pg) with 10 mM of NaCl in the reaction mixture, as shown in Figure S1 of the Supporting Information. The amplification efficiency was calculated using equation 1 and found to be 110%, within the acceptable range according to The Minimum Information for Publication of Quantitative Real-time PCR experiments (MIQE) guidelines.29 For reference, an amplification efficiency of 100% indicates that the amount of PCR product generated doubles with each cycle.

$$Efficiency = [10^{-1/slope} - 1] \times 100 \quad (1)$$

**HNB-IMSA assays**

HNB-IMSA assays for 16S rRNA targets were performed for 90 minutes at 70 °C in a 10 µL mixture containing the following components: 1.0 µL of 10X reaction buffer (500 mM Tris-HCl and 10 mM DTT), 0.2 µM each of DsF and DsR, 0.8 µM each of FIT and RIT, 1.6 µM each of SteF and SteR, 1.4 mM of each dNTP, 3.2 U of Bst 2.0 WarmStart DNA polymerase (New England Biolabs, Ipswich, MA, USA ), 0.8 M betaine (Sigma-Aldrich), 8 mM MgSO4 (NEB), 240 µM HNB (Sigma-Aldrich), and 1.0 µL of template solution. The sequences of all primers used

for IMSA can be found in Table S1 of the Supporting Information. A general schematic of the IMSA amplification process as well as primer binding sites can be found in figures S2 and S3.

**Mycobacterium smegmatis culture conditions**

Mycobacterium smegmatis was initially cultured in Middlebrook 7H9 broth supplemented with 30% glycerol, 0.05% Tween 80, ADC enrichment medium (NaCl, bovine serum albumin, and dextrose), carbenicillin (50 µg mL-1) and cycloheximide (10 µg mL-1) for 72 h in an incubator shaker (37.0 °C, 250 rpm). Following the incubation period, a 100 µL aliquot of the culture was inoculated into a second culture of equal volume (5 mL) containing the same components as the initial culture, with the exception of Tween. The secondary culture was subsequently incubated for 2 days. To accurately determine the number of cells corresponding to an OD600 value of 1, serial 10-fold dilutions were performed once this culture reached an OD600 = 1. After the dilutions were made, 100 µL was taken from each of the dilutions and plated on 7H10 agar. Colonies were counted after incubating the cells for 3 days from the lowest plated dilution, which corresponded to 1.9×107 colony forming units (cfu) mL-1 in the original solution. Prior to all extractions, cells were pelleted, washed, and resuspended in phosphate buffered saline (PBS) or Artificial Sputum.

**DNA extraction using SPME fibers**

A general schematic illustrating the workflow for the PIL-SPME based DNA extraction method is shown in Figure 1A. A 10 pg mL-1 solution of DNA in 1.5 mL TE buffer at pH 8 was prepared in a LoBind tube (Eppendorf, Hamburg, Germany) immediately prior to extraction. The tube was modified prior to extraction by piercing the cap with a syringe needle and inserting the SPME fiber through the resulting opening. The lid was closed, ensuring that the sorbent coating was immersed in the sample solution, and subjected to vortex agitation with a Fisherbrand Digital vortex mixer (Fisher Scientific, Hampton, NH, USA) for 2 min. Immediately following the extraction, the PIL-SPME fiber was desorbed in 10 µL of 1 M NaCl for 30 min. To avoid qPCR

inhibition caused by 1 M NaCl, the desorption solution was diluted 5-fold to achieve a final concentration of 10 mM NaCl in the qPCR mix. After each extraction, the fibers were washed with 2 M NaCl for 30 min to desorb any remaining DNA from the fiber. Figure S4 shows representative qPCR plots of the diluted desorption solution as well as the subsequent wash step, revealing that carryover is negligible (Cq >38) after this step.

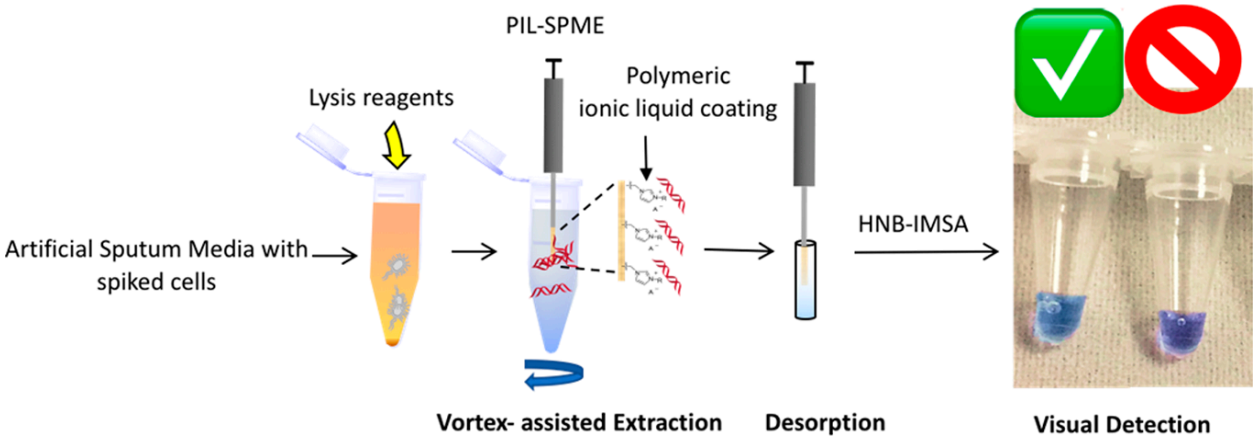


**Figure 1.** Schematic representation of the developed method for rapid extraction of mycobacterial DNA and subsequent visual detection by isothermal amplification (HNB-IMSA).

## Results and Discussion

### Optimization of extraction and desorption conditions

The chemical structure of the PIL sorbent coating used in this study is shown in Figure S5 and was prepared using a previously reported method.[30] This PIL was chosen for method optimization as it had previously been successfully applied for the extraction of DNA from aqueous solutions and *E. coli* cell lysate.

In order to develop a method that could be easily interfaced with HNB-IMSA for potential POC applications, the total analysis time should be as short as possible. The step in the PIL-SPME workflow that can be most readily expedited is the extraction time. To determine the effects of different parameters on the extraction of DNA, qPCR was used to quantify the DNA extracted by the PIL sorbent coating.

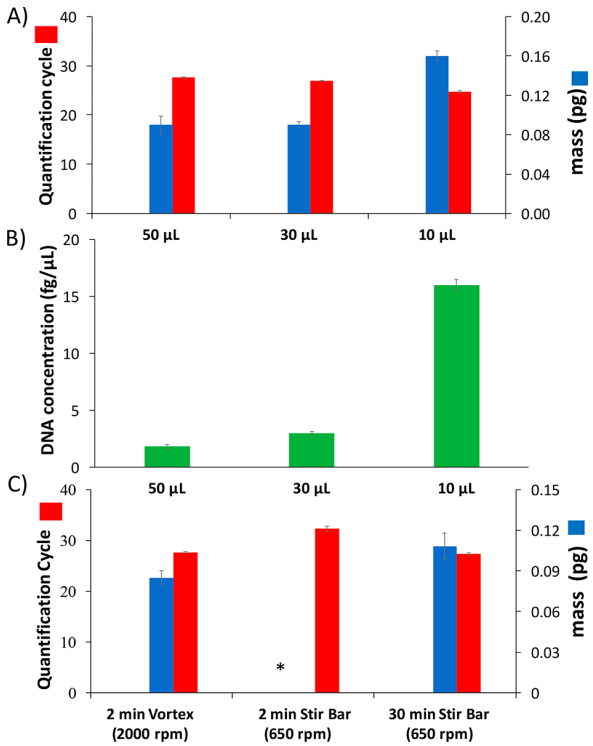


**Figure 2.** (A) Effect of desorption volume on the recovery of DNA following extractions. (B) Concentration of the desorption solution when employing different desorption volumes. (C) Effect of the agitation method on the extraction of DNA. All extractions were performed in triplicate from a 10 pg mL−1 solution of DNA: total volume, 1.5 mL, pH 8 TE buffer; extraction time, 2 min with vortex (2500 rpm); desorption time, 30 min; desorption solvent, 1 M NaCl; desorption solvent volume, 10, 30, or 50 µL. Cq values are indicated in red, while mass is indicated in blue. * Indicates insufficient DNA was extracted for quantification.

In an attempt to decrease the extraction time, vortex agitation was employed as an alternative to traditional magnetic stirring for the extraction of a 280 bp fragment of DNA. As shown in Figure 2C, vortex agitation for 2 min at 2500 rpm yielded comparable extraction efficiency to stirring at 650 rpm for 30 min. This corresponds to a drastic 15-fold decrease in extraction time while maintaining similar extraction performance. When a 2 min extraction at 650 rpm with magnetic stirring was performed, qPCR analysis of the desorption solution indicated that insufficient DNA was extracted for quantification. The vigorous mixing afforded by vortex agitation results in faster mass transfer of the nucleic acid to the PIL fiber. Short extraction times (i.e., 2 min) are achieved due to the rapid ion exchange process,[31] facilitated by the exchangeable halide anions of the PIL sorbent.[22] Furthermore, the good reproducibility (relative standard

deviation (RSD) of 0.8%, n = 3 for Cq values) indicates that there is no significant loss of fiber performance due to loss of coating when applying vortex mixing.

Faster vortex speeds should be expected to provide faster mass transfer of the DNA from the sample solution to the PIL and therefore allow for higher extraction of DNA at shorter times. To investigate this, several vortex speeds ranging from 500-2500 rpm were investigated. As shown in Figure S6, the amount of DNA extracted increased from 500-1000 rpm, remaining constant at approximately 0.030 pg of DNA. However, a sharp increase in the mass extracted was observed from 1000-2000 rpm, with masses of 0.029 ± 0.010 to 0.135 ± 0.028 pg, respectively, being achieved. A less pronounced increase was seen at 2500 rpm where the mass extracted was 0.161 ± 0.005 pg. Therefore, a vortex speed of 2500 rpm was chosen for subsequent extractions.

The effect of extraction time on the extraction of DNA was also investigated. This was carried out by performing extractions from a 10 pg $mL^{-1}$ solution of DNA in TE buffer at pH 8 and varying the extraction time from 0.5-15 min. Figure S7 shows an increase in the mass of DNA extracted in the range from 0.5-6 min. Beyond 6 min, no significant increase in the amount of DNA extracted was observed. An extraction time of 2 min was chosen for subsequent experiments as it allowed for very rapid and reproducible extractions (RSD = 3.1% based on mass extracted) and precludes exposing the fiber, sample, and analyst to long vortex times.

Dilution of the desorption solution is necessary to relieve inhibition caused by the high concentration of NaCl in qPCR. Therefore, the use of smaller desorption volumes should increase the concentration of DNA within the final desorption solution and ultimately produce better detection limits. To examine this, 3 different desorption volumes were investigated. As shown in Figure 2A, the amount of DNA recovered after a 2 min extraction was greater when a desorption volume of 10 µL was used. The difference in the mass recovered when using 10 µL instead of 30

or 50 µL could be attributed to the significantly smaller surface area of the desorption container that makes contact with the 10 µL solution (0.67 $cm^2$) versus using 50 µL or 30 µL solutions (2.45 $cm^2$ and 1.63 $cm^2$, respectively). Since DNA is known to adsorb onto polypropylene under high ionic strength conditions,[32] decreasing the surface area of the desorption container that is exposed to the 1 M NaCl desorption solution likely minimizes this effect and allows for higher DNA recoveries. Figure 2B further highlights the benefits of using 10 µL as the desorption solvent volume by showing the concentration of DNA in the desorption solution plotted as a function of the desorption volume. This results in nearly a 1 order of magnitude increase in the concentration of DNA when 10 µL are used as the desorption volume instead of 50 µL (16 fg $\mu L^{-1}$, and 1.8 fg $\mu L^{-1}$ respectively). The intraday fiber-to-fiber reproducibility was tested with 3 fibers using a 2 min extraction at 2500 rpm and a 5% RSD was found for all Cq values.

**Optimization of HNB-IMSA buffer for direct analysis of SPME desorption solution**

IMSA is an INAA technology developed by Ding et al. that is similar to LAMP. However, a particular advantage of IMSA is the creation of multiple self-matching structures, allowing for faster reaction times and better detection limits than traditional LAMP reactions.[12] IMSA reactions are commonly performed in the isothermal amplification buffer supplied by NEB. However, inhibition of the reaction was observed when 1 µL of the desorption solution (1 M NaCl) was directly transferred into the IMSA reaction mix (Figure S8). The minimum inhibitory concentration of NaCl was determined by testing a range of NaCl concentration in the HNB-IMSA mix and monitoring the fluorescence change in real-time. This allowed for reaction effectiveness to be gaged by using the threshold times obtained to determine the inhibitory effects of NaCl. As shown in Figure S8, the minimum inhibitory concentration of NaCl in the reaction mixture was 14 mM, which would require a 10-fold dilution of the 1 M NaCl desorption solution. This dilution step would severely hinder the analysis and detection of low concentrations of bacteria (e.g., $10^5$

cfu $mL^{-1}$) of cells. Ideally, a buffer compatible with the 1 M NaCl desorption solution would be used in the HNB-IMSA reaction to avoid unnecessary dilution steps and achieve optimal sensitivity.

According to NEB, the *Bst* 2.0 WarmStart polymerase used for IMSA is compatible with a variety of buffers including NEBuffer 3 (100 mM NaCl, 10 mM $MgCl_2$, 1 mM DTT, and 50 mM Tris-HCl pH 7.9). When the reaction was attempted under the same reaction conditions as the previously optimized reaction (63 °C, 60 min), no amplification was detected. However, upon increasing the reaction temperature to 70 °C, the amplification of target DNA was recovered as indicated by an increase in real-time fluorescence. The recovery in amplification can potentially be attributed to the increased melting temperature of the primers to the target due to the high concentration of NaCl. Unfortunately, visual detection was not achieved due to the difficulty in discerning between positive and negative samples. Since the color of the solution is a dependent on a combination of pH and HNB/dNTPs chelating $Mg^{2+}$,[33] these components were investigated to determine the source of the lacking color change. The concentration of $Mg^{2+}$ was varied in a mixture of 1X NEBuffer 3, dNTPs, and HNB to determine the optimal $Mg^{2+}$ concentration to produce a solution of purple color corresponding to negative amplification. Figure S9 illustrates that the negative color is not achieved until the total concentration of $Mg^{2+}$ is 24 mM. However, when this concentration of $Mg^{2+}$ is used for a standard reaction, the target was not amplified due to the excessive amounts of magnesium present in the reaction system, possibly leading to inhibition of the polymerase or a change in melting temperature of the primers.

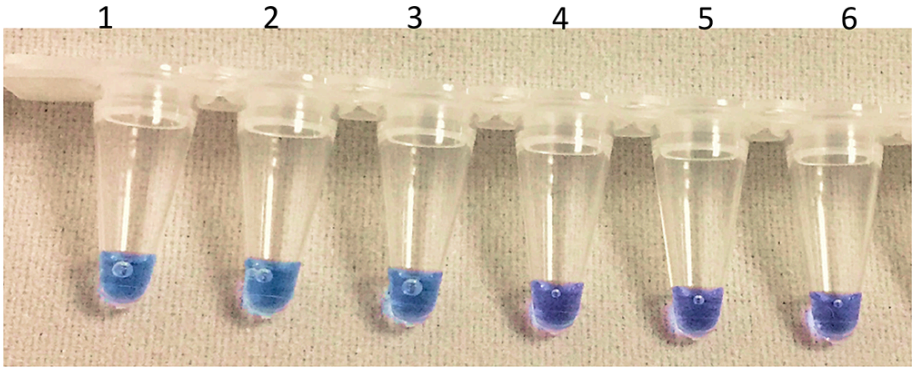


**Figure 3.** Visual detection sensitivity of HNB-loaded IMSA. HNB: 240 μM. Tubes 1−6: the reactions with templates of (1) 1.39 × 104, (2) 1.39 × 103, (3) 1.39 × 102, (4) 1.39 × 101, and (5) 1.39 × 100 copies, and (6) no-target control (NTC) with isovolumetric nuclease-free water replacing the template. Positive reactions turn light blue (1−3), while negative ones remain purple (4−6). Template: M. smegmatis genomic DNA. Reaction time: 90 min. Reaction temperature: 70 °C.

One significant difference between the Isothermal Amplification Buffer (pH 8.8) and the NEBuffer 3 (pH 7.9) is their vast difference in pH. Although previous reports have suggested that the solution color results from the chelation of $Mg^{2+}$ by the dNTPs and is independent of small changes in pH [33], it is conceivable that the large difference in pH (nearly 1 unit) influences the color of the IMSA reaction system. This hypothesis was tested and confirmed when the pH of NEBuffer 3 was raised to 8.8 and the color of the negative reaction became purple. Since 10 mM of $Mg^{2+}$ was already present in the reaction, a new buffer was prepared with 100 mM NaCl, 1 mM dithiothreitol (DTT), and 50 mM Tris-HCl at pH 8.8. Figure S10A shows a series of reactions in which the $Mg^{2+}$ concentration was varied and the color change examined prior to amplification. The reactions following amplification are illustrated in Figure S10B. A $Mg^{2+}$ concentration of 8 mM was chosen as it produced the most easily identified color change. The sensitivity of this reaction system was tested across a wide range of mycobacterial DNA concentrations ($1.39\times 10^4$-1.39 copies) and is shown in Figure 3. The data shown in Figure 3 demonstrate the capability of the method for detecting down to 139 copies of mycobacterial DNA, making it suitable for the detection of low quantities of template.

**Extraction of mycobacterial DNA from cells in artificial sputum and its visual detection using HNB-IMSA**

Extracting DNA from mycobacteria in sufficient quantity and purity for downstream molecular biology techniques represents a formidable challenge. Besides being difficult to lyse due to their notoriously thick cell walls, pathogenic mycobacteria such as Mycobacterium tuberculosis are commonly found in the sputum of the infected individual, increasing the difficulty of analysis due to the complex nature of this matrix.[34] PIL-based SPME holds promise as a sample preparation method for the extraction of DNA directly from mycobacterial cells in sputum due to its ease of use and lack of multiple centrifugation steps that are required in typical methods. Furthermore, by coupling PIL-SPME with the visual detection afforded by HNB-IMSA, this method is ideally suited for a POC-oriented application in resource limited settings. Mycobacterium smegmatis was chosen as the target organism due to its morphological similarity to M. tuberculosis.

To demonstrate the compatibility of PIL-based SPME with HNB-IMSA for the extraction of DNA from M. smegmatis, extractions were initially conducted from an aqueous cell lysate. The crude lysate was diluted to 1.5 mL with TE buffer (pH 8) and subjected to the optimized PIL-based SPME method for the extraction of DNA. The extraction performance was analyzed with HNB-IMSA using the previously optimized buffer system (50 mM Tris-HCl at pH 8.8 and 1 mM DTT) with each extraction analyzed by HNB-IMSA in triplicate. The exhaustion of $Mg^{2+}$ ions during amplification resulted in the color of the reaction turning from purple (negative) to sky blue (positive), as shown in Figure 4B, allowing for easy identification of DNA positive and negative samples. Furthermore, the reactions can be viewed under blue light (~470 nm) to exploit the fluorescent properties of both SYBR green and HNB for detection (Figure 4C).[35] As illustrated in Table 1, all the reactions showed positive for target DNA amplification, indicating that extraction

and detection of DNA from M. smegmatis is possible by coupling PIL-based SPME with HNB-IMSA. Primer specificity was also tested in triplicate each time to ensure that false positives did not interfere with the analysis. It was observed that all NTCs were negative and did not change in color, indicating good primer specificity.

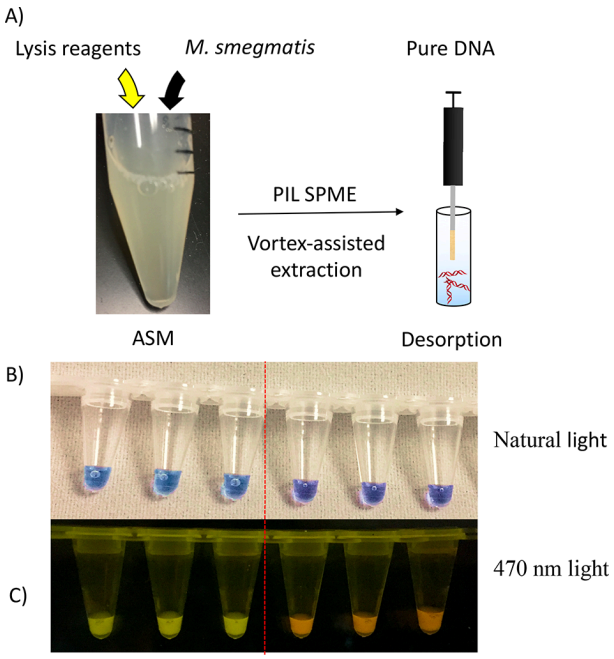


**Figure 4.** Visual representation of the artificial sputum media (ASM) used as well as the PIL-SPME workflow for DNA extractions (A). A representative example of all HNB-IMSA reactions performed and their visual detection under natural light (B) and 470 nm irradiation (C). Reactions are performed in triplicate, and three NTCs are also included to assess reaction specificity.

The capability of the method for extracting mycobacterial genomic DNA from a range of cellular suspensions was further explored. The cell suspensions were prepared by serially diluting an initial suspension of $OD_{600}$ = 1 to 3 different concentrations ($2.99\times10^{7}$-$2.99\times10^{5}$ cfu $mL^{-1}$). A 200 µL aliquot from each suspension was subjected to chemical lysis followed by PIL-SPME and visual detection with HNB-IMSA. Triplicate extractions were performed for each concentration of cells. For each extraction, triplicate HNB-IMSA reactions were performed. As shown in Table 1, the results demonstrated that all HNB-IMSA reactions performed after extractions from each of the tested concentrations gave a positive result, as indicated by the color change of the reaction

solution. This shows that sufficient mycobacterial DNA was recovered from *M. smegmatis* for detection by HNB-IMSA at cell suspension concentrations as low as $2.99\times10^5$ cfu $mL^{-1}$.

**Table 1.** Summary of visual results following the extraction of mycobacterial DNA from various cell suspensions.

| Concentration (cfu mL-1)a | No. of positive samples/no. of samples tested | NTC |
|---|---|---|
| 2.375×108 | (9/9) | 0/9 |
| 1.9×107 | (9/9) | 0/9 |
| 1.9×106 | (9/9) | 0/9 |
| 1.9×105 | (9/9) | 0/9 |

a Triplicate extractions were performed from each of the indicated concentrations. For each extraction, 3 HNB-IMSA reactions were performed along with 3 NTCs. NTC, no-target control with isovolumetric nuclease-free water replacing the template

To test the potential applicability of the method for extracting mycobacterial DNA from sputum, ASM spiked with *M. smegmatis* cells was used to closely simulate a clinical sample. ASM was prepared following an example from the literature (details can be found in page 14 of the Supporting Information).[36] Briefly, 200 µL of ASM was spiked with *M. smegmatis* at concentrations typical for infected individuals ($2.99\times10^7$ cfu $mL^{-1}$).[28] Figure 4A shows a representative example of ASM with spiked mycobacterial cells. The cells were chemically lysed and their DNA extracted using PIL-based SPME. Following HNB-IMSA, results showed that all (9/9) reactions tested positive, indicating that genomic DNA of sufficient quantity and quality was extracted from the mycobacteria to yield positive visual identification with HNB-IMSA.

The developed PIL-SPME method was then compared with TE boiling and SPE methods for the extraction of mycobacterial DNA from artificial sputum samples.[37] A comparison of the methodologies is shown in Table S3. All three methods were tested at the same concentration ($2.99\times10^7$ cfu $mL^{-1}$) of *M. smegmatis* cells in ASM. The TE boiling method is simpler and requires fewer steps than the SPE kit. However, multiple centrifugation steps are required in both cases, rendering these methods incompatible at the POC or in resource limited settings. The PIL-SPME

method is rapid and does not require sophisticated equipment. For all of the extractions performed with the SPME device, all (9/9) reactions indicated a positive result. It is also important to note that all three methods are compatible with HNB-IMSA demonstrating the compatibility of this INAA technology with a variety of sample preparation methods. The DNA extracted by the SPE kit could also be detected using a traditional qPCR-based method which amplified a region in the 16S rRNA gene giving Cq values of $17.63 \pm .79$. While detection was easily achieved using qPCR, the technique requires expensive and sophisticated equipment that is not compatible with POC applications.

## Conclusion

In summary, a rapid method based on PIL-SPME capable extracting genomic DNA from mycobacteria in ASM was developed. This method was seamlessly interfaced with HNB-IMSA to afford visual detection of the extracted nucleic acid by developing a compatible reaction buffer. The method was capable of extracting and detecting mycobacterial genomic DNA from the crude lysate of mycobacteria at concentrations as low as $2.99\times10^5$ cfu $mL^{-1}$. Moreover, extraction of DNA was also possible from clinically relevant concentrations of mycobacteria in ASM, demonstrating its incredible promise for use in POC applications.

## Acknowledgments

The authors acknowledge funding from Chemical Measurement and Imaging Program at the National Science Foundation (Grant Number CHE-1709372).

## Supporting Information

Calibration curve, IMSA primer design, representative cycling amplification, qPCR plots, chemical structure of the PIL sorbent coating, effect of vortex speed, sorption−time profile, effects of NaCl and Mg2+, sequences of IMSA primers, comparison of different sample preparation

methods, and additional experimental details can be found in Appendix A: Supporting Information

Chapter 2

## References


(1) Caliendo, A. M.; Gilbert, D. N.; Ginocchio, C. C.; Hanson, K. E.; May, L.; Quinn, T. C.; Tenover, F. C.; Alland, D.; Blaschke, A. J.; Bonomo, R. A.; Carroll, K. C.; Ferraro, M. J.; Hirschhorn, L. R.; Joseph, W. P.; Karchmer, T.; MacIntyre, A. T.; Reller, L. B.; Jackson, A. F. *Clin. Infect. Dis.* **2013**, *57*, S139–S170.

(2) Magliulo, M.; Simoni, P.; Guardigli, M.; Michelini, E.; Luciani, M.; Lelli, R.; Roda, A. *J. Agric. Food Chem.* **2007**, *55*, 4933–4939.

(3) Tok, J. B.-H.; Chuang, F. Y. S.; Kao, M. C.; Rose, K. A.; Pannu, S. S.; Sha, M. Y.; Chakarova, G.; Penn, S. G.; Dougherty, G. M. *Angew. Chemie Int. Ed.* **2006**, *45*, 6900–6904.

(4) Belgrader, P.; Benett, W.; Hadley, D.; Long, G.; Mariella, R.; Milanovich, F.; Nasarabadi, S.; Nelson, W.; Richards, J.; Stratton, P. *Clin. Chem.* **1998**, *44*, 2191–2194.

(5) Bühlmann, A.; Pothier, J. F.; Rezzonico, F.; Smits, T. H. M.; Andreou, M.; Boonham, N.; Duffy, B.; Frey, J. E. *J. Microbiol. Methods* **2013**, *92*, 332–339.

(6) Roberts, G. D.; Goodman, N. L.; Heifets, L.; Larsh, H. W.; Lindner, T. H.; Mcclatchy, J. K.; Mcginnis, M. R.; Siddiqi, S. H.; Wright, P. *J. Clin. Microbiol.* **1983**, *18*, 689–696.

(7) Drain, P. K.; Hyle, E. P.; Noubary, F.; Freedberg, K. A.; Wilson, D.; Bishai, W. R.; Rodriguez, W.; Bassett, I. V. *Lancet Infect. Dis.* **2014**, *14*, 239–249.

(8) Traggiai, E.; Becker, S.; Subbarao, K.; Kolesnikova, L.; Uematsu, Y.; Gismondo, M. R.; Murphy, B. R.; Rappuoli, R.; Lanzavecchia, A. *Nat. Med.* **2004**, *10*, 871–875.

(9) Malorny, B.; Tassios, P. T.; Rådström, P.; Cook, N.; Wagner, M.; Hoorfar, J. *Int. J. Food Microbiol.* **2003**, *83*, 39–48.

(10) Morozumi, M.; Nakayama, E.; Iwata, S.; Aoki, Y.; Hasegawa, K.; Kobayashi, R.; Chiba, N.; Tajima, T.; Ubukata, K.; Group, the A. R. D. S. *J. Clin. Microbiol.* **2006**, *44*, 1440–1446.

(11) Notomi, T.; Okayama, H.; Masubuchi, H.; Yonekawa, T.; Watanabe, K.; Amino, N.; Hase, T. *Nucleic Acids Res.* **2000**, *28*, E63.

(12) Ding, X.; Nie, K.; Shi, L.; Zhang, Y.; Guan, L.; Zhang, D.; Qi, S.; Ma, X. *J. Clin. Microbiol.* **2014**, *52*, 1862–1870.

(13) Piepenburg, O.; Williams, C. H.; Stemple, D. L.; Armes, N. A. *PLoS Biol.* **2006**, *4*, e204.

(14) Schoch, J.; Wiessler, M.; Jäschke, A. *J. Am. Chem. Soc.* **2010**, *132*, 8846–8847.

(15) Patel, R.; Kvach, J. T.; Mounts, P. *J. Gen. Microbiol.* **1986**, *132*, 541–551.

(16) Boom, R.; Sol, C. J. A.; Salimans, M. M. M.; Jancen, C. L.; Wertheim-van-Dillen, P. M. E.; J, V. der N. *J Clin Microbiol* **1990**, *28*, 495–503.

(17) Wen, J.; Legendre, L. A.; Bienvenue, J. M.; Landers, J. P. *Anal. Chem.* **2008**, *80*, 6472–6479.

(18) Arthur, C. L.; Pawliszyn, J. *Anal. Chem.* **1990**, *62*, 2145–2148.

(19) Cagliero, C.; Ho, T. D.; Zhang, C.; Bicchi, C.; Anderson, J. L. *J. Chromatogr. A* **2016**, *1449*, 2–7.

(20) Tascon, M.; Gómez-Ríos, G. A.; Reyes-Garcés, N.; Poole, J.; Boyacı, E.; Pawliszyn, J. *J. Pharm. Biomed. Anal.* **2017**, *144*, 106–111.

(21) Vas, G.; Vékey, K. *J. Mass Spectrom.* **2004**, *39*, 233–254.

(22) Nacham, O.; Clark, K. D.; Anderson, J. L. *Anal. Chem.* **2016**, *88*, 7813–7820.

(23) Nacham, O.; Clark, K. D.; Varona, M.; Anderson, J. L. *Anal. Chem.* **2017**, *89*, 10661–10666.

(24) Wang, X.; Xing, L.; Shu, Y.; Chen, X.; Wang, J. *Anal. Chim. Acta* **2014**, *837*, 64–69.

(25) Pandey, P.; Pant, N. D.; Rijal, K. R.; Shrestha, B.; Kattel, S.; Banjara, M. R.; Maharjan, B.; Rajendra, K. C. *PLoS One* **2017** DOI:10.1371/journal.pone.0169798

(26) Piatek, A. S.; Van Cleeff, M.; Alexander, H.; Coggin, W. L.; Rehr, M.; Van Kampen, S.; Shinnick, T. M.; Mukadi, Y. *Glob. Heal. Sci. Pract.* **2013**, *1*, 18–23.

(27) García-Basteiro, A. L.; DiNardo, A.; Saavedra, B.; Silva, D. R.; Palmero, D.; Gegia, M.; Migliori, G. B.; Duarte, R.; Mambuque, E.; Centis, R.; Cuevas, L. E.; Izco, S.; Theron, G. *Pulmonology* **2018**, *24*, 73–85.

(28) Kelley, S. O. *ACS Sensors* **2017**, *2*, 193–197.

(29) Huggett, J. F.; Foy, C. A.; Benes, V.; Emslie, K.; Garson, J. A.; Haynes, R.; Hellemans, J.; Kubista, M.; Mueller, R. D.; Nolan, T.; Pfaffl, M. W.; Shipley, G. L.; Vandesompele, J.; Wittwer, C. T.; Bustin, S. A. *Clin. Chem.* **2013**, *59*, 892–902.

(30) Ho, T. D.; Yu, H.; Cole, W. T. S.; Anderson, J. L. *Anal. Chem.* **2012**, *84*, 9520–9528.

(31) Chen, L.; Yang, G.; Zhang, J. *React. Funct. Polym.* **1996**, *29*, 139–144.

(32) Gaillard, C.; Strauss, F. *Tech. Tips Online* **1998**, *3*, 63–65.

(33) Goto, M.; Honda, E.; Ogura, A.; Nomoto, A.; Hanaki, K. I. *Biotechniques* **2009**, *46*, 167–172.

(34) Niemz, A.; Ferguson, T. M.; Boyle, D. S. *Trends Biotechnol.* **2011**, *29*, 240–250.

(35) Ding, X.; Wu, W.; Zhu, Q.; Zhang, T.; Jin, W.; Mu, Y. *Anal. Chem.* **2015**, *87*, 10306–10314.

(36) Diraviam Dinesh, S. *Protoc. Exch.* **2010** DOI:10.1038/protex.2010.212

(37) Aldous, W. K.; Pounder, J. I.; Cloud, J. L.; Woods, G. L. *J. Clin. Microbiol.* **2005**, *43*, 2471–2473.

## Appendix A: Supporting Information Chapter 2

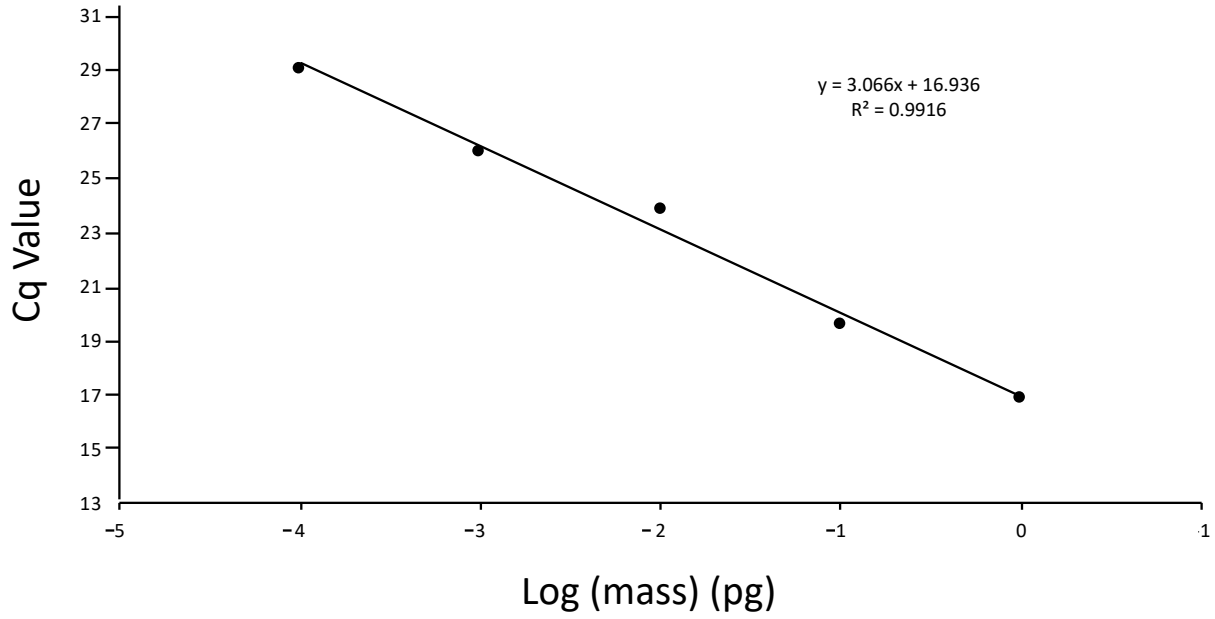


**Figure S1.** A five point calibration curve developed to quantify the amount of DNA extracted during method development.

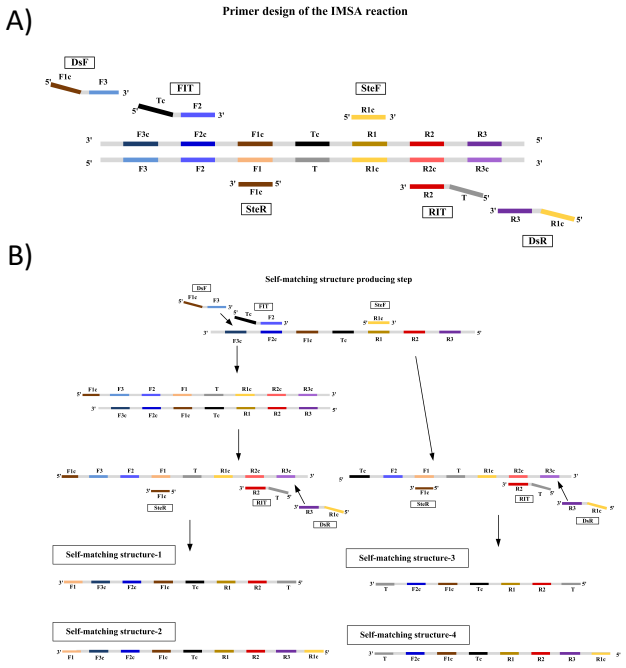


**Figure S2.** IMSA primer design and self-matching structure producing step. A) Illustrates the various primers that are used in the reaction as well their target binding regions. B) The formation of the 4 self-matching structures that will enable the exponential amplification.

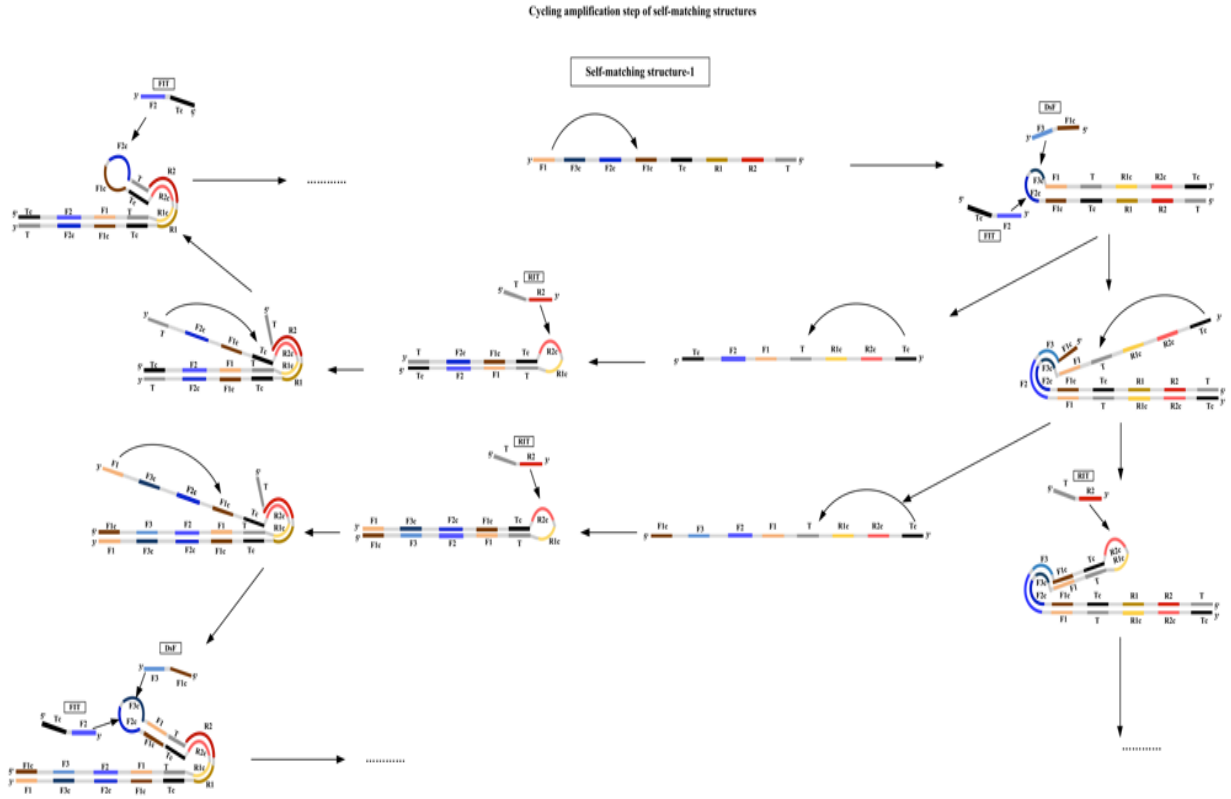


**Figure S3.** Representative cycling amplification of one of the self-matching structures in IMSA. The other 3 self-matching structures amplify in a similar manner.

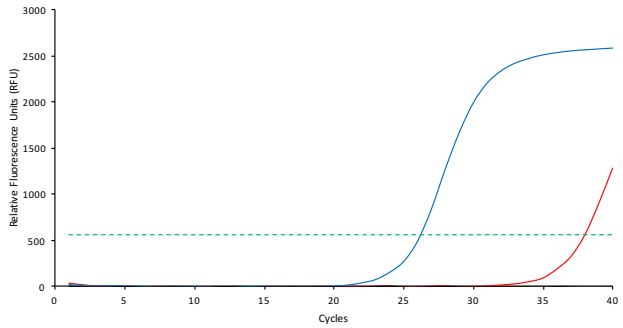


**Figure S4.** Representative qPCR plots of the desorption solution after extraction (blue) and following a 30 min wash (red) with 2 M NaCl. The washing step of the fiber shows negligible carryover (Cq = 38).

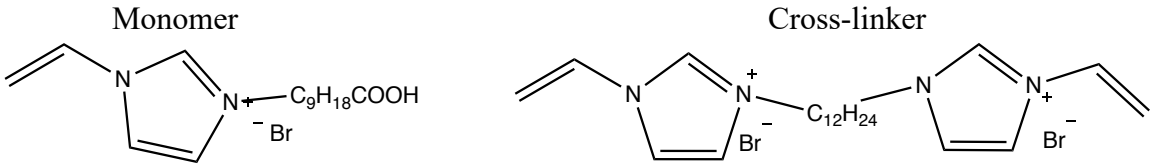


**Figure S5.** Chemical structure of the PIL sorbent coating used in this study. The fiber was prepared using 50% by weight of IL cross-linker with respect to the weight of the IL monomer.

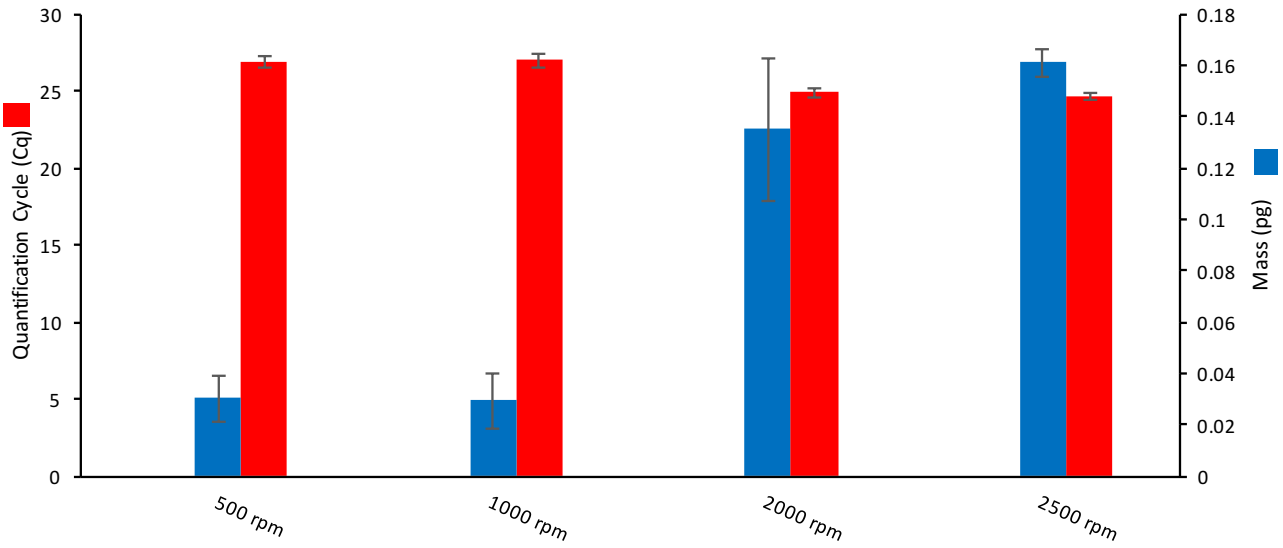


**Figure S6.** The effect of vortex speed on the extraction of a 280 bp fragment from a 10 pg mL-1 solution. Vortex speeds evaluated ranged from 500-2500 rpm. Extraction volume: 1.5 mL, pH 8 TE buffer. Extraction time: 2 minutes; desorption time: 30 min; desorption solvent: 1 M NaCl; desorption solvent volume: 10 µL. Mass of DNA is denoted in blue (■) while Cq values are indicated in red (■)

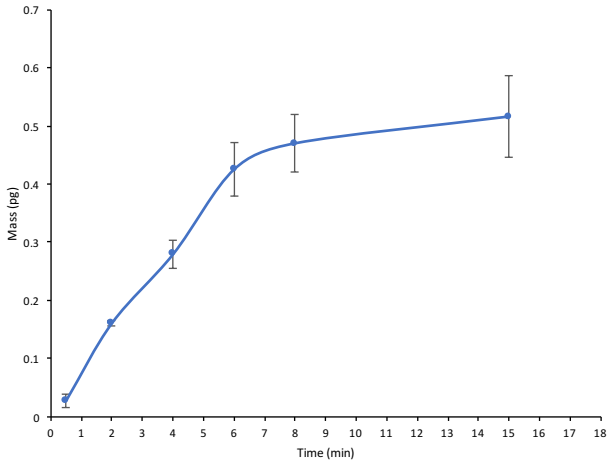


**Figure S7.** Sorption-time profile illustrating the effects of extraction time on the amount of a 280 bp fragment (10 pg/mL) extracted. Extraction volume: 1.5 mL, pH 8 TE buffer. Extraction time: 0.5, 2, 4, 6 min with vortex (2500 rpm); desorption time: 30 min; desorption solvent: 1 M NaCl; desorption solvent volume: 10 μL.

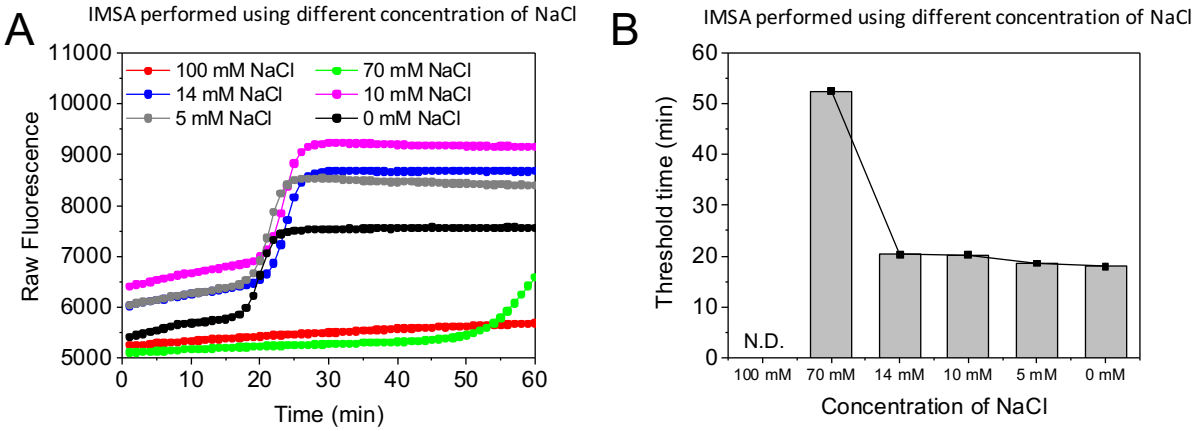


**Figure S8.** Investigation of the effects of NaCl concentration on IMSA. (A) Real-time fluorescence; (B) Comparison of threshold time. Template: 3.17×105 cps of a pCR®2.1 plasmid inserted with HBV S protein gene sequence. Reaction time: 60 min. Reaction temperature: 63ºC. N.D.: not detected.

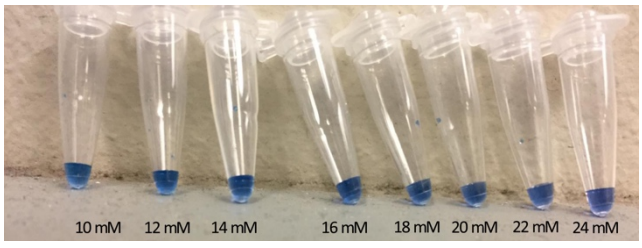


**Figure S9.** Effect of Mg2+ on the initial color of the HNB-IMSA reaction. NEBuffer 3 was used along with HNB, DNTPs, and supplemented with various amounts of Mg2+

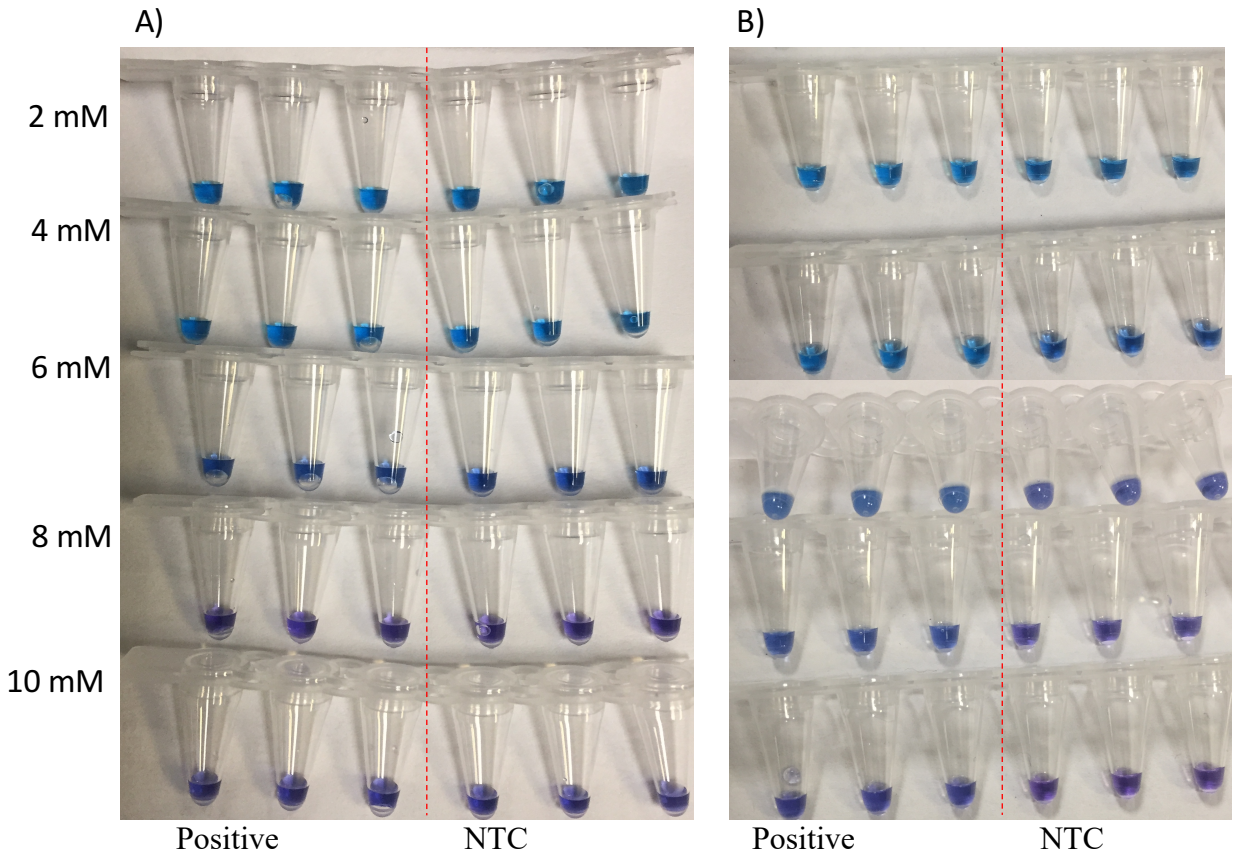


**Figure S10.** The color change of the HNB-IMSA reaction is tested before and after amplification with varying concentration of Mg2+. The visual appearance of HNB-IMSA reactions with varying concentrations of Mg2+ prior to amplification is shown in (A) while (B) shows the color change achieved after 100 pg of M. smegmatis DNA is amplified. Triplicate reactions were performed for each Mg2+ concentration along with three NTCs.

**Table S1.** Sequences of IMSA primers for the amplification of a region of the 16S rRNA gene in the Mycobacterium smegmatis genome

| Description | Sequence 5'-3' |
|---|---|
| DsF IMSA primer | GCAGTCTCTCACGAGTCCCGCGCAACCCTTGTCTCAT |
| DsR IMA primer | ACGTCAAGTCATCATGCCCCTTAGATTCGCTCCACCTCACG |
| FIT IMSA primer | TCCCCACCTTCCTCCGAGT-GTTGCCAGCACGTTATGGT |
| RIT IMSA primer | ACTCGGAGGAAGGTGGGGA-TGTACCGGCCATTGTAGCA |
| SteF IMSA primer | ACGTCAAGTCATCATGCCCCTTA |
| SteR IMSA primer | GCAGTCTCTCACGAGTCCC |

**Table S2.** Comparison of different sample preparation methods for the extraction of mycobacterial DNA from artificial sputum medium.

| Method | Workflow | Total extraction time (min) | Compatible with direct sputum sampling | HNB-IMSA compatible | Reusability |
|---|---|---|---|---|---|
| PIL-SPME | 1) Chemical Lysis<br>2) Vortex SPME<br>3) Desorption | 45 | yes | yes | ~50 extractions [a] |
| TE boiling | 1) Centrifugation<br>2) Add TE Buffer, boiling step<br>3) Centrifugation | 35 | no | yes | Not Applicable |
| SPE kit | 1) Centrifugation<br>2) Incubation with lysozyme<br>3) Incubation with lysis buffer and proteinase K<br>4) Boiling step<br>5) Addition of ethanol, centrifugation<br>6) Mixture is applied to spin column followed by centrifugation<br>7) 2 washing steps with centrifugation<br>8) Elution with centrifugation of the DNA | >120 | no | yes | Not recommended |

a From aqueous samples, cell lysate, and ASM

**Materials**

7H9 and 7H10 broth base and agar were obtained from Sigma-Aldrich (St. Louis, MO, USA). Electrophoresis grade BSA, diethylene triamine pentaacetic acid, cycloheximide, Tris Base, dextrose, and Tween 80 were acquired from P212121 (Yipsilanti, MI, USA). Mucin from porcine stomach and salmon testes DNA was acquired from Sigma-Aldrich. KCl and NaCl were obtained from Fisher Scientific (Waltham, MA, USA). Casamino Acids were purchased from Difco (Detroit, MI, USA). Carbenicillin was obtained from Goldbio (Olivette, MO, USA). Deionized water (18.2 MΩ cm) used for all solutions was obtained from a Milli-Q water purification system (Millipore, Bedford, MA, USA). DNA LoBind polypropylene microcentrifuge tubes were purchased from Eppendorf (Hamburg, Germany). IMSA primer design was done using the free PrimerExplorer software. Proteinase K, Guanidinium hydrochloride and Tween 20 were purchased from Sigma-Aldrich. Hydroxy Napthol Blue (HNB) was acquired from Millipore (Billerica, MA, USA).

**Surface area determination of desorption container**

By treating the desorption container as a cone, the surface area of the container that was in contact with each of the desorption solutions was calculated using equation 2:

$$Surface\ Area = \pi r\sqrt{h^2 + r^2} \quad (2)$$

Both the height (h) and radius (r) of the desorption container are needed for the calculation. The calculated surface areas were 2.45 cm2, 1.63 cm2, and 0.67 cm2 for 50, 30, and 10 µL of desorption solution, respectively.

**Lysis Conditions**

All cell lyses prior to extraction using PIL-SPME were performed as follows: 20 µL of 20 mg mL-1 Proteinase K was added to the bottom of a centrifuge tube. 200 µL of the sample was subsequently added to the Proteinase K and mixed thoroughly. After mixing, 200 µL of the lysis buffer (3M Guanadine Hydrochloride, 20% Tween 20) was added to the mixture and quickly pulse-vortexed for 15 seconds. The tubes were then incubated at 56 °C for 10 minutes.

**Preparation of Artificial Sputum Matrix**

Briefly, 5 g of mucin, 4 g Salmon testes DNA, 5.9 mg of diethylene triamine pentaacetic acid, 5 g NaCl, 2.2 g of KCl, and 1.81 g of Tris-base are added to 800 mL of water in a beaker and stirred. Once dissolved, 5 g of Casamino acids are added to the mixture. Subsequently, the pH is adjusted to 7.0 and the volume is brought up to 1000 mL. The solution is autoclaved and afterwards 5 mL of egg yolk emulsion is added to the mixture

# CHAPTER 3. VISUAL DETECTION OF SINGLE-NUCLEOTIDE POLYMORPHISMS USING MOLECULAR BEACON LOOP-MEDIATED ISOTHERMAL AMPLIFICATION WITH CENTRIFUGE-FREE DNA EXTRACTION

Reprinted with permission from *Analytical Chemistry* 2019, 91, 11, 6991-6995



Marcelino Varona, and Jared L. Anderson

## Abstract

Loop-mediated isothermal amplification (LAMP) is a powerful nucleic acid amplification technique due to its rapid and sensitive nature. These characteristics, in addition to low-cost and robustness, make LAMP an attractive alternative to polymerase chain reaction for point-of-care applications. However, sequence-specific detection remains a formidable challenge, particularly when single-nucleotide resolution is required. In this study, a LAMP method is developed for facile visual detection of single-nucleotide polymorphisms (SNPs) using molecular beacons (MBs) by exploiting the dual-fluorescence of fluorescein (6-FAM) and hydoxynaphthol blue (HNB). The method is coupled with solid-phase microextraction (SPME) to facilitate rapid extraction and detection of the target sequence. This work expands the use of MBs in LAMP for the visual detection of SNPs and facilitates the development of future LAMP assays for a wide-range of targets.

## Results and Discussion

Nucleic acid amplification techniques are some of the most useful and widely employed in the biological and biomedical fields. Quantitative polymerase chain reaction (qPCR) is an established amplification method that has been extensively used for pathogen identification,[1] gene expression analysis,[2] and genotyping.[3] A qPCR instrument is composed of a thermal cycler, which accurately controls the temperature of the reaction containers, and an optical module to measure

fluorescence. However, these requirements preclude the facile implementation of this technique in resource-limited settings for point-of-care (POC) applications.[4]

Isothermal nucleic acid amplification (INAA) techniques have been developed to overcome some of the limitations posed by traditional methods.[5] Loop-mediated isothermal amplification (LAMP) is a popular INAA technique that relies on 4-6 primers for the amplification of a target sequence.[6] Since it is performed at a constant temperature and can be easily coupled with colorimetric detection, it is ideally-suited for use at the POC.[7] One significant drawback to traditional visual detection methods for LAMP is the inability to detect specific amplicons. SYBR Green I is a DNA binding dye that fluoresces strongly in the presence of any double-stranded DNA that is produced, meaning spurious amplification is indistinguishable from specific amplification.[8] Hydroxynapthol blue (HNB)[9] and Calcein[10] have also been used to visually distinguish between negative and positive reactions. More specifically, when HNB is present in the reaction solution prior to amplification the dye chelates excess $Mg^{2+}$ in the solution and produces a violet color change. During the amplification process, insoluble magnesium pyrophosphate is formed[11] which removes free $Mg^{2+}$ from solution and changes the appearance of HNB in solution from violet to sky-blue.[9] However, these metal indicators only monitor the presence of $Mg^{2+}$ in the reaction system and cannot provide direct evidence of specific amplification. Furthermore, certain clinically-relevant applications require single-nucleotide resolution for accurate identification of drug resistant microorganisms[12] and cancer diagnoses.[13] While careful primer design can be used to mitigate non-specific amplification, it does not negate the indirect nature of traditional colorimetric methods.

Strand displacement probes have been successfully used for sequence-specific detection of LAMP amplicons and single-nucleotide polymorphisms (SNPs) using real-time detection.[14,15]

Similarly, molecular beacon (MB) probes were recently shown to be effective in the real-time detection of LAMP amplification;[16] however, their ability to discriminate SNPs has not been demonstrated. While the aforementioned methods have been shown with real-time detection, they require further study and modification for use at the POC. The ideal LAMP detection method for POC applications should be capable of detecting specific amplification sequences, possess single-nucleotide resolution, and produce results that can be easily visualized and interpreted. Herein, we demonstrate a MB-LAMP method that exploits the fluorescence of HNB and fluorescein (FAM) to achieve single-nucleotide differentiation that can be identified visually with a transilluminator. Furthermore, we demonstrate the use of a SPME method for rapid, centrifuge-free isolation of DNA in less than 5 minutes and subsequent visual detection.

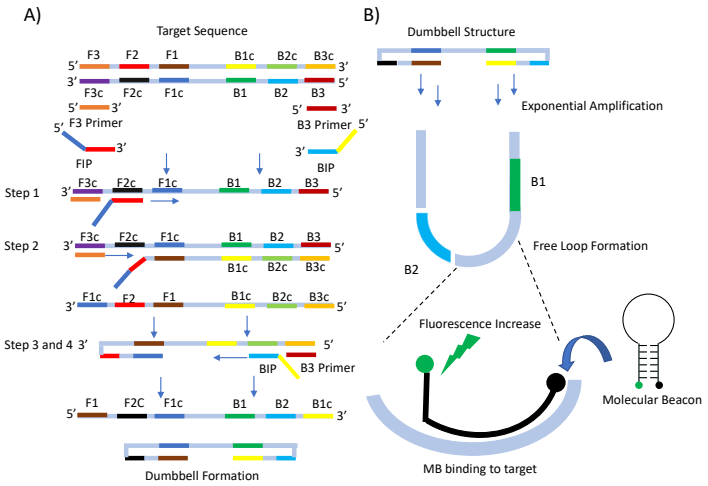


**Figure 1.** A) General loop-mediated isothermal amplification (LAMP) schematic of the amplification process up to the formation of the self-matching dumbbell structure as well as illustration of primers and primer-binding sites. B) Schematic demonstrating the binding of the molecular beacon to the loop region between the B1 and B2 regions of the target.

Figure 1A and 1B show a general schematic of the LAMP amplification process and the detection using a MB probe, respectively. During MB-LAMP, single-stranded loops are generated between the B1 and B2 regions of the target. A real-time calibration curve was performed with the MB-LAMP method previously developed by Liu et al. and used as a comparison for subsequent

experiments.[16] Figure S1 shows the method can detect down to $2.38\times10^2$ copies of the target, which is consistent with previous results.

To develop a visual detection method compatible with MB-LAMP, the addition of HNB was investigated. HNB has previously been coupled with SYBR Green I[17] and FAM[18] to develop a system that exploits the fluorescence of both dyes for easy visual identification of amplified targets. Since the MB used in this study utilizes FAM as the fluorophore, it was hypothesized that a similar system could be developed. Several samples with HNB concentrations ranging from 120 to 360 µM were tested and the amplification measured in real-time. Figure S2A shows a decrease in the threshold times when HNB is added to the reaction. Threshold times ($T_t$) are the real-time LAMP equivalents of quantification cycle ($C_q$) values in qPCR and indicate when the observed fluorescence is appreciably higher than the background. They are useful for assessing effects of changing reaction conditions on the amplification of the target. Increasing threshold times are an indication of inhibition of the reaction system.[19] The obtained maximum relative fluorescence units (RFUs) decreased significantly with the addition of more HNB, a four-fold difference in RFUs is observed from 0 µM to 360 µM (Figure S2B). The effect of HNB concentration on the visual identification of the reaction products was subsequently studied. Three positive reactions and three no template controls (NTC) were incubated for one hour at 63 °C and the reaction containers subsequently visualized with a transilluminator. Shown in Figure S3, as the concentration of HNB is increased, the appearance of green fluorescence in the positive reaction containers was reduced. Conversely, red fluorescence derived from the NTC appeared to increase with the addition of more HNB.

To investigate the source for the change in visual appearance, fluorescence spectra of the reactions were obtained by exciting at 470 nm and recording fluorescence using a 10 nm step size,

as shown in Figure S4. Maximum fluorescence was observed at 520 nm for the positive reactions while the negative reactions exhibited a broad peak starting at 600 nm. Endpoint measurements were subsequently taken by recording emission spectra at 520 nm and 660 nm with excitation at 470 nm. As shown in Figure S5, the fluorescence observed at 520 nm remains constant for both the positive and negative reactions. However, the fluorescence obtained at 660 nm from the negative reaction increased noticeably as higher concentrations of HNB were used. This indicates that the concentration of HNB directly influenced the intensity of the red-light emission derived from the NTC, as determined by fluorescence measurements. On the other hand, the visual appearance of the positive reactions appear to change with increasing HNB concentration. However, the fluorescence at 520 nm remains constant regardless of how much HNB was added. Therefore, 240 µM was chosen for subsequent experiments as it provided the most clear and visually apparent fluorescence for both the positive control and NTC. A calibration curve using the method with 240 µM HNB was performed and is shown in Figure S6. The detection limit of this system ($2.38\times 10^2$) is identical to the reaction system without HNB.

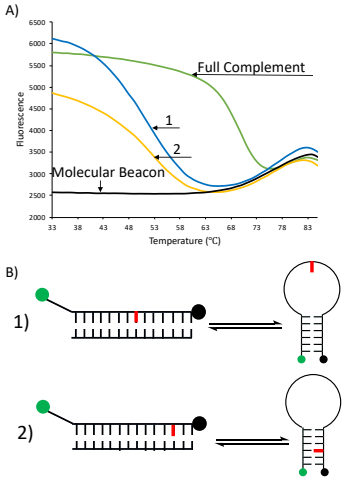


**Figure 2.** A) Real-time results of the performed molecular beacon annealing profiles. B) Representative illustration of the single nucleotide polymorphism (SNP) location within the sequences tested. The green circle represents the fluorophore while the black circle represents the quencher.

Molecular beacons are able to detect single-nucleotide mismatches due to their unique structure.[20] The various conformations of a MB are illustrated in Figure S7A. When a target is present, the molecular beacon will unfold from its hairpin structure to bind the target, resulting in separation of the fluorophore-quencher pair and an increase in fluorescence. If mismatches are present in the sequence, binding will not occur until the temperature is sufficiently reduced, allowing differentiation of mismatched sequences if the appropriate conditions are chosen. Since MBs have not been previously employed in LAMP assays for SNP detection, it was necessary to investigate the effect of the SNP location on MB binding. As illustrated in Figure S7A, the 3' end of the MB stem used in this study binds to the target. Therefore, it was necessary to ascertain whether the MB could discriminate single-nucleotide differences occurring in the stem and/or loop binding region. Annealing profiles were performed to determine the stability of MB binding to different mismatched sequences. The sequences studied are shown in Table S1. In this approach, the temperature is slowly reduced at a rate of 1 °C $min^{-1}$ and fluorescence recorded after each minute.[20,21] Two different mismatched sequences were tested and a schematic representation of the location of these can be seen in Figure S7B. From the results shown in Figure 2, it was observed that the MB did not produce a stable duplex with sequences containing a mismatch in the loop or stem structure. In contrast, the stability of the MB-target duplex was much higher. The mismatched structures are not stable at elevated temperatures; therefore, a fluorescence increase cannot be observed until the temperature is below 58 °C. Conversely, the MB binds with a higher stability to its complementary sequence enabling fluorescence at higher temperatures (65°C).

To determine whether or not discrimination of mismatched sequences was possible using MB-LAMP, amplification was performed with a sequence containing a single-nucleotide difference in the loop binding region of the MB. The mismatched sequence can be found in Table

S1. The SNP was placed in the same location as the mismatch used for the annealing profile experiments described previously. Figure S8 shows the real-time results indicating a significantly reduced fluorescence signal from the SNP-containing target. An 850 RFU difference is observed in the qPCR plots between the maximum fluorescence from the target and the SNP. When the reaction containers were visualized with a transilluminator, there was a clear and unambiguous difference in the appearance of the target and mismatched sequence, as shown in Figure 3 Furthermore, due to HNB in the reaction, a color-change from purple to light blue using natural light could be observed between the positive and negative reactions (Figure 3). This has potential to be exploited in the future development of a visual, multiplexed detection system by employing natural light and a transilluminator to differentiate between amplification products.

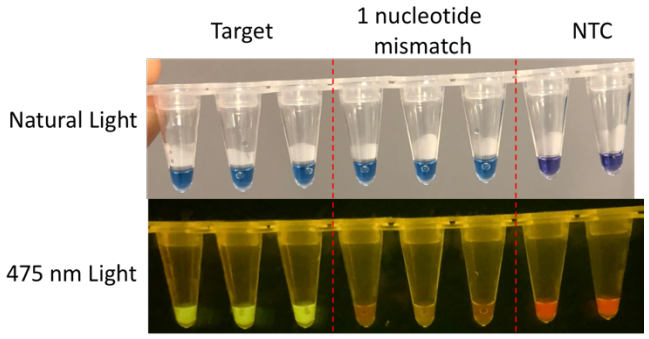


**Figure 3.** MB-LAMP reaction containers following amplification for 60 min at 63 °C as visualized under natural light or 475 nm light. For the assays containing the target and mismatched sequence, 1.0 pg of DNA was used.

In order to improve discrimination of the target from the mismatched products, the effect of different reaction temperatures on the resulting fluorescence was examined. Six reactions containing the mismatched sequences were carried out at 63 °C, 64 °C, and 65 °C, along with three positive reactions containing the target. After incubating for one hour at the aforementioned temperatures, the fluorescence at 520 nm was recorded. Results shown in Figure S9 indicate a slight decrease in the fluorescence of the positive reaction at a reaction temperature of 65 °C. A

more noticeable difference was observed in the reactions containing the SNP, as there was a significant change in the fluorescence signal as the temperature is increased. This was highlighted by nearly a two-fold decrease in the fluorescence intensity observed from 63 °C to 65 °C. The difference between the two temperatures can be attributed to the destabilization of the MB-mismatch complex, as increased temperature reduces non-specific binding, leading to a total decrease in the fluorescence output.[22]

Certain applications requiring single-nucleotide resolution involve the detection of low quantities of the desired sequence within a large excess of the wild type sequence. To test the ability of the MB-LAMP method in the detection of the target sequence in the presence of interfering DNA, a series of reactions were performed in which the ratio of target DNA to non-target DNA containing the SNP was varied. Reactions were performed at 65 °C and the fluorescence was monitored in real-time. Furthermore, the reaction containers were visualized after amplification under a transilluminator to verify that results could be visually interpreted. Results shown in Figure S8 demonstrate that the method is capable of detecting the target when it comprises 1% of the total mass of nucleic acid present, where 99% is the mismatched sequence.

In addition to the detection method, POC applications also require robust sample preparation techniques for the isolation of nucleic acids from complex samples. We have previously developed a rapid SPME method using polymeric ionic liquid sorbents for the extraction of DNA from complex samples.[23] An overview of the method can be seen in Figure 4A. One drawback to this method was the long desorption time (30 min) compared to the 2 min extraction time. To improve the overall speed of the method, different desorption containers were explored. By using a small vial featuring an insert, desorption into 50 µL NaCl could be achieved in just 2 min by using vortex agitation. Results shown in Figure 4B demonstrate that comparable

recoveries of the target DNA are observed when using 2 min vortex for the recovery in comparison to a 30 min static desorption step. Conversely, when a 2 min static desorption is performed nearly half as much DNA is recovered versus using vortex for 2 min (0.51 pg and 0.93 pg).

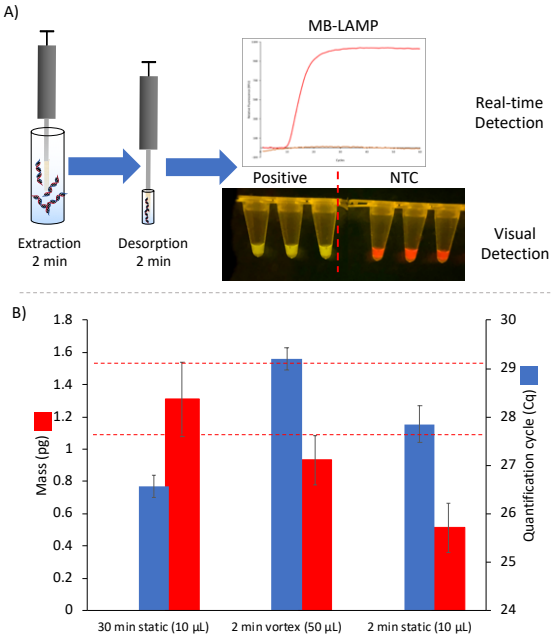


**Figure 4.** A) Representative schematic of a SPME-based extraction from a cell lysate with real-time and visual MB-LAMP detection. B) Comparison of desorption conditions following a 2 min SPME-DNA extraction. All extractions were performed in triplicate from a 84 pg $mL^{-1}$ solution of DNA: total volume, 1.5 mL, 2 mM TE buffer pH 8; extraction time, 2 min with vortex (2500 rpm); desorption solvent, 1 M NaCl.

The compatibility of the extraction method to MB-LAMP was subsequently explored. As illustrated in Figure S10, the method was not tolerant to high concentrations of the desorption solution as evidenced by the increase in threshold times when more NaCl is added to the LAMP reaction. This would require a 10-fold dilution of the desorption solution. To circumvent this, a previously optimized isothermal reaction buffer compatible with 1 M NaCl was tested.[23] Inhibition caused by the NaCl was negated using this buffer allowing for direct interfacing of the SPME desorption solution to the isothermal reaction, thereby eliminating the need for dilution. In order to demonstrate the practical applicability of the method, extractions were performed from a cell

lysate prepared from *Escherichia coli* K–12 cells containing a plasmid with the sequence of interest. Detailed culture, lysis and extraction conditions can be found in the ESI. After performing extractions from cellular suspensions of $10^6$ colony forming units $mL^{-1}$, sufficient DNA was recovered for easy visualization with MB-LAMP. Triplicate extractions were performed to verify the reproducibility of the method. A representative image of the results from one extraction can be seen in Figure 4A. Three positive reactions and 3 NTCs were performed for each extraction.

To determine whether or not SNP discrimination could be possible following SPME-based extraction, annealing profiles were performed in the custom buffer and compared to the annealing profiles previously performed in the traditional Isothermal Buffer. As observed in Figure S11, the annealing profiles are virtually identical when performed in either buffers. This indicates that the specificity of the MB-LAMP method remains when coupled to SPME-based extraction.

The developed method provides a foundation for further development of MB-LAMP for POC applications. Through coupling MB-LAMP to SPME-based sample preparation, a rapid and "user-friendly" method for visually identifying specific amplification products was established. This MB-LAMP method can be readily applied in applications requiring single-nucleotide specificity for diagnostic applications. Future work will focus on expanding the use of SPME as a sample preparation tool with MB-LAMP analysis for cancer diagnostics and drug resistance in pathogens. We also aim to develop sequence-selective methods compatible with MB-LAMP for more sensitive analysis of low-abundance sequences.

**Acknowledgements**

The authors acknowledge funding from the Chemical Measurement and Imaging Program at the National Science Foundation (Grant No. CHE-1709372)

## Supporting Information

Reagents and instrumentation, cell culture conditions, cell lysate extraction conditions, all oligonucleotide and target sequences used, LAMP calibration curves, HNB optimization including real-time plots, fluorescent measurements, and emission spectra, molecular beacon conformations, target/mismatch representative real-time plots, temperature optimization, NaCl effects on LAMP, annealing profiles in custom and Isothermal Buffer can be found in Appendix B: Supporting Information Chapter 3

## References


(1) Postollec, F.; Falentin, H.; Pavan, S.; Combrisson, J.; Sohier, D. *Food Microbiol.* **2011**, *28* (5), 848–861.

(2) Derveaux, S.; Vandesompele, J.; Hellemans, J. *Methods* **2010**, *50* (4), 227–230.

(3) Lefever, S.; Rihani, A.; Van der Meulen, J.; Pattyn, F.; Van Maerken, T.; Van Dorpe, J.; Hellemans, J.; Vandesompele, J. *Sci. Rep.* **2019**, *9* (1), 2150.

(4) St John, A.; Price, C. P. *Clin. Biochem. Rev.* **2014**, *35* (3), 155–167.

(5) Zhao, Y.; Chen, F.; Li, Q.; Wang, L.; Fan, C. *Chem. Rev.* **2015**, *115* (22), 12491–12545.

(6) Notomi, T.; Okayama, H.; Masubuchi, H.; Yonekawa, T.; Watanabe, K.; Amino, N.; Hase, T. *Nucleic Acids Res.* **2000**, *28* (12), E63.

(7) Xie, S.; Yuan, Y.; Song, Y.; Zhuo, Y.; Li, T.; Chai, Y.; Yuan, R. *Chem. Commun.* **2014**, *50* (100), 15932–15935.

(8) Njiru, Z. K.; Mikosza, A. S. J.; Armstrong, T.; Enyaru, J. C.; Ndung'u, J. M.; Thompson, A. R. C. *PLoS Negl. Trop. Dis.* **2008**, *2* (2), e147.

(9) Goto, M.; Honda, E.; Ogura, A.; Nomoto, A.; Hanaki, K. I. *Biotechniques* **2009**, *46* (3), 167–172.

(10) Xu, G.; Zhao, H.; Cooper, J. M.; Reboud, J. *Chem. Commun.* **2016**, *52* (82), 12187–12190.

(11) Mori, Y.; Kitao, M.; Tomita, N.; Notomi, T. *J. Biochem. Biophys. Methods* **2004**, *59* (2), 145–157.

(12) Sayyed, D. R.; Nimse, S. B.; Song, K. S.; Kim, T. *Chem. Commun.* **2014**, *50* (82), 12344–12347.

(13) Flaherty, K. T.; Puzanov, I.; Kim, K. B.; Ribas, A.; McArthur, G. A.; Sosman, J. A.; O'Dwyer, P. J.; Lee, R. J.; Grippo, J. F.; Nolop, K.; Chapman, P. B. *N. Engl. J. Med.* **2010**, *363* (9), 809–819.

(14) Jiang, Y. S.; Bhadra, S.; Li, B.; Wu, Y. R.; Milligan, J. N.; Ellington, A. D. *Anal. Chem.* **2015**, *87* (6), 3314–3320.

(15) Cai, S.; Jung, C.; Bhadra, S.; Ellington, A. D. *Anal. Chem.* **2018**, *90* (14), 8290–8294.

(16) Liu, W.; Huang, S.; Liu, N.; Dong, D.; Yang, Z.; Tang, Y.; Ma, W.; He, X.; Ao, D.; Xu, Y.; Zou, D.; Huang, L. *Sci. Rep.* **2017**, *7* (1), 40125.

(17) Ding, X.; Wu, W.; Zhu, Q.; Zhang, T.; Jin, W.; Mu, Y. *Anal. Chem.* **2015**, *87* (20), 10306–10314.

(18) Ding, X.; Wang, G.; Sun, J.; Zhang, T.; Mu, Y. *Chem. Commun.* **2016**, *52* (76), 11438–11441.

(19) Nixon, G. J.; Svenstrup, H. F.; Donald, C. E.; Carder, C.; Stephenson, J. M.; Morris-Jones, S.; Huggett, J. F.; Foy, C. A. *Biomol. Detect. Quantif.* **2014**, *2* (2), 4–10.

(20) Mhlanga, M. M.; Malmberg, L. *Methods* **2001**, *25* (4), 463–471.

(21) Vet, J. A. M.; Marras, S. A. E. *Oligonucleotide Synthesis: Methods and Applications*; Piet Herdewijn, Ed.; Humana Press: Totowa, 2005; pp 273–289.

(22) Tyagi, S.; Kramer, F. R. *Nat. Biotechnol.* **1996**, *14* (3), 303–308.

(23) Varona, M.; Ding, X.; Clark, K. D.; Anderson, J. L. *Anal. Chem.* **2018**, *90* (11), 6922–6928.

## Appendix B: Supporting Information Chapter 3

### Reagents and Instrumentation

All synthetic oligonucleotide primers were purchased from Integrated DNA Technologies (Coralville, IA, USA). The molecular beacon was ordered with HPLC purification while the remaining primers were purified with standard desalting. The three 3.9 kB plasmids were obtained from Eurofin Genomics (Louisville, KY, USA). Tris(hydroxymethyl)aminomethane (Tris) was obtained from P212121 (Ypsilanti, MI, USA). Isothermal Buffer (10X), Bst 2.0 WarmStart DNA

polymerase, 100 mM MgSO4, dNTPs, molecular biology grade Proteinase K, and NEB 5-alpha Competent E. coli cells were obtained from New England Biolabs (Ipswich, MA, USA ). Betaine, Guanidine Hydrochloride, Tween-20, and hydroxynapthol blue (HNB) were obtained from Sigma-Aldrich (St. Louis, MO, USA). For qPCR experiments, SsoAdvanced Universal SYBR Green Supermix was obtained from Bio-Rad laboratories (Hercules, CA, USA). Sodium chloride was obtained from Fisher Scientific (Hampton, NH, USA). Fluorescence assays were performed on CorningTM 384-well black microplates (Corning, NY, USA). Eppendorf Lo-bind centrifuge tubes were used for all extractions (Hamburg, Germany). Carbenicillin was purchased from GoldBio (St. Louis, MO, USA).

All qPCR and LAMP assays were performed on either a Bio-Rad CFX96 TouchTM Real Time PCR System or a Bio-Rad CFX ConnectTM Real Time PCR system. All fluorescence experiments were performed using a BioTek Synergy Hybrid H1 Microplate Reader. Deionized water (18.2 MΩ cm) used during this study was obtained from a Millipore Milli-Q water purification system (Bedford, MA, USA). An Eppendorf, New Brunswick Scientific I 24 incubator shaker was used for the incubation of cell cultures.

**Culture Conditions**

A 2 mL Luria broth culture (100 µg mL-1 Carbenicillin) of E. coli K12, transformed with a plasmid containing the sequence of interest, was inoculated and incubated at 37 °C, 250 rpm overnight in an incubator shaker. Once an OD600 of 1.00 was reached, the culture was removed from the incubator shaker. Three, tenfold serial dilutions were performed to reach a cellular concentration of 106 colony forming units (cfu) mL-1.

**Extractions from Cell Lysate**

A 200 µL aliquot of the 106 cfu mL-1 cell suspension was added to 20 µL of Proteinase K (800 units mL-1) and 200 µL of 3 M Guanidine-HCl and 20% Tween-20. The mixture was briefly vortexed and incubated for 10 min at 56 °C. Following incubation, 2 mM tris-buffer pH 8 was added to bring the total volume to 1.5 mL. The extraction was performed using SPME for 2 min using vortex agitation (2500 rpm). The fiber was then washed with water and subsequently desorbed into 50 µL of 1 M NaCl using 2500 rpm of vortex agitation.

**Table S1.** Sequences used in this study including LAMP primers, LAMP target and SNP-containing sequence as well as the oligonucleotides used for annealing profiles.

| Name | Sequence |
|---|---|
| BIP | 5'-ACCATTTGCCTAGCCGTACTACAATAAAGTCACCTTCTTGG-3' |
| FIP | 5'-TCCTTTTTTGTAGGGCTATGTTGTTGTTTGTGTGATTTTTGTGTGC-3' |
| B3 | 5'-GTCATTAGGTACTACCGAGG-3' |
| F3 | 5'-CCTAAATGTAGCAAATTGATTTCCT-3' |
| LF | 5'-TGTGTTGCGCGCACAGTA-3' |
| MB | 5'-FAM-AGCGGCTGCAGCCCTACTAGCCGCT-Dabcyl-3' |
| Target | 5'-<br>CCTAAATGTAGCAAATTGATTTCCTACAAGTTTGTGTGATTTTTGTGT<br>GCTACTGTGCGCGCAACACAAAGATAACAACATAGCCCTACAAAAA<br>AGGAAAACGTCATGAAACAAACCATTTGCCTAGCCGTACTTGCAGC<br>CCTACTAGCCGCTCCTGTATTTGCTCACCAAGAAGGTGACTTTATTG<br>TGCGCGCGGGTATTGCCTCGGTAGTACCTAATGAC<br>-3' |
| Target + SNP* | 5'-<br>CCTAAATGTAGCAAATTGATTTCCTACAAGTTTGTGTGATTTTTGTG<br>TGCTACTGTGCGCGCAACACAAAGATAACAACATAGCCCTACAAAA<br>AAGGAAAACGTCATGAAACAAACCATTTGCCTAGCCGTACTTGCAG<br>CC**G**TACTAGCCGCTCCTGTATTTGCTCACCAAGAAGGTGACTTTATT<br>GTGCGCGCGGGTATTGCCTCGGTAGTACCTAATGAC-3' |
| MB complement | 5' – AGCGGCTAGTAGGGCTGCA – 3' |
| MB mismatch loop* | 5' – AGCGGCTAGTA**C**GGCTGCA – 3' |
| MB mismatch stem* | 5' – AGC**C**GCTAGTAGGGCTGCA – 3' |

*Bold Letters indicate bases that are different from the target sequence

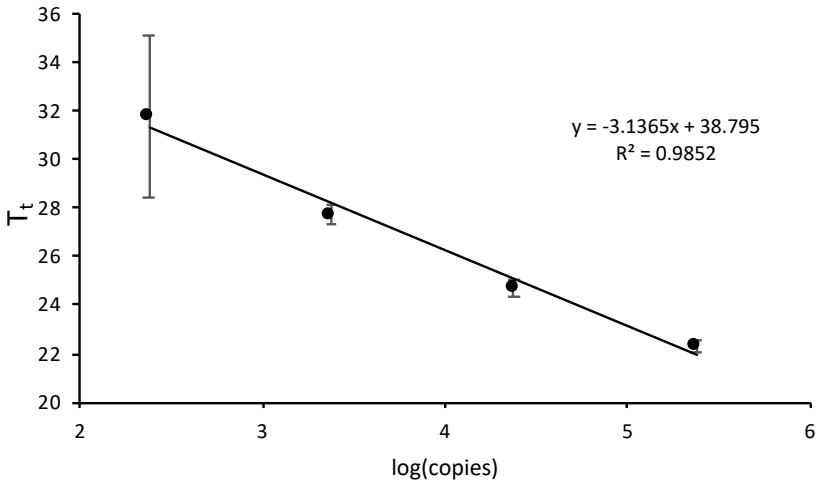


**Figure S1.** Molecular Beacon-LAMP calibration curve of a fragment of the ompW gene to determine limit of detection. A series of concentrations ranging from $2.38\times10^5$ copies to $2.38\times10^2$ were tested in triplicate.

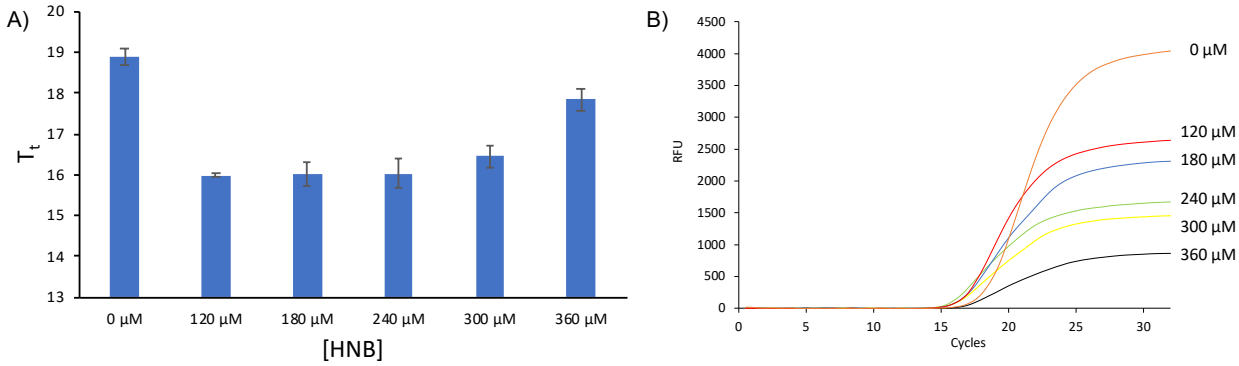


**Figure S2.** Effect of HNB concentration on MB-LAMP. Mass of template: 1.0 pg; reaction temperature: 63 °C; MB concentration: 0.32 µM; HNB concentration: 0 µM , 120 µM, 180 µM, 240 µM, 300 µM, 360 µM.

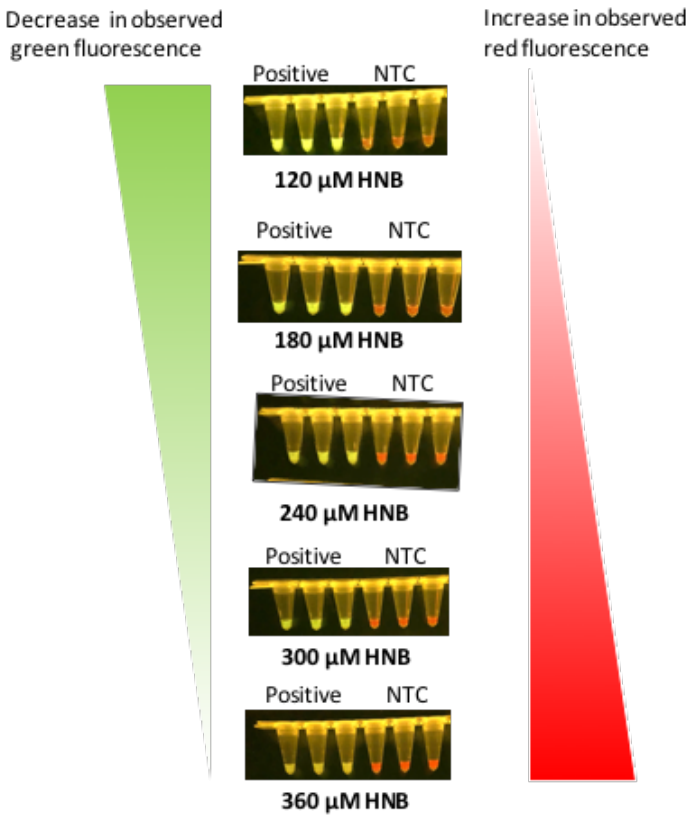


**Figure S3.** Reaction containers visualized using a transilluminator following LAMP with HNB concentrations ranging from 120 µM to 360 µM. An excitation wavelength of 470 nm was employed. Three positive reactions and three no template controls were performed for each HNB concentration. A DNA mass of 1.0 pg was used for all reactions.

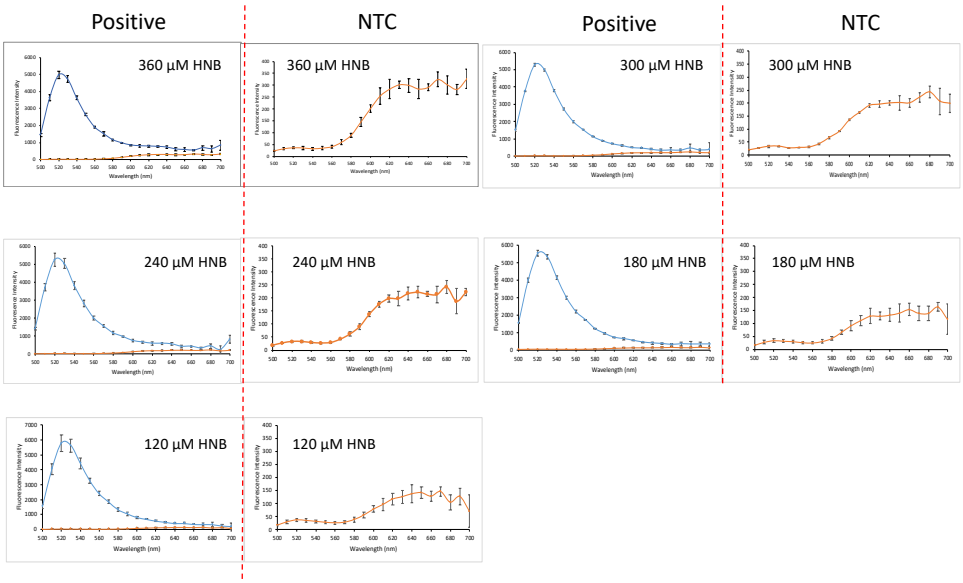


**Figure S4.** Fluorescence emission spectra of reaction containers following LAMP at various concentration levels of HNB. An excitation wavelength of 470 nm was employed with a step-size of 10 nm. All measurements were performed in triplicate.

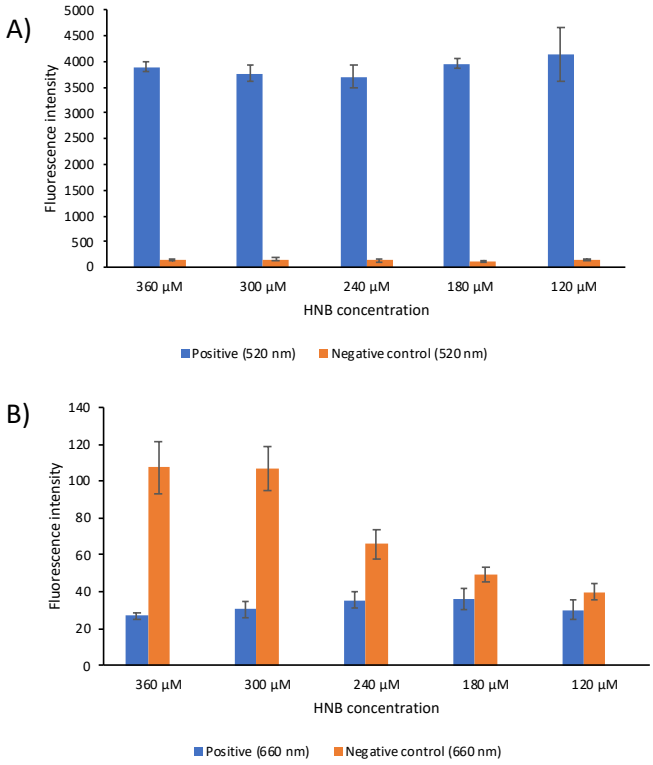


**Figure S5.** Endpoint fluorescence measurements following LAMP with various concentrations of HNB. An excitation wavelength of 470 nm was employed. Emission wavelength: A) 520 nm or B) 660 nm. All measurements were performed in triplicate.

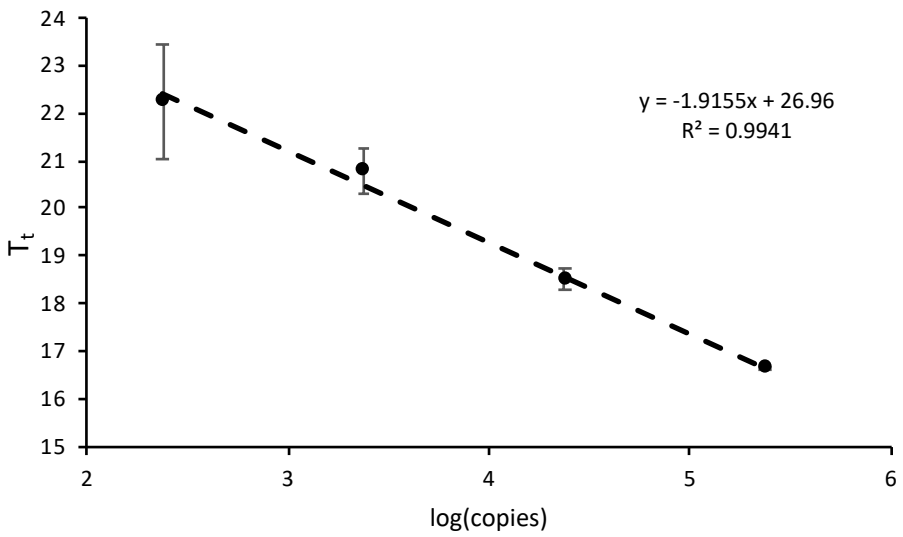


**Figure S6.** Limit of detection of a fragment of the ompW gene using LAMP and real-time detection with a molecular beacon probe. A series of concentrations were tested in triplicate ranging from $2.38\times10^5$ copies to $2.38\times10^2$. A 240 µM amount of HNB was included in all reactions.

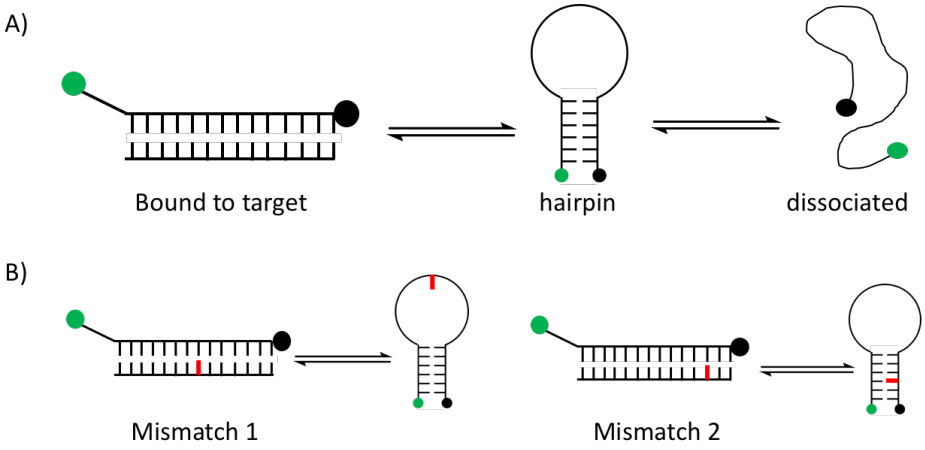


**Figure S7.** A) Possible molecular beacon conformations depending on temperature and presence of target. B) Representative illustration of the location for the two mismatches tested using annealing profiles. The sequences are drawn from 5' to 3' ends.

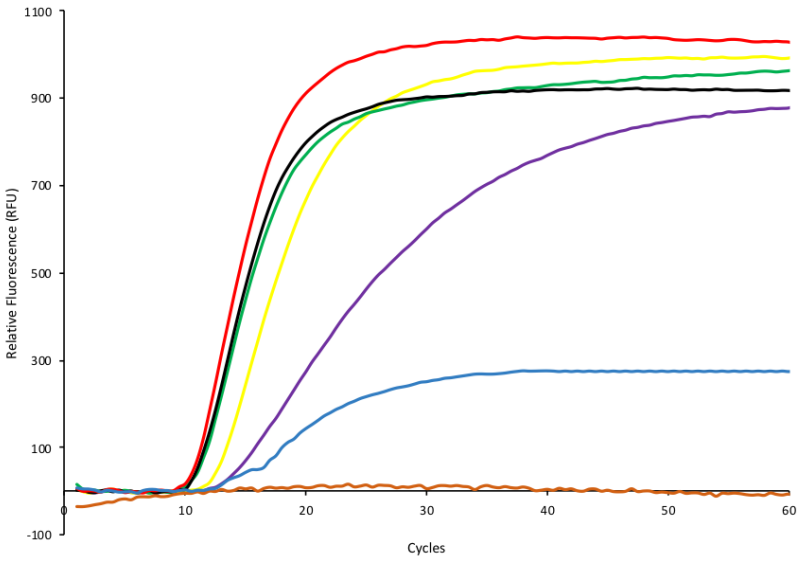


**Figure S8.** MB-LAMP real- time amplification curves resulting from different target to mismatch ratios. 100% Target ( ), 75% ( ), 50% ( ), 5% ( ), 1% ( ) , and 100% ( ) mismatch.

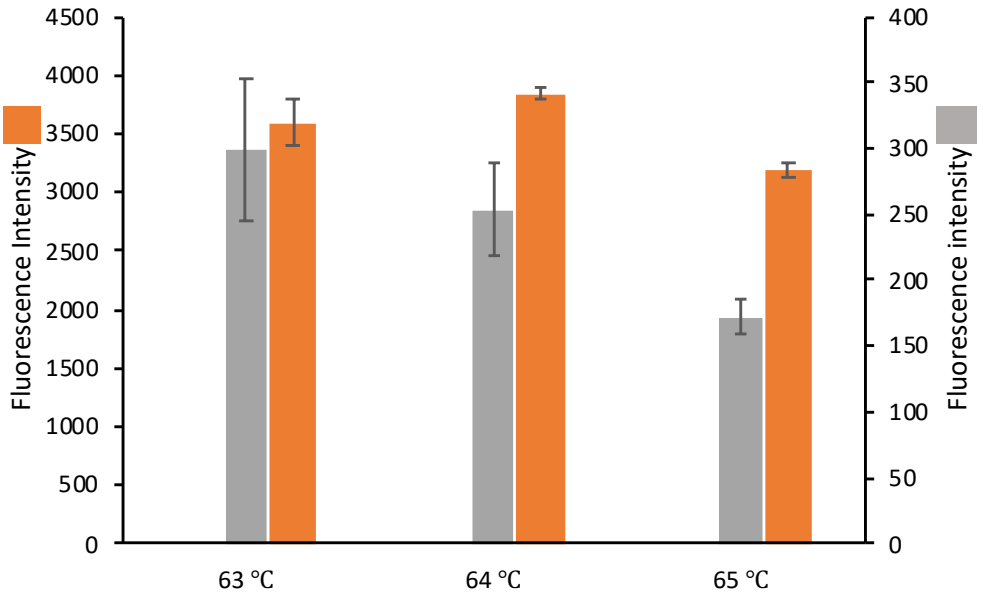


Figure S9. Fluorescence measurements of the reaction containers following amplification of the target ( ) or the mismatched sequence ( ). Reactions were performed at three different temperatures. An excitation wavelength of 470 nm was employed with an emission wavelength of 520 nm.

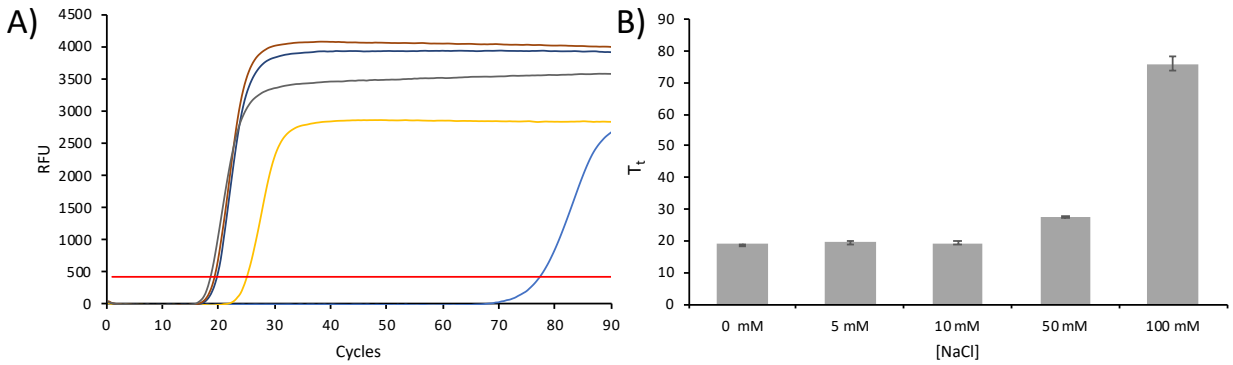


**Figure S10**. Effect of NaCl concentration on LAMP amplification with real-time detection. Mass of template: 1.0 pg ($2.38\times10^5$ cps); reaction temperature: 63 °C; MB concentration: 0.32 µM; NaCl concentration: 0 mM, 5 mM, 10 mM, 50 mM, 100 mM. A) Real-time fluorescence curves. B) Comparison of threshold times.

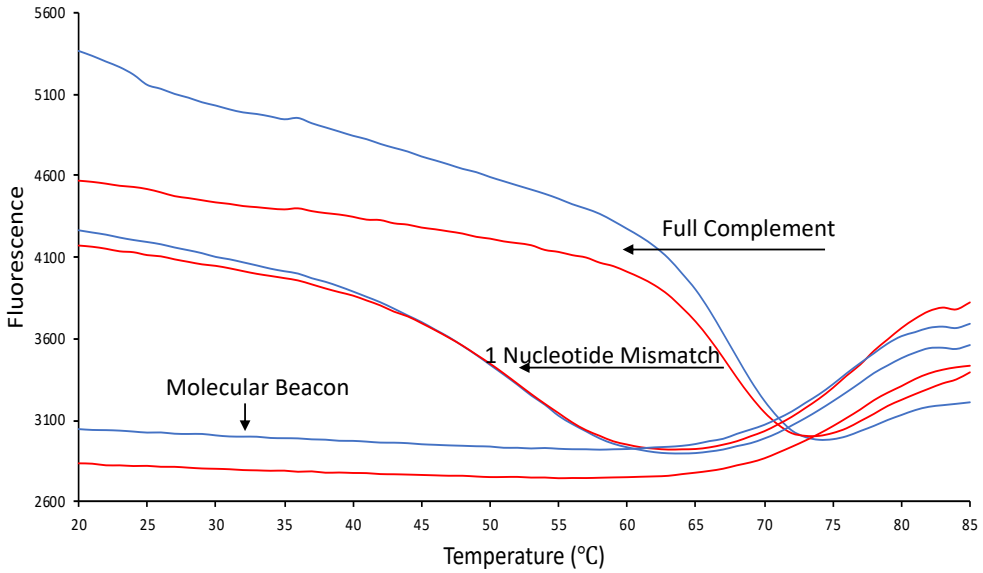


**Figure S11.** Comparison of molecular beacon annealing profiles performed in ( ) Isothermal Buffer or ( ) custom-made buffer. All reactions contained 8 mM $MgSO_4$, .2 µM MB and 1 µM of the complement or mismatched sequence.

# CHAPTER 4. SOLID-PHASE MICROEXTRACTION ENABLES ISOLATION OF BRAF V600E CTDNA FROM HUMAN PLASMA FOR DETECTION WITH A MOLECULAR BEACON LOOP-MEDIATED ISOTHERMAL AMPLIFICATION ASSAY

Reprinted with permission from *Analytical Chemistry* 2020, 92, 4, 3346-3353



Marcelino Varona, Derek R. Eitzmann, Darshna Pagariya, Robbyn K. Anand and Jared L. Anderson

## Abstract

Circulating tumor DNA (ctDNA) is a promising biomarker that can provide a wealth of information regarding the genetic makeup of cancer as well as provide a guide for monitoring treatment. Methods for rapid and accurate profiling of ctDNA are highly desirable in order to obtain the necessary information from this biomarker. However, isolation of ctDNA and its subsequent analysis remains a challenge due to the dependence on expensive and specialized equipment. In order to enable widespread implementation of ctDNA analysis, there is a need for low-cost and highly accurate methods that can be performed by non-expert users. In this study, an assay is developed that exploits the high specificity of molecular beacon (MB) probes with the speed and simplicity of loop-mediated isothermal amplification (LAMP) for the detection of the BRAF V600E single-nucleotide polymorphism (SNP). Furthermore, solid-phase microextraction (SPME) is applied for the successful isolation of clinically-relevant concentrations (73.26 fM) of ctDNA from human plasma. In addition, the individual effects of plasma salts and protein on the extraction of ctDNA with SPME are explored. The performed work expands the use of MB-LAMP for SNP detection as well as demonstrates SPME as a sample preparation tool for nucleic acid analysis in plasma.

## Introduction

Early and accurate detection of cancer is paramount for prompt administration of treatment and positive patient outcomes.[1] Tissue biopsy is the most commonly used technique for the diagnosis of cancer. During a biopsy, tissue suspected of being cancerous is obtained from the patient and subsequently analyzed using microscopy. However, biopsies are time consuming, invasive, and often difficult to obtain. Moreover, obtaining a sufficient amount of tissue for histological analysis as well as genotyping can present a significant challenge. As a result, minimally invasive methods that can provide rapid results are highly desirable for reliable diagnosis and treatment of cancer.

Circulating tumor DNA (ctDNA) represents a promising biomarker for the diagnosis of cancer and monitoring of treatment efficacy.[2,3] The genomic profile of ctDNA provides dynamic insight into the tumor's genetic makeup. Since ctDNA can be found in blood and plasma, it can be obtained from patients with more frequency while being significantly less invasive than traditional tissue biopsies. This has led to the popularization of personalized medicine, an approach which seeks to tailor medical treatment in an individual rather than a 'one size fits all' basis, as a strategy for the development of more effective therapies.[4]

Vemurafenib is a representative example of an anticancer drug that was developed to combat metastatic melanomas that specifically possess the BRAF V600E mutation.[5] The mutation is caused by the substitution of a thymine (T) base to an adenine (A) within the gene encoding for BRAF – a serine/threonine protein kinase that promotes cell mobility and proliferation. The resulting mutation causes the amino acid to change from valine (V) to glutamate (E), promoting an increase in activity of the protein. Up to 90% of BRAF-mutant melanomas contain this specific mutation.[6,7] Not only is this mutation relevant for melanomas, it has also been observed in various other cancers including lung adenocarcinomas.[8] Therefore, to successfully obtain accurate

identification of BRAF V600E positive ctDNA, assays must be capable of achieving single-nucleotide resolution.

There are several challenges associated with ctDNA analysis that preclude it from being widely implemented, particularly in resource-limited settings. The first challenge involves the isolation of ctDNA from plasma samples. Traditional extraction methods rely on silica-based sorbents that can require complex vacuum apparatuses, organic solvents (e.g., isopropanol and ethanol), and significant user intervention.[9,10] Furthermore, commonly used detection methods such as digital PCR and qPCR, while highly sensitive, require sophisticated thermal cycling equipment and complex fluorescence detection modules.[11]

Solid-phase microextraction (SPME) was developed as an alternative to traditional solid-phase extraction (SPE).[12] It relies on a thin sorbent film immobilized on a support that preconcentrates desired analytes from a sample. Advantages of SPME over traditional SPE include ease of automation, low cost, and short analysis times.[13] Recently, SPME sorbent coatings comprised of polymeric ionic liquids (PILs) have been developed and applied for the analysis of ultraviolet filters,[14] organophosphorous pesticides,[15] and free fatty acids[16] from a variety of matrices. Our group has utilized PIL-SPME for the rapid isolation and detection of nucleic acids from aqueous cell lysates and artificial sputum samples.[17–19] PIL-SPME holds promise as a rapid, user-friendly technique for the isolation of ctDNA from plasma for subsequent molecular analysis.

Loop-mediated isothermal amplification (LAMP) is a powerful isothermal amplification technique capable of amplifying nucleic acid sequences with equal or better sensitivity than traditional PCR-based methods and shorter analysis times (<1 h).[20] Due to its rapid and isothermal nature, LAMP is a promising substitute for PCR, particularly in resource-limited settings. While possessing several advantages over PCR-based methods, LAMP does not have a universal

sequence-specific detection method analogous to the TaqMan probe in qPCR. As a result, sequence-specific methodologies are highly desired, particularly for ctDNA analysis where single-nucleotide resolution is required.

Sequence-specific detection following LAMP amplification is a challenge that has been addressed through a variety of strategies including the incorporation of additional enzymes,[21] use of competitive primers,[22] strand displacement probes,[23-24] and molecular beacons (MBs).[25] MBs are dual-labeled oligonucleotide probes that can be designed to be highly specific to their target.[26] Recently, our group demonstrated that MB-LAMP was capable of visually discriminating between single-nucleotide polymorphisms (SNPs).[27] Due to its high specificity, MB-LAMP has the potential to be applied in ctDNA analysis.

In this study, we demonstrate for the first time the isolation of BRAF V600E ctDNA from human plasma samples using PIL-SPME and its subsequent LAMP detection using allele-specific MBs. The performance of PIL-SPME in plasma was systematically evaluated to identify the effects of protein, salt content, and anticoagulant used during plasma collection on the extraction of DNA. Furthermore, the utility of MB-LAMP for ctDNA analysis was expanded to demonstrate the positive identification of wild type and mutant sequences. The MB-LAMP reaction was also investigated with dual-labeled probes of various lengths to understand the relationship between the probe-structure and the observed fluorescence signal. Moreover, a plate reader assay capable of detecting 5% of the BRAF V600E mutation was developed and implemented, thereby eliminating the necessity of a qPCR instrument and increasing its potential as a point-of-care tool.

## Experimental

### Reagents and Instrumentation

All synthetic oligonucleotide primers and dual-labeled probes were purchased from Integrated DNA Technologies (Coralville, IA, USA). MBs and dual-labeled probes were prepared

using HPLC purification while primers were ordered with standard desalting. Tris(hydroxymethyl)aminomethane (Tris) and bovine serum albumin (BSA) were obtained from P212121 (Ypsilanti, MI, USA). Trisodium citrate, ethylenediaminetetraacetic acid dipotassium salt dihydrate, and dehydrated plasma were ordered from Sigma-Aldrich (St. Louis, MO, USA). Pooled human plasma apheresis derived was obtained from Innovative Research (Novi, MI, USA). Sodium chloride was obtained from Fisher Scientific (Hampton, NH, USA). Eppendorf Lobind centrifuge tubes (Hamburg, Germany) were used for all extractions. An Agilent Technologies Poroshell 120 column (50 mm × 4.6 mm i.d. × 2.7 μm particle size) was used for BSA analysis. All fluorescence experiments were performed using a BioTek Synergy Hybrid H1 microplate reader. Deionized water (18.2 MΩ cm) used was obtained from a Millipore Milli-Q water purification system (Bedford, MA, USA). For BSA extraction experiments, an Agilent 1260 HPLC with a diode array detector coupled to an Agilent 6230B Accurate Mass Time of Flight (TOF) mass spectrometer with an electrospray source was used.

**Template DNA Preparation**

Three 3.9 kbp plasmids containing different insertions of 280 bp, 210 bp, and 210 bp were obtained from Eurofin Genomics (Louisville, KY, USA). The 280 bp fragment was employed in the extraction experiments. The two 210 bp fragments contained a portion of the BRAF gene. One fragment contained the BRAF V600E mutation while the other contained the wild type allele. All sequences, primers, and probes used in this study can be found in Table S1. PCR amplification of each inserted sequence was followed by agarose gel electrophoresis using a horizontal gel electrophoresis system H4 chamber from Bethesda Research Laboratories (Gaithersburg, MD) with a Neo/Sci (Rochester, NY) dual-output power supply. After electrophoresis, the amplicon bands were removed and purified by a QIAquick gel extraction kit (Qiagen, Hilden, Germany).

The recovered DNA fragments were subsequently quantified by a NanoDrop 2000c spectrophotometer from Thermo Scientific (Waltham, MA) and stored at -20 °C.

**qPCR Conditions**

All qPCR experiments were carried out on a CFX96 Touch real-time PCR detection system from Bio-Rad Laboratories (Hercules, CA). The amplification protocol used for thermocycling was as follows: an initial denaturation step of 5 min at 95.0 °C, followed by 40 cycles of 95.0 °C for 10 s and 58.0 °C for 30 s. All data points recorded were performed in triplicate unless otherwise specified. Each reaction contained the following reagents: 10 µL (2X) SsoAdvanced Universal SYBR green supermix (Bio-Rad), 8.2 µL of deionized water, 0.8 µL of 10 µM forward and reverse primers, and 1.0 µL of template DNA.

**PIL-SPME Extraction Procedure**

Preparation of the PIL-SPME sorbents was performed following a previously reported method.[28] The chemical structure of the sorbent is shown in Figure S1. All extractions were carried out using the following procedure. A 1.0 mL volume of extraction solution containing 10 pg $mL^{-1}$ template DNA was pipetted into a 1.5 mL DNA LoBind tube. The cap of the tube was pierced using a needle to allow the PIL fiber to be immersed into the extraction solution upon closing. The centrifuge tube was then agitated with a Fisher-Brand digital vortex mixer (Fisher Scientific, Hampton, NH) for 2 min at 2500 rpm. Next, the fiber was removed from the extraction solution and washed in deionized water. After washing, the fiber was then transferred into 10 µL of 1 M NaCl (desorption solution) for 30 min. To alleviate qPCR inhibition caused by the high salt concentration in the desorption solution, a 5-fold dilution was performed prior to qPCR analysis. Following desorption, the PIL fiber was placed in saturated (6.14 M) NaCl for 1 h prior to subsequent extractions.

**Magnetic Bead Extractions**

Extractions were performed using Dynabeads Myone Silane magnetic beads (Thermo-Fisher Scientific) as suggested by the manufacturer, with some modifications. Extraction solutions (1.0 mL) were prepared containing 10 pg $mL^{-1}$ DNA. A volume of 750 µL 6.0 M guanidine HCl was added to the extraction solution along with 30 µL of beads (40 mg $mL^{-1}$ stock). The beads were subjected to vortex agitation for 2 minutes and were subsequently collected, washed with ethanol, air dried, and the DNA finally desorbed in 400 µL of 2.0 mM Tris at pH 8.

**LC-TOF-MS Conditions for BSA analysis**

LC-MS grade water (Fisher Scientific) supplemented with 0.1% formic acid (Sigma-Aldrich) was used as mobile phase A while acetonitrile with 0.1% formic acid was used as mobile phase B. An injection volume of 5.0 µL was used. Gradient elution was performed using the following separation program: 5% B to 100% B from 0-10 min, held at 100% B from 10 to 15 min, decreased to 5% B from 15 to 20 min, and finally held at 5% B for 5 min.

An external calibration curve was prepared (Figure S2) by analyzing standard solutions of BSA and measuring the peak area obtained from the extracted ion chromatogram using the +50 charge state of the protein (1329.63 m/z)

**LAMP Conditions**

LAMP amplification of the BRAF sequences was performed by heating at 60.5°C for 1 h on a CFX96 Touch real-time PCR detection system. For real-time assays, fluorescence measurements were taken every 30 seconds. End-point fluorescence measurements were recorded using a BioTek Synergy Hybrid H1 Microplate Reader (Winooski, VT). Each 10 µL reaction mixture contained the following components: 1.4 mM of each dNTP (New England Biolabs, Ipswich, MA), 10× Isothermal Buffer (NEB), 6 mM $MgSO_4$ (NEB), 0.5 µM wild type and mutant

MBs, 1.6 µM FIP and BIP primers, 0.2 µM F3 and B3 primers, 0.4 µM LoopB primer, 3.2 U Bst 2.0 WarmStart DNA polymerase (NEB), and 1 µL of template DNA solution.

## Results and Discussion

### MB-LAMP assay design

During LAMP, single-stranded loop regions are generated between the F1 and F2 regions of the target DNA.[24] These single-stranded loops are available for hybridization with the MB probe. For this assay, a primer set containing the V600E mutation between the F1 and F2 region of the target was designed using Primer Explorer V4.0 software. Initially, the molecular beacon (MB1) was created as described by Liu. et al.[25] As illustrated in Figure 1A, the loop primer was modified by adding additional bases to the 3' end to generate the MB stem. This design allows part of the stem to be fully hybridized to the target. However, as shown in Figure 1B, sufficient discrimination between the wild type and mutant sequences was not observed when this strategy was implemented. This was likely due to the location of the SNP in the last nucleotide of the 3' end of the loop primer.

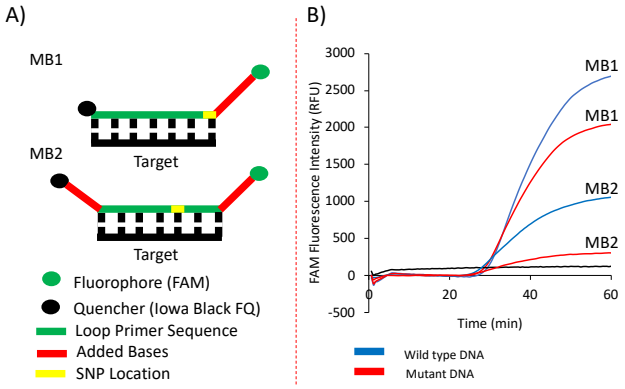


**Figure 1.** (A) Representative illustrations of the molecular beacons used to discriminate between wild type and mutant BRAF V600E sequences. (B) Real-time MB-LAMP amplification plots of wild type (blue) and mutant (red) BRAF in the presence of wild type (FAM labeled) MB1 or MB2.

Therefore, a different molecular beacon (MB2) was designed in order to obtain better discrimination. This was done by selecting a different loop primer and adding several nucleotides

to generate the MB stem (Figure 1A). In this case, additional nucleotides were incorporated to both 5' and 3' ends of the loop primer, unlike MB1 which only had nucleotides added to the 3' end. Figure 1B shows representative real-time amplification curves when this MB was used for the detection of the wild type and mutant sequences. Greater differentiation between the wild type and mutant sequence was observed when MB2 was used compared to MB1. Annealing profiles between MB2 and its complementary sequence are shown in Figure S3 and confirm the ability of MB2 to discriminate between wild type and mutant sequences.

The reaction temperature is an important parameter to optimize in order to obtain sufficient discrimination between wild type and mutant sequences. Reactions were performed using several temperatures ranging from 60-62.8 °C. Representative amplification plots in Figure S4 show that 60.5 °C affords the highest fluorescence for the wild type sequence while maintaining discrimination from the mutant sequence. Subsequently, the concentration of the MB in the reaction was optimized. It was found that 0.5 µM MB yielded the highest fluorescence after amplification of the wild type sequence (Figure S5 A-C).

Previous studies have suggested that 0.8 M betaine was required in the MB-LAMP assay, potentially limiting its usefulness due the destabilizing nature of the zwitterionic molecule.[29,30] Betaine is often used as a qPCR and LAMP additive for the amplification of GC-rich regions as it decreases the stability of GC base pairs to be similar to AT base pairs.[31] In order to determine whether betaine was an essential component of the MB-LAMP reaction mixture, reactions were performed without it. As shown in Figure S6, the reaction progressed even in the absence of betaine. Moreover, the removal enabled a higher maximum fluorescence signal in the presence of the target. Sufficient discrimination was also obtained when betaine was removed, indicating that

SNP detection could still be achieved. These results strongly suggest that betaine is not a requisite component of MB-LAMP assays.

In order to detect both wild type and mutant sequences independently, a second MB targeting the mutant allele was incorporated into the assay. This MB was structurally similar to MB2 with the exception of using HEX (mutant) as the reporter dye instead of FAM (wild type). A representative illustration of the MBs used in the assay are shown in Figure 2A. Real-time reactions were performed using the multiplexed assay and representative homozygous mutant, homozygous wild type, and heterozygous samples. Figure 2B demonstrates the capability of the assay for allelic discrimination. Discrete populations of each genotype are clearly observed when the endpoint fluorescence of each channel obtained from qPCR (FAM and HEX channels) are plotted for each reaction performed.

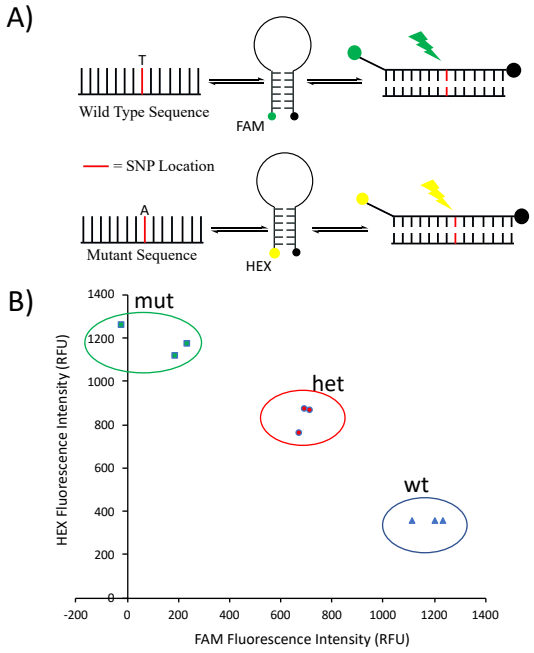


**Figure 2.** (A) General schematic of the molecular beacons used in this study to identify wild type (FAM) and mutant (HEX) BRAF sequences. (B) Allelic discrimination plot derived from end point fluorescence measurements obtained from the qPCR instrument.

**End point detection using a plate reader**

One significant advantage of LAMP over traditional qPCR-based techniques is cost effectiveness. LAMP can be performed without sophisticated thermal-cycling equipment or expensive fluorescence modules that are often required for qPCR. Due to the real-time monitoring inherent to qPCR, it is necessary to obtain fluorescence measurements after every amplification cycle performed. In order to design the MB-LAMP assay to be more amenable for point-of-care applications, a plate reader was proposed as an alternative to the qPCR instrument for end-point detection and discrimination, thereby reducing assay costs.

To determine the feasibility of using a plate reader for endpoint detection, triplicate reactions containing either the wild type or mutant sequence and no template controls (NTCs) were performed. Following amplification at 60.5 °C, a plate reader was used to obtain endpoint fluorescent readings of the HEX (excitation λ, 530 nm; emission λ, 560 nm) and FAM (excitation λ, 485 nm; emission λ, 528 nm) probes for each reaction performed. Figure S7A illustrates the fluorescence values obtained for the HEX and FAM channels for each reaction. In order to more clearly visualize discrimination of the two sequences, Figure S7B plots the fluorescence values of HEX and FAM channels from each reaction performed. This graph shows a clear separation between the mutant, wild type, and NTC reactions indicating the viability of the plate reader as an alternative detection method.

Mutant ctDNA sequences comprise a small percentage of the total amount of cell-free DNA present in plasma.[32] Therefore, it is necessary to assess whether the plate reader could detect the mutant sequence in the presence of excess wild type sequence. MB-LAMP reactions containing $2.34\times10^5$ copies $\mu L^{-1}$ of the BRAF fragment (wild type + mutant) were carried out with either 1%, 5%, or 10% of the mutant sequence. Fluorescence measurements obtained from the plate reader

assay are shown in in Figure 3. These results indicate that the MB-LAMP can detect down to 5% of the mutant BRAF sequence when the plate reader is used. In comparison, traditional Sanger sequencing can typically detect 15-20% of the mutant sequence, pyrosequencing can detect down to 2% and modified PCR-based methods down to 0.1%.[33,34] Probe-based LAMP methods such as one-step strand displacement (OSD)-LAMP have reported similar results to the developed assay (5%).[24]

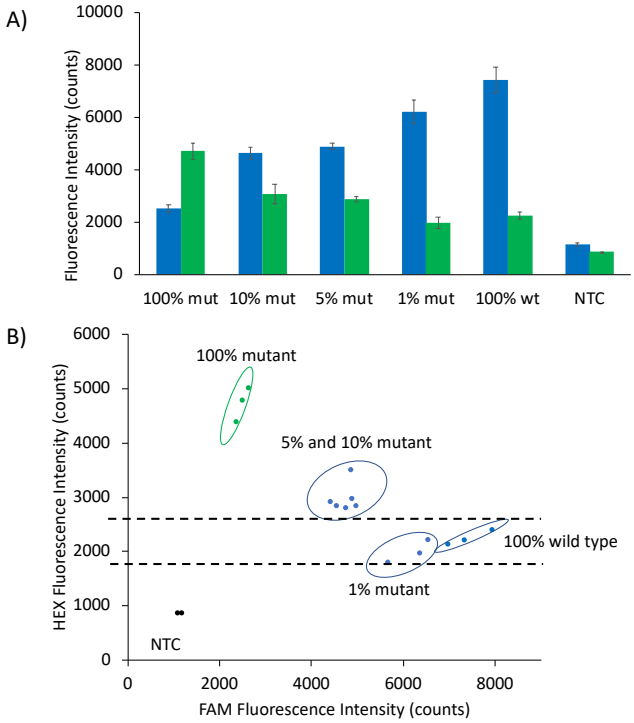


**Figure 3.** (A) Fluorescence values obtained using the plate reader from reactions containing 2.34×105 copies µL-1 of the BRAF fragment with different percentages of the mutant sequence. (B) Fluorescence plot illustrating the mutant positive reactions. The dotted line represents a 95% confidence interval created using the average HEX value for the 100% wild type reactions. Blue columns represent FAM fluorescence while green columns represent HEX.

**Investigation of probe structure and its effect on the resulting fluorescence**

Careful design of the MB is essential for obtaining single-nucleotide specificity and sufficient fluorescence for identification of positive reactions. As mentioned previously, MB1 was designed as described by Liu et al. and did not afford significant discrimination between the wild type and mutant sequences. However, it was observed that the fluorescence values obtained with

MB1 and the wild-type sequence were higher than MB2. The length of the two MBs are similar, with MB1 and MB2 containing 24 and 23 nucleotides, respectively. During stem design, seven additional nucleotides were added onto the 3' end to create the stem, allowing the 5' end to fully hybridize with the target. MB2 was designed by adding 9 additional nucleotides to the loop primer, 4 nucleotides to the 5' end and 5 nucleotides to the 3' end.

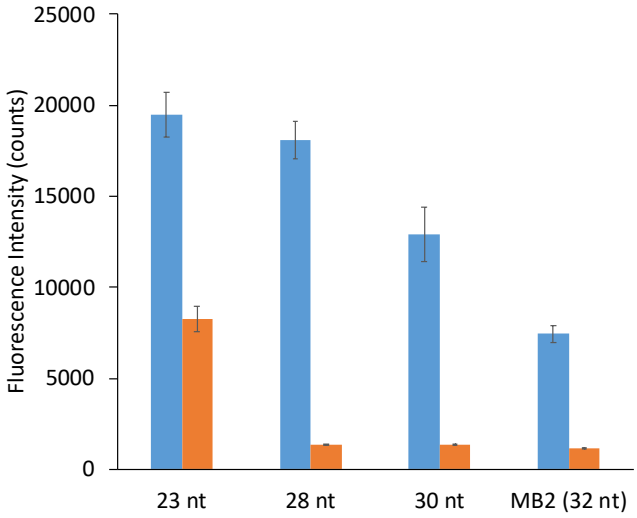


**Figure 4.** Fluorescence measurements of the FAM channel (excitation λ, 485 nm; emission λ, 528 nm) following LAMP amplification with different length of dual-labeled probes. The blue bars represent the positive reactions while the orange bars the NTCs. Triplicate reactions were performed for each probe

Due to the formation of single-stranded DNA loops during LAMP amplification, it is possible that hybridization of the MB to the loop structure could allow the fluorophore-quencher pair to interact in space, leading to quenching by FRET.[35] To test this, the length of MB2 (32 nt) was modified by reducing the length to 30, 28, and 23 nt. LAMP reactions were performed with each sequence, as previously optimized, and FAM fluorescence recorded using the plate reader. As shown in Figure 4, a noticeable increase in fluorescence was observed as the length of the probe decreased. These results suggest that quenching of MB2 could be responsible for the decreased fluorescence when compared to MB1. When designing MBs for LAMP applications, decreasing the number of added nucleotides to the loop primer may lead to higher fluorescence values. Studies

are ongoing in our laboratory to understand if these observations can be generalized to all MB-LAMP assays.

**SPME preconcentration from plasma**

PIL-SPME has previously been applied in a variety of complex samples (cell lysate and artificial sputum) for the extraction of nucleic acids.[17,19] To determine the feasibility of PIL-SPME for DNA isolation from plasma, extractions were performed from plasma that was collected and stored using the anticoagulant trisodium citrate (4%). All extractions were performed using a 280 bp sequence at clinically-relevant ctDNA concentrations (10 pg $mL^{-1}$ = 54.94 fM). As observed in Figure 5A, there was an approximate 6 quantification cycle (Cq) increase when the extraction was performed from the plasma (31.49±0.58) compared to 2.0 mM tris buffer pH 8.0 (25.21±0.28). For reference, a Cq value increase of 1 indicates a 2-fold decrease in the amount of DNA present in the reaction under optimal reaction conditions.[36] This increase in Cq value indicates that some component of the plasma significantly affected the extraction or inhibited the qPCR reaction. It is important to emphasize that direct addition of the plasma to qPCR yielded no observable amplification. Therefore, these results demonstrate PIL-SPME as a useful technique for the isolation and preconcentration of sufficiently pure nucleic acid for qPCR analysis.

To determine whether the plasma was causing inhibition of qPCR, the extraction procedure was performed without any DNA in the plasma, allowing the SPME sorbent coating to extract potential inhibitors. A 10 fg mass of target DNA was subsequently added to the desorption solution after 30 min, diluted 5-fold, and analyzed by qPCR. This was compared to an identical procedure using Tris buffer instead of the plasma and spiking the same amount of DNA into the desorption solution. As shown in Figure S8, amplification of the two solutions was identical, indicating that no inhibitory components were co-extracted by the PIL fiber from the plasma.

These data strongly suggest that the higher Cq values observed are due to a component of the plasma affecting the extraction process, not qPCR inhibition by plasma components.

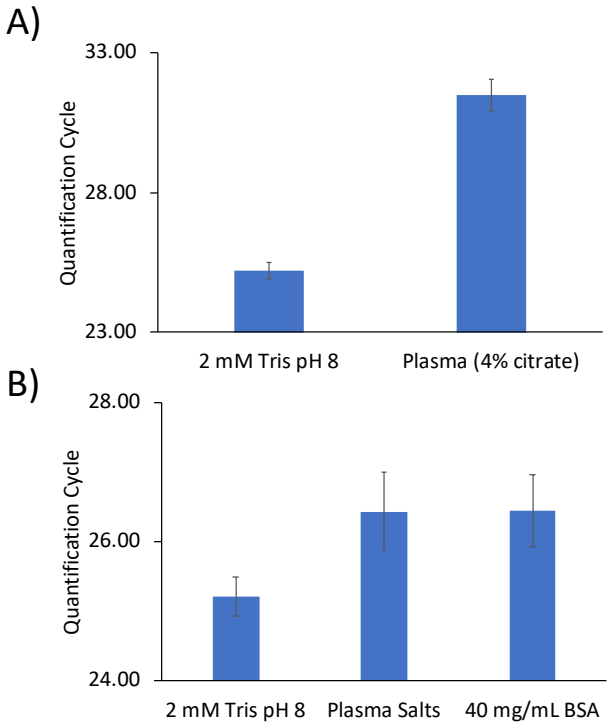


**Figure 5.** qPCR results following PIL-SPME of a model 280 bp DNA from different matrices. (A) Comparison of extractions from Tris buffer and plasma containing 4.0% trisodium citrate. (B) Evaluation of the salts from plasma as well as protein on the extraction of DNA.

Various salts responsible for maintaining osmotic balance in the plasma are potential culprits that are known to influence the DNA extraction process.[37] Since PIL-based sorbent coatings predominantly extract DNA through an ion exchange mechanism,[17] it is possible that higher ionic strength extraction solutions can affect interactions between the sorbent and DNA. To determine the effect of these salts on the extraction, a solution was prepared to mimic the salts present in plasma.[38] Extractions were performed from this salt solution, resulting in Cq values (26.43±0.52) higher than those from Tris (25.21±0.28), as shown in Figure 5B. These results suggest that the salts present in plasma can cause a moderate decrease in the extraction. However,

the observed Cq value difference of 1.22 is significantly lower than the 6.28 cycle difference between Tris and plasma extractions.

Protein represents another major component of plasma that has the potential to negatively affect PIL-SPME. Figure 5B demonstrates the results obtained following extractions from a 40 mg $mL^{-1}$ BSA solution mimicking the concentration of serum albumin. The Cq values from these extractions (26.45±0.57) were very similar to those obtained from extractions performed from the salt solution. These results suggest possible co-extraction of protein by the PIL, which could cause a competitive effect with DNA for ion-exchange sites on the fiber coating.

There are various species of anticoagulants that can be employed during plasma collection and storage. The plasma used in previous experiments contained 4.0% trisodium citrate, resulting in a concentration of 155 mM. It is possible that the high concentration of anionic species such as citrate could reduce the strength of electrostatic interactions between the PIL sorbent coating and DNA. To investigate this, extractions were performed from a 4.0% trisodium citrate solution containing the different plasma salts. The Cq values obtained (31.81±0.46) were comparable to those obtained from extractions of human plasma (31.49±0.58) collected with 4.0% trisodium citrate.

It was hypothesized that using a different anticoagulant such as K2EDTA or Na2EDTA could enable lower Cq values to be achieved. However, extractions performed from plasma collected using K2EDTA and Na2EDTA yielded nearly identical results as the citrate-treated plasma (data not shown). To determine whether the presence of the EDTA was responsible for increased Cq values, extractions were performed using 4.0 mM K2EDTA in a solution containing the plasma salts. The Cq values obtained (26.45±45) from these extractions were not significantly

different than those performed in the salt solution (26.43±0.52). These data indicate that another component of the plasma is responsible for affecting the extraction behavior of the PIL sorbent.

Since the PIL sorbent was affected by the components in the plasma, it is possible that commercially-available DNA extraction materials also exhibit negative effects when used in plasma. The extraction performance of PIL-SPME was compared with that of magnetic beads for DNA extraction from Tris buffer and K2EDTA plasma. Figure S9 compares the extraction results of PIL-SPME and the magnetic beads. Interestingly, the Cq values are nearly identical for both methods in the two different sample matrices. These results show that reduced performance in plasma also occurs with silica-based extraction techniques.

**Effects of protein on PIL-SPME DNA extractions**

Interactions between the PIL-SPME sorbent coating evaluated in this study and protein have not been previously investigated. Due to the lower DNA extraction achieved from the BSA solution, it was hypothesized that protein could interact with the PIL coating. In order to evaluate the interaction of the PIL sorbent with BSA, extractions were performed from a 40 mg $mL^{-1}$ BSA solution and the desorption solution subsequently analyzed by LC-TOF-MS. Using an external calibration curve for quantification (Figure S2), it was determined that the sorbent extracted 4.11±0.61 µg of BSA.

The effect of BSA on the qPCR efficiency was subsequently studied. As established by the MIQE guidelines,[36] acceptable qPCR efficiencies range from 90-110% and are obtained using equation (1).

$$Efficiency = [10^{-1/slope} - 1] \times 100 \quad (1)$$

An efficiency of 100% indicates the doubling of DNA during every qPCR cycle. DNA extractions were performed at 4 different DNA concentration levels in solutions containing 40 mg

$mL^{-1}$ and 4.0 mg $mL^{-1}$ BSA. Figure S10 shows the efficiency of the calibration curves to be 90.64% and 99.91% from the 40 mg $mL^{-1}$ and 4 mg $ml^{-1}$ BSA solutions, respectively. These results indicate that while high BSA concentrations cause a decrease in the qPCR efficiency, the obtained values remain within acceptable limits.

**Extractions of BRAF V600E from plasma for MB-LAMP detection**

The applicability of PIL-SPME for the isolation of clinically-relevant ctDNA sequences from plasma for subsequent MB-LAMP analysis was explored. Briefly, 1.0 mL of K2EDTA plasma was spiked with 10 pg of the BRAFV600E fragment corresponding to a clinically-relevant concentration (73.26 fM) of the mutant sequence.[32] PIL-SPME was performed and the desorption solution analyzed using MB-LAMP with the plate reader, as previously described. To prevent any dilution of the desorption solution, a previously optimized MB-LAMP buffer was used.[19]

Figure 6A shows the fluorescence results using the plate reader following PIL-SPME from the spiked plasma sample. Following triplicate extractions, the custom-buffer enabled the detection of all extractions performed. A comparison was also performed using the Isothermal Buffer provided by New England Biolabs. Due to the high salt concentration of the desorption solution, a 10-fold dilution prior to analysis must be performed. Two of the reactions were unable to be positively identified as BRAF V600E due to the required dilution. These results can be more clearly seen in Figure 6B where the HEX fluorescence of these reactions does not rise above the set threshold. This indicates the custom-buffer is a necessary component for the successful coupling of PIL-SPME with MB-LAMP.

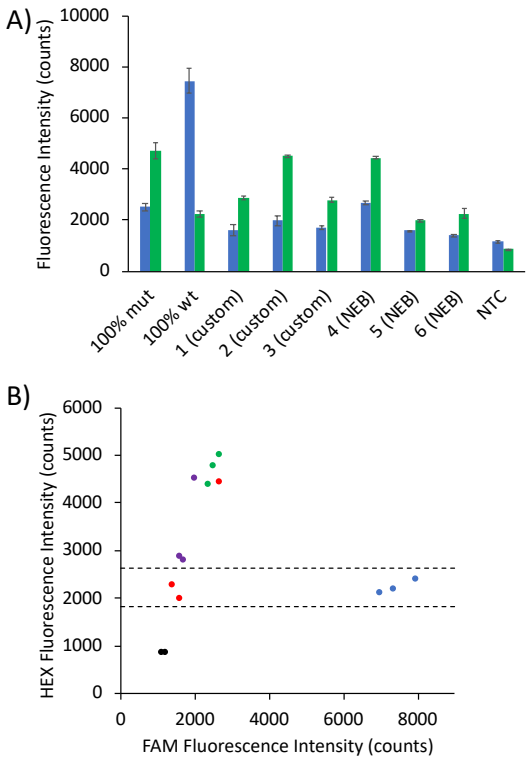


Figure 6. (A) Fluorescence results following PIL-SPME with MB-LAMP detection performed in the custom-buffer or NEB's isothermal buffer. Blue columns represent FAM fluorescence while green columns represent HEX. (B) Plot generated using the values obtained from the fluorescence readings following MB-LAMP for each extraction performed. Fluorescence values from 100 % wild type reactions (blue) and 100% mutant reactions (green) were used as a control. Reactions performed in the custom buffer are visualized in purple while the isothermal buffer reactions are in red. The dotted line represents a 95% confidence interval created using the average HEX value for the 100% wild type reactions.

## Conclusion

In summary, a MB-LAMP assay was designed and implemented to enable detection of the clinically-relevant BRAF V600E mutation. To simplify the application of the assay in resource-limited settings for point-of-care applications, a plate reader was used for detection. During assay development, dual-labeled probes (fluorophore-quencher) of different lengths were employed to investigate the relationship between the probe structure and the observed fluorescence. These experiments will serve as a guide in future MB design for LAMP applications. Furthermore, PIL-SPME was utilized as a simple, centrifuge-free sample preparation technique for the isolation of

DNA from human plasma samples in clinically-relevant concentrations. The effects of various plasma components on the extraction was also systematically evaluated. Future work will focus on lowering the cost of the assay by implementing a water bath for amplification and smartphone-based detection. Furthermore, to make the current method more user friendly, the number of steps can be reduced by using lyophilized reagents. This study demonstrates the potential of MB-LAMP for the detection of ctDNA mutations and further expands the use of PIL-SPME for DNA extraction from complex biological samples.

## Acknowledgements

Research reported in this manuscript was supported the Chemical Measurement and Imaging Program at the National Science Foundation (Grant No. CHE-1709372) and the National Institutes of Biomedical Imaging and Bioengineering of the National Institutes of Health under award number R21EB028583.

## Supporting Information

DNA sequences and oligonucleotide probes used. PIL chemical composition, BSA LC-MS calibration curve, MB-annealing profiles, real-time LAMP plots optimizing temperature, MB concentration, and betaine. End-point results using plate reader. Comparison of PIL-SPME and magnetic beads. Calibration curves from plasma. Can be found in Appendix D: Supporting Information Chapter 4

## References

(1) Hiom, S. C. *Br. J. Cancer* **2015**, *112*, S1–S5.

(2) Heitzer, E.; Ulz, P.; Geigl, J. B. *Clin. Chem.* **2015**, *61*, 112–123.

(3) Gorgannezhad, L.; Umer, M.; Islam, M. N.; Nguyen, N. T.; Shiddiky, M. J. A. *Lab Chip* **2018**, *18*, 1174–1196.

(4) Hamburg, M. A.; Collins, F. S. *N. Engl. J. Med.* **2010**, *363*, 301–304.

(5) Flaherty, K. T.; Yasothan, U.; Kirkpatrick, P. *Nat. Rev. Drug Discov.* **2011**, *10*, 811–812.

(6) Flaherty, K. T.; Puzanov, I.; Kim, K. B.; Ribas, A.; McArthur, G. A.; Sosman, J. A.; O'Dwyer, P. J.; Lee, R. J.; Grippo, J. F.; Nolop, K.; Chapman, P. B. *N. Engl. J. Med.* **2010**, *363*, 809–819.

(7) Davies, H.; Bignell, G. R.; Cox, C.; Stephens, P.; Edkins, S.; Clegg, S.; Teague, J.; Woffendin, H.; Garnett, M. J.; Bottomley, W.; Davis, N.; Dicks, E.; Ewing, R.; Floyd, Y.; Gray, K.; Hall, S.; Hawes, R.; Hughes, J.; Kosmidou, V.; Menzies, A.; Mould, C.; Parker, A.; Stevens, C.; Watt, S.; Hooper, S.; Wilson, R.; Jayatilake, H.; Gusterson, B. A.; Cooper, C.; Shipley, J.; Hargrave, D.; Pritchard-Jones, K.; Maitland, N.; ChenevixTrench, G.; Riggins, G. J.; Bigner, D. D.; Palmieri, G.; Cossu, A.; Flanagan, A.; Nicholson, A.; Ho, J. W. C.; Leung, S. Y.; Yuen, S. T.; Weber, B. L.; Seigler, H. F.; Darrow, T. L.; Paterson, H.; Marais, R.; Marshall, C. J.; Wooster, R.; Stratton, M. R.; Futreal, P. A. Nature **2002**, 417, 949−954.

(8) Paik, P. K.; Arcila, M. E.; Fara, M.; Sima, C. S.; Miller, V. A.; Kris, M. G.; Ladanyi, M.; Riely, G. J. *J Clin Oncol* **2011**, *29*, 2046–2051.

(9) Lee, H.; Na, W.; Park, C.; Park, K. H.; Shin, S. *Sci. Rep.* **2018**, *8*, 5467.

(10) Stemmer, C.; Beau-Faller, M.; Pencreac'h, E.; Guerin, E.; Schneider, A.; Jaqmin, D.; Quoix, E.; Gaub, M. P.; Oudet, P. *Clin. Chem.* **2003**, *49*, 1953–1955.

(11) Pratt, E. D.; Cowan, R. W.; Manning, S. L.; Qiao, E.; Cameron, H.; Schradle, K.; Simeone, D. M.; Zhen, D. B. *Anal. Chem.* **2019**, *91*, 7516–7523.

(12) Arthur, C. L.; Pawliszyn, J. *Anal. Chem.* **1990**, *62*, 2145–2148.

(13) Kasperkiewicz, A.; Gómez-Ríos, G. A.; Hein, D.; Pawliszyn, J. *Anal. Chem.* **2019**, *28*, 59.

(14) An, J.; Anderson, J. L. *Talanta* **2018**, *182*, 74–82.

(15) Gionfriddo, E.; Souza-Silva, É. A.; Ho, T. D.; Anderson, J. L.; Pawliszyn, J. *Talanta* **2018**, *188*, 522–530.

(16) Pacheco-Fernández, I.; Trujillo-Rodríguez, M. J.; Kuroda, K.; Holen, A. L.; Jensen, M. B.; Anderson, J. L. *Talanta* **2019**, *200*, 415–423.

(17) Nacham, O.; Clark, K. D.; Anderson, J. L. *Anal. Chem.* **2016**, *88*, 7813–7820.

(18) Nacham, O.; Clark, K. D.; Varona, M.; Anderson, J. L. *Anal. Chem.* **2017**, *89*, 10661–10666.

(19) Varona, M.; Ding, X.; Clark, K. D.; Anderson, J. L. *Anal. Chem.* **2018**, *90*, 6922–6928.

(20) Notomi, T.; Okayama, H.; Masubuchi, H.; Yonekawa, T.; Watanabe, K.; Amino, N.; Hase, T. *Nucleic Acids Res.* **2000**, *28*, E63.

(21) Fu, Y.; Duan, X.; Huang, J.; Huang, L.; Zhang, L.; Cheng, W.; Ding, S.; Min, X. *Sci. Rep.* **2019**, *9*.

(22) Malpartida-Cardenas, K.; Rodriguez-Manzano, J.; Yu, L. S.; Delves, M. J.; Nguon, C.; Chotivanich, K.; Baum, J.; Georgiou, P. *Anal. Chem.* **2018**, *90*, 11972–11980.

(23) Cai, S.; Jung, C.; Bhadra, S.; Ellington, A. D. *Anal. Chem.* **2018**, *90*, 8290–8294.

(24) Jiang, Y. S.; Bhadra, S.; Li, B.; Wu, Y. R.; Milligan, J. N.; Ellington, A. D. *Anal. Chem.* **2015**, *87*, 3314–3320.

(25) Liu, W.; Huang, S.; Liu, N.; Dong, D.; Yang, Z.; Tang, Y.; Ma, W.; He, X.; Ao, D.; Xu, Y.; Zou, D.; Huang, L. *Sci. Rep.* **2017**, *7*, 40125.

(26) Mhlanga, M. M.; Malmberg, L. *Methods* **2001**, *25*, 463–471.

(27) Varona, M.; Anderson, J. L. *Anal. Chem.* **2019**, *91*, 6991–6995.

(28) Ho, T. D.; Toledo, B. R.; Hantao, L. W.; Anderson, J. L. *Anal. Chim. Acta* **2014**, *843*, 18–26.

(29) Nanayakkara, I. A.; White, I. M. *Analyst* **2019**, *144*, 3878–3885.

(30) Becherer, L.; Bakheit, M.; Frischmann, S.; Stinco, S.; Borst, N.; Zengerle, R.; Von Stetten, F. *Anal. Chem* **2018**, *90*, 4741–4748.

(31) Rees, W. A.; Korte, J.; Von Hippel, P. H.; Yager, T. D. *Biochemistry* **1993**, *32*, 137–144.

(32) Kelley, S. O. *ACS Sensors* **2017**, *2*, 193–197.

(33) Lee, S. T.; Kim, S. W.; Ki, C. S.; Jang, J. H.; Shin, J. H.; Oh, Y. L.; Kim, J. W.; Chung, J. H. *J. Clin. Endocrinol. Metab.* **2012**, *97*, 2299–2306.

(34) Huang, T.; Zhuge, J.; Zhang, W. W. *Biomark. Res.* **2013**, *1*, 3.

(35) Johansson, M. K.; Fidder, H.; Dick, D.; Cook, R. M. *J. Am. Chem. Soc.* **2002**, *124*, 6950–6956.

(36) Huggett, J. F.; Foy, C. A.; Benes, V.; Emslie, K.; Garson, J. A.; Haynes, R.; Hellemans, J.; Kubista, M.; Mueller, R. D.; Nolan, T.; Pfaffl, M. W.; Shipley, G. L.; Vandesompele, J.; Wittwer, C. T.; Bustin, S. A. *Clin. Chem.* **2013**, *59*, 892–902.

(37) Tan, S. C.; Yiap, B. C. *J. Biomed. Biotechnol.* **2009**, 1–10.

(38) Przondziono, J.; Walke, W.; Hadasik, E.; Młynarski, R. *Adv. Mater. Sci. Eng.* **2013**, 1–6.

## Appendix C: Supporting Information Chapter 4

**Table S1.** DNA sequences, primers, and probes used in this study.

| | |
|---|---|
| 280 bp sequence | 5'-<br>GGATGTGTCTGCGGCGTTTTATCATCTTCCTCTTCATCCTGCTGCTATGC<br>CTCATCTTCTTGTTGGTTCTTCTGGACTATCAAGGTATGTTGCCCGTTTGT<br>CCTCTAATTCCAGGATCATCAACAACCAGCACCGGACCATGCAAAACCT<br>GCACAACTCCTGCTCAAGGAACCTCTATGTTTCCCTCATGTTGCTGTACA<br>AAACCTACGGACGGAAACTGCACCTGTATTCCCATCCCATCATCTTGGG<br>CTTTCGCAAGTAACCTATGGGAGTGGGCCTC-3' |
| qPCR Primers | Forward-5′-<br>GGATGTGTCTGCGGCGTTTT-3′ Reverse- 5′-<br>GAGGCCCACTCCCATAGGTT-3 |
| Wild type BRAF | 5'-<br>TATATTTCTTCATGAAGACCTCACAGTAAAAATAGGTGATTTTGGTCTAGC<br>TACAGTGAAATCTCGATGGAGTGGGTCCCATCAGTTTGAACAGTTGTCTG<br>GATCCATTTTGTGGATGGTAAGAATTGAGGCTATTTTTCCACTGATTAAAT<br>TTTTGGCCCTGAGATGCTGCTGAGTTAC<br>TAGAAAGTCATTGAAGGTCTCAACTATAGT-3' |
| Mutant V600E BRAF | 5'-<br>TATATTTCTTCATGAAGACCTCACAGTAAAAATAGGTGATTTTGGTCTAGC<br>TACAG**A**GAAATCTCGATGGAGTGGGTCCC<br>ATCAGTTTGAACAGTTGTCTGGATCCATTT<br>TGTGGATGGTAAGAATTGAGGCTATTTTTCCACTGATTAAATTTTTGGCC<br>CTGAGATGCTGCTGAGTTACTAGAAAGTCATTGAAGGTCT<br>CAACTATAGT-3' |
| BRAF_FIP | 5'-TCCAGACAACTGTTCAAACTGATGGTGATTTTGGTCTAG-3' |
| BRAF_BIP | 5'-TTGTGGATGGTAAGAATTGAGGC-TTTCTAGTAACTCAGCAGCA-3' |
| BRAF_F3 | 5’-TCTTCATGAAGACCTCACAG-3’ |
| BRAF_B3 | 5’-CTATAGTTGAGACCTTCAATGAC-3’ |
| BRAF_LB | 5’-TCCACTGATTAAATTTTTGGCCCTG-3 |
| MB1 | 5’-IABkFQ–GGGACCCACTCCATCGAGATTTCAGGGTCCC-FAM-3’ |
| MB2 | 5’-FAM-CGCGCCCACTCCATCGAGATTTCACTGGCGCG-IABKFQ-3' |
| MB2-MUT | 5’-HEX-CGCGCCCACTCCATCGAGATTTCTCTGGCGCG-Dabcyl-3' |
| MB2 Complement | 5'-CAGTGAAATCTCGATGGAGTGGG-3' |
| MB2 Mismatch | 5'-CAG**A**GAAATCTCGATGGAGTGGG-3' |
| 30 nt probe | 5’-FAM-CCGCCCACTCCATCGAGATTTCACTGGCGG-IABKFQ-3' |
| 28 nt probe | 5’-FAM-CGCCCACTCCATCGAGATTTCACTGGCG-IABKFQ-3' |
| 23 nt probe | 5’-FAM-CCCACTCCATCGAGATTTCACTG-IABKFQ-3' |

Bolded letter denotes the location of the BRAF V600E mutation

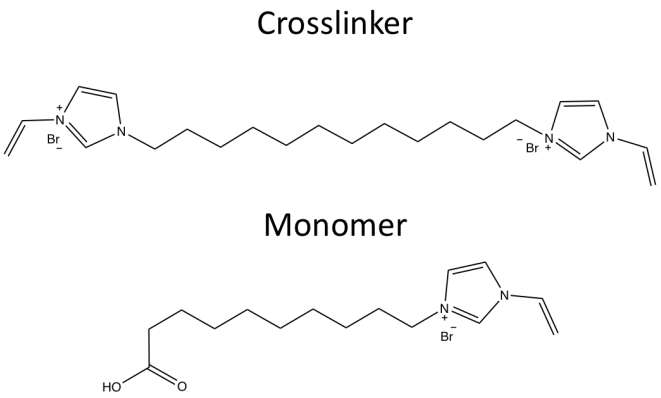


**Figure S1.** Chemical composition of the PIL-based sorbent coating used in the study.

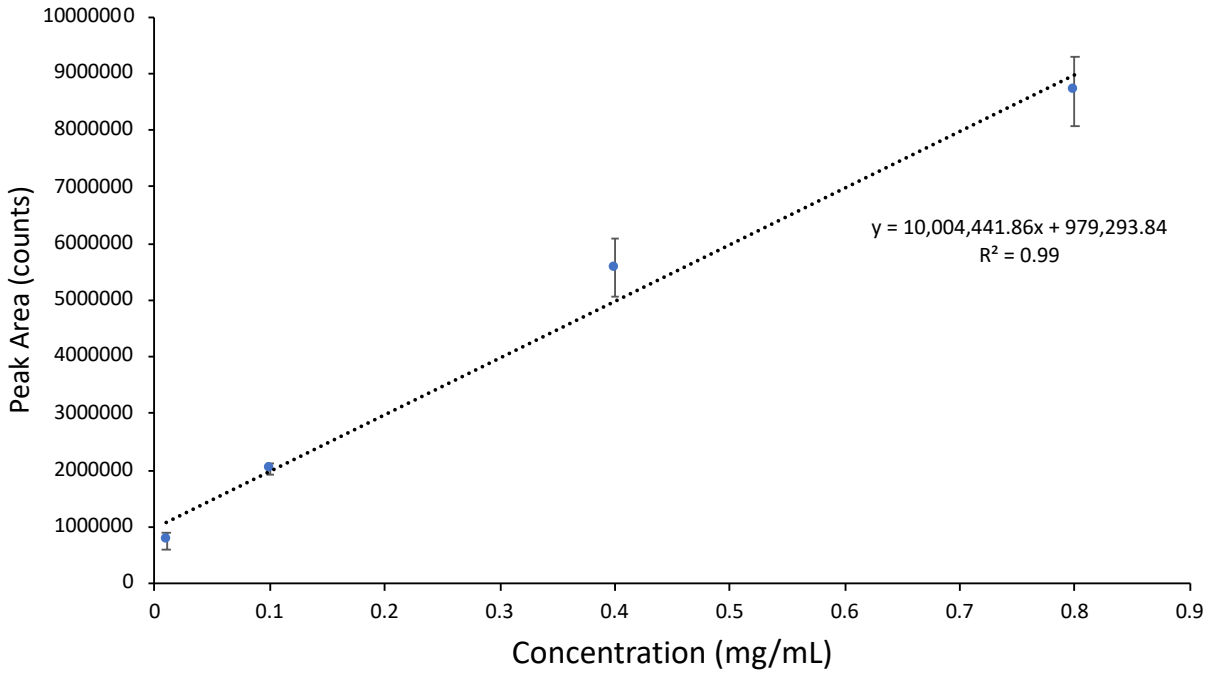


**Figure S2.** LC-MS calibration curve generated for BSA extraction experiments. The peak area of the +50 charge state (1329.6 m/z) of the protein was used.

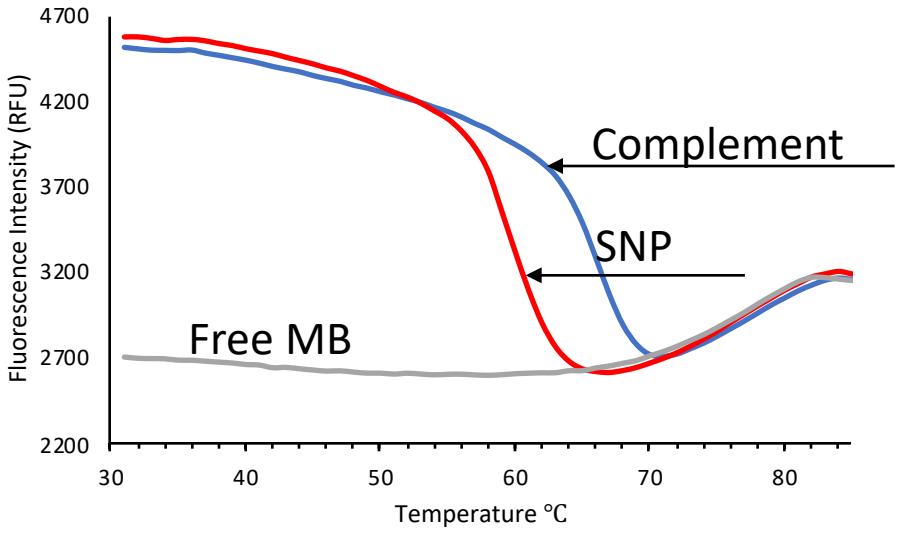


**Figure S3.** Annealing profiles using MB2 in the presence of the target or a sequence containing a 1 nucleotide mismatch.

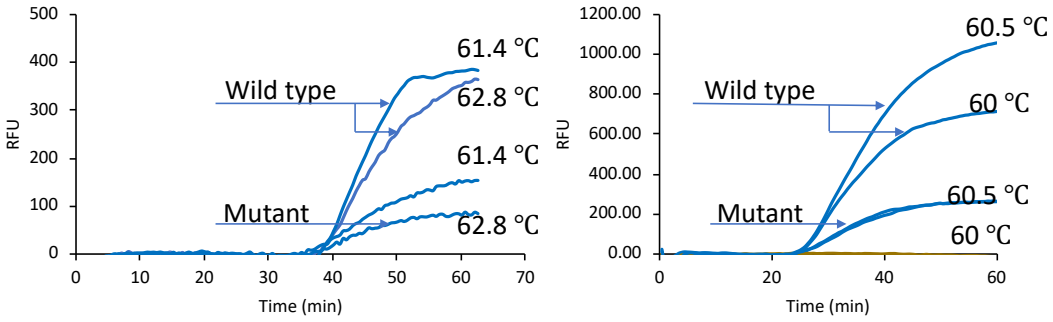


**Figure S4.** Temperature optimization of the MB-LAMP reaction. Representative real-time amplification plots of the FAM channel when MB-LAMP reactions were performed with $2.34\times 10^5$ copies of wild type and mutant BRAF V600E.

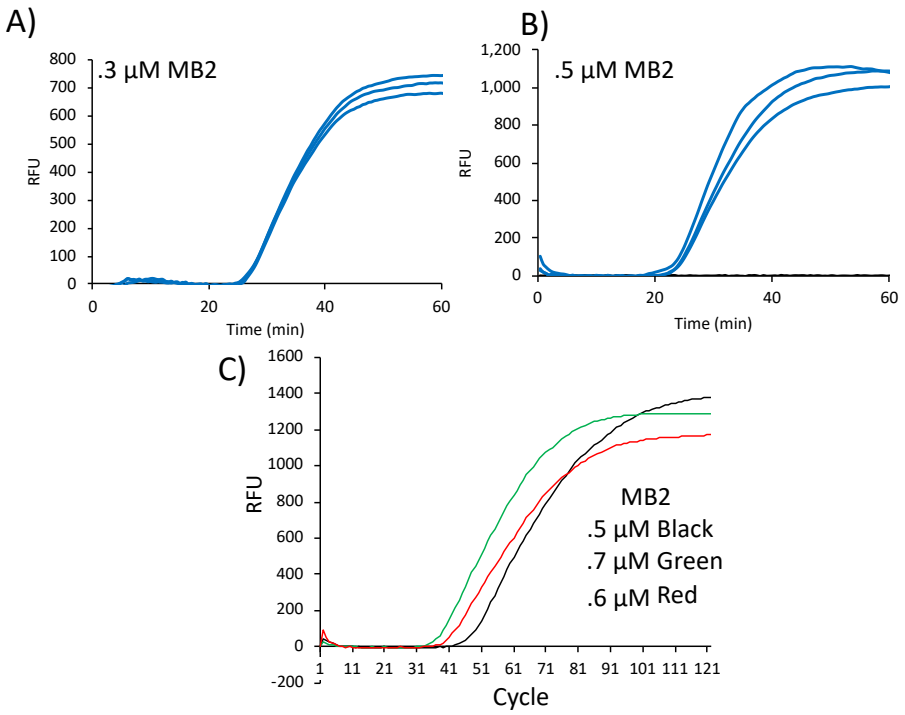


**Figure S5.** Real-time amplification plots demonstrating the effect of having (A) 0.3 µM, (B,C) 0.5 µM, (C) 0.6 µM, and (C) 0.7 µM of MB2 present in the reaction.

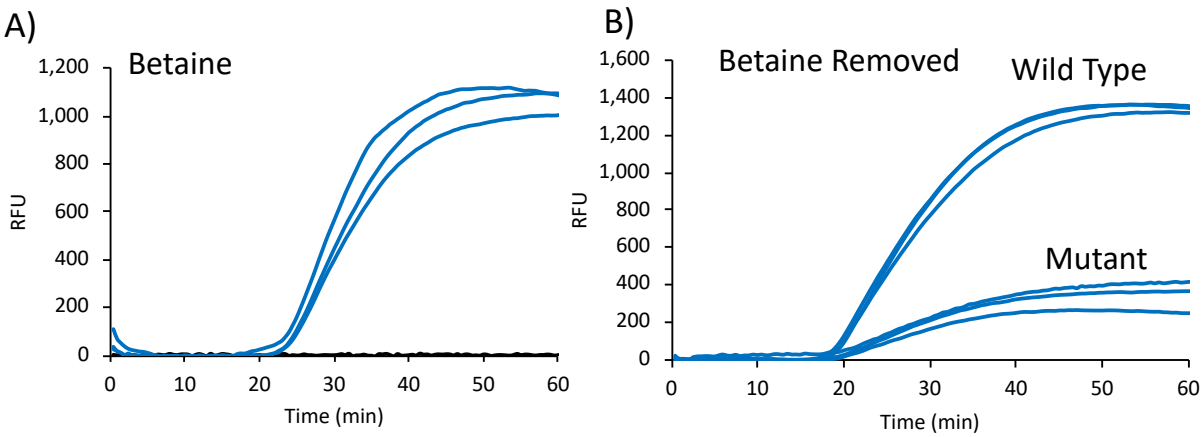


**Figure S6.** Real-time MB-LAMP amplification using MB2 demonstrating the effect of having betaine present in the MB-LAMP reaction (A) versus removing it from the system (B).

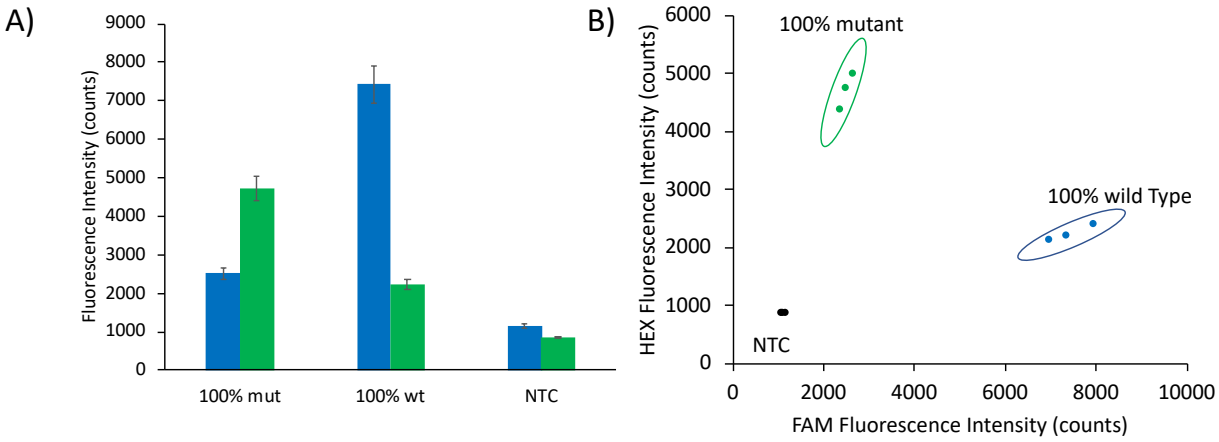


**Figure S7.** (A) End-point fluorescence measurements of reactions containing 100% mutant, 100% wild type, and no template control reactions obtained with a plate reader. (B) Plot of HEX and FAM fluorescence values obtained from each performed reaction.

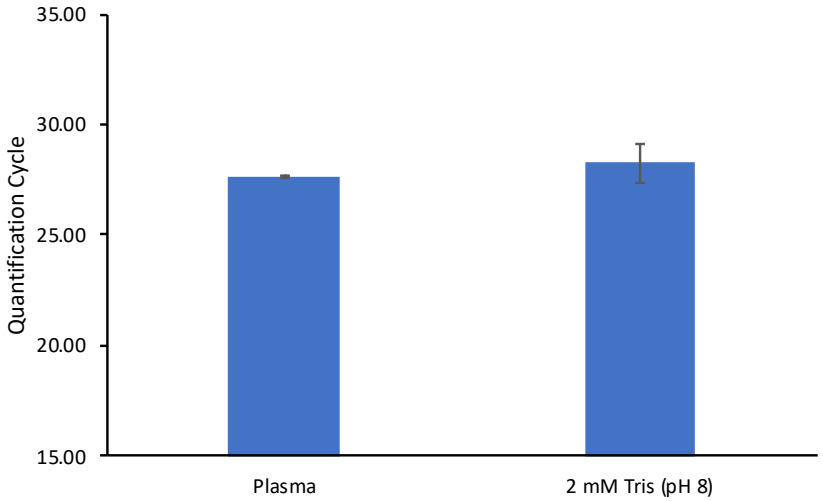


**Figure S8.** qPCR results following blank extractions in either plasma or Tris buffer. Following the blank extraction and desorption, 10 fg of target DNA was added to the desorption solution.

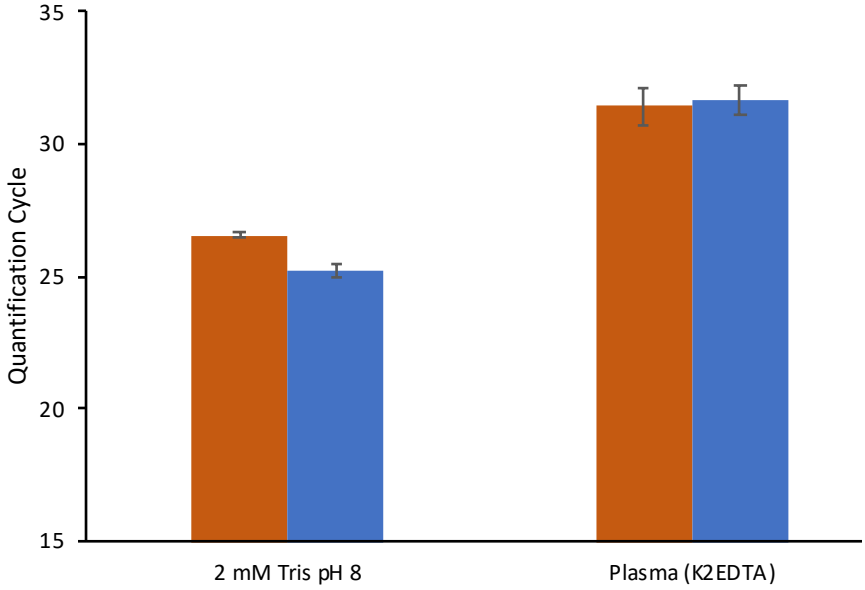


**Figure S9**. Comparison of the extraction from a 10 pg $mL^{-1}$ solution of DNA in Tris and plasma using PIL-SPME or silica-coated magnetic beads. The brown columns represent results from the magnetic beads while the blue columns represent the PIL-SPME results.

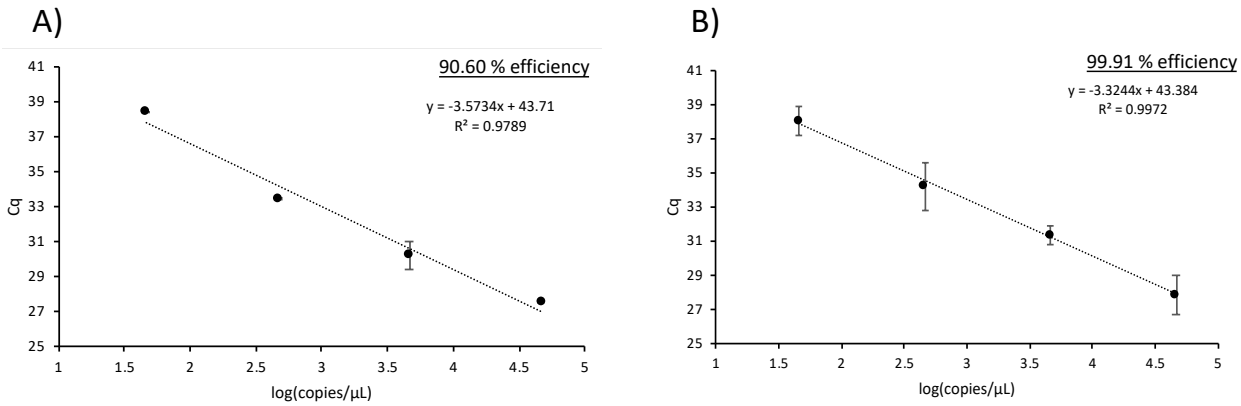


**Figure S10.** Calibration curves constructed by performing PIL-SPME at 4 different concentration-levels of DNA. Extractions were performed in (A) 40 mg $mL^{-1}$ and (B) 4 mg $mL^{-1}$ BSA solutions. Triplicate extractions were performed for each DNA concentration.

# CHAPTER 5. SEQUENCE-SPECIFIC DETECTION OF ORF1A, BRAF, AND OMPW DNA SEQUENCES WITH LOOP MEDIATED ISOTHERMAL AMPLIFICATION ON LATERAL FLOW IMMUNOASSAY STRIPS ENABLED BY MOLECULAR BEACONS

Reprinted with permission from *Analytical Chemistry* 2021, 93, 9, 4149-4153



Marcelino Varona, Derek R. Eitzmann, and Jared L. Anderson

## Abstract

Loop-mediated isothermal amplification (LAMP) holds great potential for point-of-care (POC) diagnostics due to its speed and sensitivity. However, differentiation between spurious amplification and amplification of the target sequence is a challenge. Herein, we develop the use of molecular beacon (MB) probes for the sequence-specific detection of LAMP on commercially-available lateral flow immunoassay (LFIA) strips. The detection of three unique DNA sequences, including ORF1a from SARS-CoV-2, is demonstrated. In addition, the method is capable of detecting clinically-relevant single-nucleotide polymorphisms (BRAF V600E). For all sequences tested, the LFIA method offers similar sensitivity to fluorescence detection using a qPCR instrument. We also demonstrate the coupling of the method with solid-phase microextraction to enable isolation and detection of the target sequences from human plasma, pond water, and artificial saliva. Lastly, a 3D printed device is designed and implemented to prevent contamination caused by opening the reaction containers after LAMP

## Introduction

The SARS-CoV-2 pandemic has revealed the dire need for robust and accurate diagnostic platforms that facilitate rapid detection of pathogens. In particular, diagnostic tools that can provide rapid and accurate information with limited laboratory equipment are highly desirable. These tools shorten the time between receiving a clinical sample and obtaining a result,

significantly increasing sample throughput and allowing prompt administration of treatment. In addition, easy-to-use diagnostics allow for minimally trained individuals to perform analyses and interpret the results, allowing for the facile establishment of testing centers and enabling in-home testing.

Loop-mediated isothermal amplification (LAMP) is a technique that offers distinct advantages over polymerase chain reaction (PCR) including shorter run-times while maintaining lower or equal detection limits.[1,2,3] In addition, LAMP offers increased robustness and resistance to inhibitors compared to PCR.[4] LAMP also possesses high potential for use in point-of-care (POC) diagnostics due to its simplicity of use and compatibility with colorimetric detection methods. Colorimetric LAMP assays have previously been developed for the detection of various targets including *M. tuberculosis*,[5] *E. coli*,[6] and SARS-COV-2.[7–11]

Traditional detection methods for LAMP include turbidimetry, the use of metal indicators such as calcein and hydroxynapthol blue (HNB)[12] and double-stranded DNA binding dyes such as SYBR Green I.[13] These non-specific methods become a hinderance when designing LAMP diagnostics, as false positives become indistinguishable from actual positive samples. Several attempts have been made to develop probe-based systems for the sequence-specific detection of LAMP. These include, but are not limited to, the use of strand displacement probes,[14–16] detection of amplification by release of quenching,[17] fluorogenic bidirectional displacement probes,[18] and more recently molecular beacons (MBs).[19] We have recently exploited MBs in LAMP for the development of POC assays.[20,21] However, these studies required a dedicated instrument for the detection step. To further simplify detection, a system that does not necessitate additional equipment would be highly beneficial. Phillips et al. developed an instrument-free method which used strand displacement probes to enable specific detection on commercially-available lateral

flow immunoassay (LFIA) strips.[16] However, strand displacement probes require a pre-annealing step, thereby increasing the number of overall steps and total assay time. Moreover, these probes, unlike TaqMan and MBs, are not commonly used for PCR-based diagnostics.

In this study, we the leverage the specificity of MBs to enable detection of LAMP on commercially-available LFIA strips. This strategy is implemented for the qualitative detection of three unique, clinically-relevant sequences. Successful detection of the ompW gene of *Vibrio cholera*, BRAF V600E SNP, and ORF1a gene from SARS-CoV-2 is demonstrated. In addition, this detection scheme yields identical sensitivity to real-time fluorescence detection for all studied sequences. In addition to challenges posed by the specific detection of LAMP, the rapid isolation of sufficiently pure nucleic acid (NA) from complex biological matrixes remains a limiting factor in NA-based diagnostics. To address this challenge, we demonstrate the compatibility of this detection method with solid-phase microextraction (SPME) to enable rapid NA isolation and detection from pond water, human plasma, and artificial saliva.

## Experimental

### SPME Extraction Procedure

A schematic of the SPME procedure and chemical composition of the sorbent can be found in Figure S1. A 1.0 mL volume of either pond water, plasma, or artificial saliva was placed in a 1.5 mL DNA LoBind tube (Eppendorf, Hamburg, Germany) and spiked with DNA. The SPME sorbent was inserted through the cap of the tube, immersed in the extraction solution, and agitated with a Fisher-Brand digital vortex mixer (Fisher Scientific, Hampton, NH) for 2 min at 2500 rpm. The fiber was then washed in deionized water and transferred into 10 µL of 1 M NaCl desorption solution for 30 min. A 1 µL aliquot of the desorption solution was then subjected to MB-LAMP with lateral-flow detection.

**SPME Compatible LAMP Buffer**

Reaction mixtures (10 µL) were prepared with the following components: 1.4 mM of each dNTP, 50 mM Tris-HCl pH: 8.8, 8 mM $MgSO_4$, 1.6 µM FIP and BIP primers, 0.2 µM F3 and B3 primers, 0.5 µM of MB, 0.4 µM of biotinylated loop backward primer, 3.2 U Bst 2.0 WarmStart DNA polymerase, and 1 µL of template DNA solution. A 1 µL volume from the SPME desorption solution composed of 1 M NaCl was added into the reaction mixture. Amplification was performed by heating at 60.5 °C for 1 h on a CFX96 Touch real-time PCR detection system with fluorescence measurements being recorded every 30 seconds. All primers and DNA sequences are shown in Table S1. Detailed information regarding the reagents and standard LAMP reactions are provided in the Supporting Information

**3D Printed Device**

The 3D printed device was modeled using Autodesk Inventor Professional 2020. An Ultimaker S3 (Utrecht, Netherlands) was used with Ultimaker ABS filament (2.85 mm). A layer height of 0.2 mm, infill density of 100%, and extruder temperature of 220 °C was used. Additionally, the bed temperature was set to 85 °C.

**Lateral-Flow Immunoassay Assays**

A HybriDetect Universal Lateral Flow Assay Kit was obtained from Milenia Biotec (Giessen, Germany) and used for all lateral-flow experiments. Assays were performed according to the manufacturer's instructions. Additional details can be found in the supporting information.

## Results and Discussion

**MB-LAMP-LFIA Assay Design and Implementation**

The general MB-LAMP-LFIA design is shown in Figure 1A. Briefly, one of the loop primers is converted to a MB labeled with a FAM fluorophore while the other loop primer is biotinylated on the 5' end. This enables incorporation of the biotinylated primer into the amplicon.

The MB imparts specificity by hybridizing to the opposite loop, allowing for detection on the LFIA strip only when the biotinylated primer is incorporated into the amplicon and the MB is hybridized to its complementary loop sequence. MBs are dual-labeled oligonucleotide probes possessing a stem-loop structure.[22] Figure 1B shows a representative depiction of the visual appearance that would be expected on a positive and negative LFIA strip.

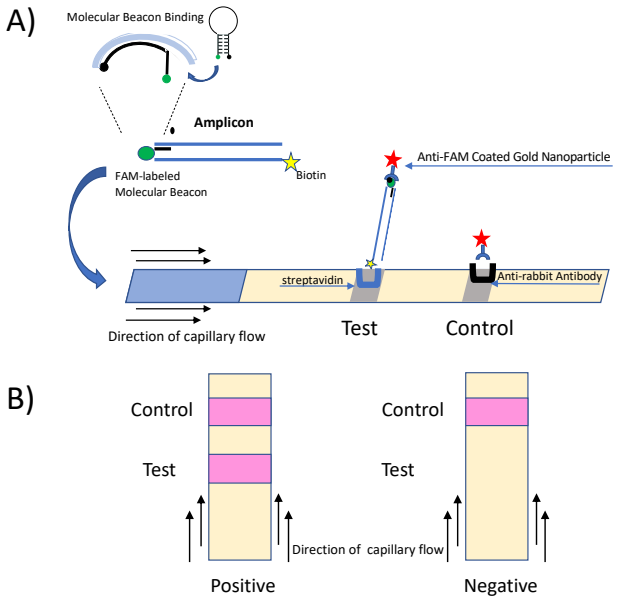


**Figure 1.** A) Schematic representation of MB-LAMP detection on a commercially-available LFIA strip. B) Representative illustration of LFIA strips indicating positive or negative samples.

In a proof-of-concept experiment, LFIA detection was first attempted with the ompW and BRAF sequences. Initial experiments demonstrated clear, specific detection of amplicons on the LFIA strips, as evidenced by the dark test band that appeared when the target sequence was present. Figure S2 demonstrates the sensitivity of the method for each of the chosen sequences. For the ompW sequence, 226 copies per reaction could be observed on the LFIA strips based on triplicate reactions. In addition, two-thirds of the reactions containing 22.6 copies yielded positive results. This sensitivity is equal to that obtained using real-time detection (Figure S3), indicating no decrease in performance when the MB-LAMP-LFIA method was employed. It should also be noted that the intensity of the test bands remained virtually identical when examining different

template concentrations. This can be observed by both visual examination of the LFIA strips (Figure 2 A,C) and by ImageJ analysis (Figure 2 B,D). The ability to obtain high test band intensities even when low concentrations of target are amplified is highly beneficial for the unambiguous determination of positive samples. Similarly, as few as 22.4 copies per reaction of the BRAF sequence could be detected in triplicate. These results were also consistent with real-time sensitivity values (Figure S4).

The developed method was then compared with a previous strategy for LAMP detection on LFIA strips that relied on the labeling of the loop primers with either a biotin or FAM moiety.[23,24] As demonstrated in Figures S5 and S6, the labeled primer strategy yielded similar sensitivity to the MB-LAMP method for both the ompW and BRAF sequences. However, light test bands could be observed for the NTCs and the $10^0$ copies per reaction of the ompW sequence, indicating lack of specificity of the traditional method (Figure S5 A,B) .

**Single-Nucleotide Polymorphism (SNP) Detection**

To determine whether MB-LAMP could enable SNP detection on a LFIA strip, triplicate MB-LAMP reactions for a wild-type BRAF sequence and the BRAF V600E variant were performed with a MB complementary to the wild-type BRAF. Figure 2 shows the resulting images and ImageJ analysis following MB-LAMP with LFIA analysis of both wild-type and mutant sequences. Visually, the wild-type can be easily differentiated from the mutant sequence. While a faint test band does appear when the mutant is amplified, the resulting intensity from the wild-type sequence is over 2-times greater, as shown in Figure 2B. As shown in Figure S7, there is no difference in intensity, either visually or with ImageJ analysis, between the wild-type and mutant sequences when the traditional strategy is employed. This result highlights the specificity imparted by the MB when used in LAMP for LFIA detection.

SNPs often represent a small percentage of the total NA population within a sample. Therefore, detecting the target sequence in the presence of interfering sequence is highly desirable. The ability of the MB-LAMP-LFIA method to detect the wild-type sequence in the presence of various amounts of mutant DNA was investigated. It can be observed in Figure 2C that the method is able to detect the wild-type sequence in a 1:1 copy number ratio with the mutant sequence. However, when higher amounts of the mutant sequence are present, the method is unable to detect the wild-type sequence. Future work will focus on developing strategies to enable detection of lower target:mutant ratios.

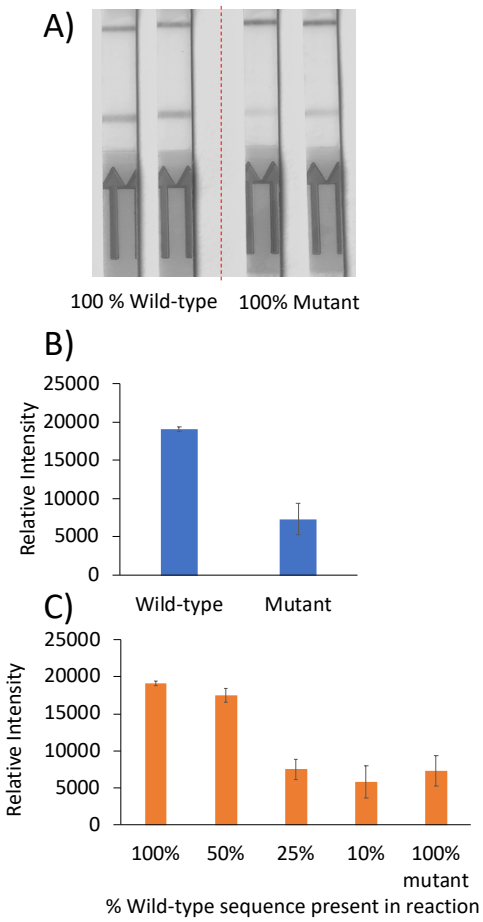


**Figure 2.** A) MB-LAMP-LFIA strips of the wild-type or mutant BRAF sequences using a FAM-labeled MB complementary to the wild-type sequence. B) Intensity of the test bands following ImageJ analysis of 100% wild-type and 100% mutant BRAF sequences. C) Resulting intensities of the test-bands following ImageJ analysis of various ratios of wild-type:mutant sequence. Triplicate reactions were used for analyses performed on ImageJ.

**Assay design for ORF1a detection**

Enabling the rapid and simple detection of the SARS-CoV-2 virus is of high worldwide significance. Traditional reverse transcription (RT)-PCR methods can detect extremely low quantities of the viral target ($10^1$-$10^2$ copies per reaction)[25]; however, centralized laboratories are required to perform the analysis due to the specialized instruments required and need for highly trained personnel. Enzyme linked immunosorbent assays are an alternative to RT-PCR and require less equipment. However, these tests have higher rates of false negatives compared to RT-PCR tests which can lead to an underestimation of total positive cases.[26]The development of an MB-LAMP method compatible with the LFIA detection scheme would be highly beneficial. Such a method would provide high accuracy, due to the specificity imparted by the MB probe, and facilitate easy interpretation of results. Several LAMP methods have been developed for SARS-CoV-2 detection. However, the majority of these methods rely on non-specific, colorimetric indicators for positive sample identification. Very recently, a preprint by Sherrill-Mix et al. demonstrated the use of molecular beacons containing locked nucleic acid bases in LAMP for the fluorescence detection of SARS-CoV-2.[27]

A recently developed LAMP primer set by Zhang et al. targeting the ORF1a gene of the SARS-CoV-2 virus was used for the assay in this study, with some modifications.[10] The forward loop primer was chosen to be converted into a MB, while the backward loop primer was biotinylated at the 5' end. MB stem length plays an important role in determining the MB's annealing temperature to its desired target. Two MBs with stems consisting of 5 and 6 nucleotides (nt) were designed and used for LAMP analysis with real-time fluorescence and LFIA detection. Figure 3A shows the LFIA strips following amplification with each MB. Visually, the test band is significantly darker when the 5-nt stem MB is used. ImageJ analysis, shown in Figure 3B, reveals

that the 5-nt stem MB yields an approximate two-fold increase in band intensity compared to the 6-nt stem MB. In both cases, the NTCs remained clear without a test-band. Annealing profiles were performed with both MBs to determine whether the annealing temperature to the target was dependent on stem length and if these results correlated to the observed band intensities. Fluorescence plots in Figure S8 show an apparent decrease in the melting temperature of the MB to its target when the stem length is increased from 5 to 6 nucleotides.

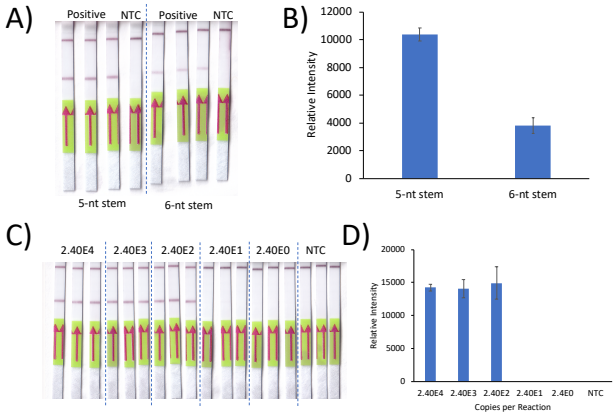


**Figure 3**. A) MB-LAMP-LFIA analysis of the ORF1a gene from SARS-CoV-2 using either a 5-nt stem or 6-nt stem MB for analysis. B) ImageJ analysis of the band intensities obtained from the 5-nt stem and 6-nt stem molecular beacons following MB-LAMP. C) Image of sensitivity results using the 5-nt stem MB and D) ImageJ analysis of the test-bands. Triplicate reactions were performed for all ImageJ analyses.

MB concentration could play a significant role in the perceived intensity of the test band, and therefore in assay efficacy. Initially, several concentrations of MB ranging from 0.1-0.6 µM were tested using real-time fluorescence monitoring and LFIA analysis. Results in Figure S9 (A-B) show that test-band intensity remains fairly constant across the concentrations tested, with minimal drop-off between the highest (0.6 µM) and lowest (0.1 µM) concentrations. Interestingly, when compared with the real-time fluorescence results, the decrease in the endpoint fluorescence with lower MB concentrations following amplification is significant (Figure S9 C,D). Several lower concentrations of MB (0.05 µM-0.005 µM) were also tested to identify where a decrease in the test-band intensity may be observed. Results shown in Figure S10 illustrate a perceived

decrease in the test band intensity for the concentrations tested. In particular, 0.025 μM and 0.005 μM have significantly different appearance and intensities when compared with 0.05 μM. When compared to the real-time results, the 0.025 μM and 0.005 μM samples were unable to be detected. These results suggest that LFIA detection is more tolerant to changes in MB concentration than real-time fluorescence detection. The sensitivity was then determined for LFIA detection using the 5-nt stem MB. Results in Figure 3 C and D show the method is capable of detecting as few as $2.3\times10^2$ copies per reaction. These results are consistent with the real-time data obtained in our laboratory as well as previously demonstrated colorimetric and real-time results.[11]

**Isolation of DNA from Complex Matrices using SPME**

NA isolation from complex samples is a critical step in order to minimize the introduction of inhibitors into the enzymatic reaction and increase DNA concentration for optimal detection. SPME is a sample preparation technique that circumvents some of the drawbacks of traditional methods. Recently, polymeric ionic liquids (PIL) have been shown as SPME sorbent phases for the isolation of NAs from complex samples.[28,29] During the desorption step, 1 M NaCl is used to desorb DNA from the PIL-based sorbent phase. However, high salt concentration is known to inhibit and delay LAMP reactions.[28] To circumvent this, a custom-buffer was developed that used NaCl from the desorption solution to avoid dilution.[28] Figure S11 illustrates a comparison between LFIA following MB-LAMP of pure ORF1a sequence in either NEB Isothermal Buffer or the custom-buffer. As shown, the resulting test-band intensities are similar between the two buffers, indicating similar performance on the LFIA strips. Triplicate extractions were performed from human plasma spiked with the wild-type BRAF sequence at clinically-relevant concentrations ($10^7$ copies $mL^{-1}$).[30] Successful detection was achieved on the LFIA strips in all extractions performed. Table S2 contains a summary of the MB-LAMP-LFIA results after SPME from all matrices tested. Detection was also achieved for ompW and ORF1a in pond water and artificial saliva, respectively.

A recent study suggested that saliva may yield better sensitivity for SARS-CoV-2 virus detection compared to nasopharyngeal swabs,[31] which would allow for easier sample collection and lower detection limits.

**Integration of 3D Printed Device to Minimize Contamination**

A significant disadvantage of LFIA is the need to open the reaction containers following amplification to add the assay diluent and the strip. Opening the reaction container can lead to widespread contamination of the environment with the amplicon, leading to positive NTCs. A closed system where the amplification and subsequent detection step can be performed is highly desirable. Commercially-available systems that can enclose reaction systems post-amplification to enable detection on LFIA do exist. However, this system increases the cost and complexity of analysis. A closed system where the amplification step and LFIA detection can be performed all-in-one would be highly beneficial.

3D printing represents a promising alternative for the creation of cheap, simple, and easy-to-use diagnostic devices. In this study, fused-deposition modeling is used to create a device that can mitigate contamination by enclosing amplification and LFIA detection. Figure S12 shows a model and image of the device. The device is composed of two "trap doors" and one inlet to enable the addition of the LFIA buffer. During amplification, the device is placed over a conventional polypropylene PCR tube and a 3D printed covering is placed through slit #1 and slit #2 (Figure S12). The LFIA strip is placed in the device and rests on slit #2 while amplification progresses. After amplification, the covering on slit #1 can be removed and the assay buffer inserted through the diluent port. Once the reaction mixture and assay buffer are mixed, the covering from slit #2 can be removed to allow the LFIA strip to reach the resulting mixture and enable detection through the LFIA test viewing window. This device is also compatible with PCR, recombinase polymerase amplification or any other amplification-based technique coupled with LFIA detection.

## Conclusion

In this study, the instrument-free, specific detection of LAMP enabled by molecular beacons was demonstrated on commercially-available LFIA strips. The versatility of the method was demonstrated by the successful detection of three unique, clinically relevant sequences (ompW, BRAF, and ORF1a). High specificity was also demonstrated through the detection and differentiation of a clinically-relevant SNP (BRAF V600E). In addition, SPME is shown to be compatible with the developed MB-LAMP-LFIA method to enable detection of nucleic acid sequences from pond water, human plasma, and artificial saliva. The developed method has potential for use in low-resource settings and peripheral laboratories to enable sensitive and specific detection of diseases.

## Supporting Information

DNA primers and sequences used, PIL structure, SPME extraction results, sensitivity for LAMP assays, annealing profiles, MB concentration optimization, 3D printed device diagram and image, reagents, and LAMP conditions can be found in Appendix E: Supporting Information Chapter 5

## Acknowledgements

J.L.A. acknowledges funding from the Chemical Measurement and Imaging Program at the National Science Foundation (Grant No. CHE-1709372). J.L.A. and D.R.E. thank the Alice Hudson Professorship for support.

## References

(1) Notomi, T.; Okayama, H.; Masubuchi, H.; Yonekawa, T.; Watanabe, K.; Amino, N.; Hase, T. Loop-Mediated Isothermal Amplification of DNA. *Nucleic Acids Res.* **2000**, *28*, E63.

(2) Zhang, S. Y.; Dai, D. J.; Wang, H. D.; Zhang, C. Q. One-Step Loop-Mediated Isothermal Amplification (LAMP) for the Rapid and Sensitive Detection of Fusarium Fujikuroi in Bakanae Disease through NRPS31, an Important Gene in the Gibberellic Acid Bio-Synthesis. *Sci. Rep.* **2019**, *9*.

(3) Khan, M.; Wang, R.; Li, B.; Liu, P.; Weng, Q.; Chen, Q. Comparative Evaluation of the LAMP Assay and PCR-Based Assays for the Rapid Detection of Alternaria Solani. *Front. Microbiol.* **2018**, *9*, 2089.

(4) Alhassan, A.; Thekisoe, O. M. M.; Yokoyama, N.; Inoue, N.; Motloang, M. Y.; Mbati, P. A.; Yin, H.; Katayama, Y.; Anzai, T.; Sugimoto, C.; Igarashi, I. Development of Loop-Mediated Isothermal Amplification (LAMP) Method for Diagnosis of Equine Piroplasmosis. *Vet. Parasitol.* **2007**, *143*, 155–160.

(5) Yee, E. H.; Sikes, H. D. Polymerization-Based Amplification for Target-Specific Colorimetric Detection of Amplified Mycobacterium Tuberculosis DNA on Cellulose. *ACS Sensors* **2020**, *5*, 308–312.

(6) Carnevale, M. L.; Roche, P. J. R.; Najih, M.; Paliouras, M.; Beitel, L. K.; Trifiro, M. A. A Rapid Diagnostic Method for E. Coli Serogroups Responsible for Gastro-Intestinal Diseases Using Loop-Mediated Isothermal Amplification. *Anal. Methods* **2015**, *7*, 287–295.

(7) Yang, W.; Dang, X.; Wang, Q.; Xu, M.; Zhao, Q.; Zhou, Y.; Zhao, H.; Wang, L.; Xu, Y.; Wang, J.; Han, S.; Wang, M.; Pei, F.; Wang, Y. Rapid Detection of SARS-CoV-2 Using Reverse Transcription RT-LAMP Method. *medRxiv* **2020**. https://doi.org/10.1101/2020.03.02.20030130.

(8) Lamb, L.; Bartolone, S.; Ward, E.; Chancellor, M. Rapid Detection of Novel Coronavirus (COVID-19) by Reverse Transcription-Loop-Mediated Isothermal Amplification. *medRxiv* **2020**. https://doi.org/10.1101/2020.02.19.20025155.

(9) El-Tholoth, M.; Bau, H. H.; Song, J. A Single and Two-Stage, Closed-Tube, Molecular Test for the 2019 Novel Coronavirus (COVID-19) at Home, Clinic, and Points of Entry. *ChemRxiv* **2020**. https://doi.org/10.26434/chemrxiv.11860137.

(10) Zhang, Y.; Odiwuor, N.; Xiong, J.; Sun, L.; Nyaruaba, R. O.; Wei, H.; Tanner, N. Rapid Molecular Detection of SARS-CoV-2 (COVID-19) Virus RNA Using Colorimetric LAMP. *medRxiv* **2020**. https://doi.org/10.1101/2020.02.26.20028373.

(11) Yu, L.; Wu, S.; Hao, X.; Dong, X.; Mao, L.; Pelechano, V.; Chen, W. H.; Yin, X. Rapid Detection of COVID-19 Coronavirus Using a Reverse Transcriptional Loop-Mediated Isothermal Amplification (RT-LAMP) Diagnostic Platform. *Clin. Chem.* **2020**, *66*, 975–977.

(12) Goto, M.; Honda, E.; Ogura, A.; Nomoto, A.; Hanaki, K. I. Colorimetric Detection of Loop-Mediated Isothermal Amplification Reaction by Using Hydroxy Naphthol Blue. *Biotechniques* **2009**, *46*, 167–172.

(13) Ding, X.; Wu, W.; Zhu, Q.; Zhang, T.; Jin, W.; Mu, Y. Mixed-Dye-Based Label-Free and Sensitive Dual Fluorescence for the Product Detection of Nucleic Acid Isothermal Multiple-Self-Matching-Initiated Amplification. *Anal. Chem.* **2015**, *87*, 10306–10314.

(14) Du, Y.; Pothukuchy, A.; Gollihar, J. D.; Nourani, A.; Li, B.; Ellington, A. D. Coupling Sensitive Nucleic Acid Amplification with Commercial Pregnancy Test Strips. *Angew. Chemie - Int. Ed.* **2017**, *56*, 992–996.

(15) Jiang, Y. S.; Bhadra, S.; Li, B.; Wu, Y. R.; Milligan, J. N.; Ellington, A. D. Robust Strand Exchange Reactions for the Sequence-Specific, Real-Time Detection of Nucleic Acid Amplicons. *Anal. Chem.* **2015**, *87*, 3314–3320.

(16) Phillips, E. A.; Moehling, T. J.; Bhadra, S.; Ellington, A. D.; Linnes, J. C. Strand Displacement Probes Combined with Isothermal Nucleic Acid Amplification for Instrument-Free Detection from Complex Samples. *Anal. Chem.* **2018**, *90*, 6580–6586.

(17) Gadkar, V. J.; Goldfarb, D. M.; Gantt, S.; Tilley, P. A. G. Real-Time Detection and Monitoring of Loop Mediated Amplification (LAMP) Reaction Using Self-Quenching and De-Quenching Fluorogenic Probes. *Sci. Rep.* **2018**, *8*, 1–10.

(18) Ding, X.; Wang, G.; Sun, J.; Zhang, T.; Mu, Y. Fluorogenic Bidirectional Displacement Probe-Based Real-Time Isothermal DNA Amplification and Specific Visual Detection of Products. *Chem. Commun.* **2016**, *52*, 11438–11441.

(19) Liu, W.; Huang, S.; Liu, N.; Dong, D.; Yang, Z.; Tang, Y.; Ma, W.; He, X.; Ao, D.; Xu, Y.; Zou, D.; Huang, L. Establishment of an Accurate and Fast Detection Method Using Molecular Beacons in Loop-Mediated Isothermal Amplification Assay. *Sci. Rep.* **2017**, *7*, 40125.

(20) Varona, M.; Anderson, J. L. Visual Detection of Single-Nucleotide Polymorphisms Using Molecular Beacon Loop-Mediated Isothermal Amplification with Centrifuge-Free DNA Extraction. *Anal. Chem.* **2019**, *91*, 6991–6995.

(21) Varona, M.; Eitzmann, D. R.; Pagariya, D.; Anand, R. K.; Anderson, J. L. Solid-Phase Microextraction Enables Isolation of BRAF V600E Circulating Tumor DNA from Human Plasma for Detection with a Molecular Beacon Loop-Mediated Isothermal Amplification Assay. *Anal. Chem.* **2020**, *92*, 3346–3353.

(22) Tyagi, S.; Kramer, F. R. Molecular Beacons: Probes That Fluoresce upon Hybridization. *Nat. Biotechnol.* **1996**, *14*, 303–308.

(23) Rodriguez, N. M.; Linnes, J. C.; Fan, A.; Ellenson, C. K.; Pollock, N. R.; Klapperich, C. M. Paper-Based RNA Extraction, in Situ Isothermal Amplification, and Lateral Flow Detection for Low-Cost, Rapid Diagnosis of Influenza A (H1N1) from Clinical Specimens. *Anal. Chem.* **2015**, *87*, 7872–7879.

(24) Singleton, J.; Osborn, J. L.; Lillis, L.; Hawkins, K.; Guelig, D.; Price, W.; Johns, R.; Ebels, K.; Boyle, D.; Weigl, B.; LaBarre, P. Electricity-Free Amplification and Detection for Molecular Point-of-Care Diagnosis of HIV-1. *PLoS One* **2014**, *9*.

(25) Vogels, C. B. F.; Brito, A. F.; Wyllie, A. L.; Fauver, J. R.; Ott, I. M.; Kalinich, C. C.; Petrone, M. E.; Casanovas-Massana, A.; Catherine Muenker, M.; Moore, A. J.; Klein, J.; Lu, P.; Lu-Culligan, A.; Jiang, X.; Kim, D. J.; Kudo, E.; Mao, T.; Moriyama, M.; Oh, J. E.; Park, A.; Silva, J.; Song, E.; Takahashi, T.; Taura, M.; Tokuyama, M.; Venkataraman, A.; Weizman, O. El; Wong, P.; Yang, Y.; Cheemarla, N. R.; White, E. B.; Lapidus, S.; Earnest, R.; Geng, B.; Vijayakumar, P.; Odio, C.; Fournier, J.; Bermejo, S.; Farhadian, S.; Dela Cruz, C. S.; Iwasaki, A.; Ko, A. I.; Landry, M. L.; Foxman, E. F.; Grubaugh, N. D. Analytical Sensitivity and Efficiency Comparisons of SARS-CoV-2 RT–QPCR Primer–Probe Sets. *Nat. Microbiol.* **2020**, *5*, 1299–1305.

(26) Grant, B. D.; Anderson, C. E.; Williford, J. R.; Alonzo, L. F.; Glukhova, V. A.; Boyle, D. S.; Weigl, B. H.; Nichols, K. P. SARS-CoV-2 Coronavirus Nucleocapsid Antigen-Detecting Half-Strip Lateral Flow Assay toward the Development of Point of Care Tests Using Commercially Available Reagents. *Anal. Chem.* **2020**, *92*, 11305–11309.

(27) Sherrill-Mix, S.; Hwang, Y.; Roche, A. M.; Weiss, S. R.; Li, Y.; Graham-Wooten, J.; Taylor, L. J.; Collman, R. G.; Van Duyne, G. D.; Bushman, F. D. LAMP-BEAC: Detection of SARS-CoV-2 RNA Using RT-LAMP and Molecular Beacons. *medRxiv* **2020**. https://doi.org/10.1101/2020.08.13.20173757.

(28) Varona, M.; Ding, X.; Clark, K. D.; Anderson, J. L. Solid-Phase Microextraction of DNA from Mycobacteria in Artificial Sputum Samples to Enable Visual Detection Using Isothermal Amplification. *Anal. Chem.* **2018**, *90*, 6922–6928.

(29) Nacham, O.; Clark, K. D.; Anderson, J. L. Extraction and Purification of DNA from Complex Biological Sample Matrices Using Solid-Phase Microextraction Coupled with Real-Time PCR. *Anal. Chem.* **2016**, *88*, 7813–7820. https://doi.org/10.1021/acs.analchem.6b01861.

(30) Kelley, S. O. What Are Clinically Relevant Levels of Cellular and Biomolecular Analytes? *ACS Sensors* **2017**, *2*, 193–197.

(31) Wyllie, A. L.; Fournier, J.; Casanovas-Massana, A.; Campbell, M.; Tokuyama, M.; Vijayakumar, P.; Geng, B.; Muenker, M. C.; Moore, A.; Vogels, C.; Petrone, M.; Ott, I.; Lu, P.; Lu-Culligan, A.; Klein, J.; Venkataraman, A.; Earnest, R.; Simonov, M.; Datta, R.; Handoko, R.; Naushad, N.; Sewanan, L.; Valdez, J.; White, E.; Lapidus, S.; Kalinich, C.; Jiang, X.; Kim, D.; Kudo, E.; Linehan, M.; Mao, T.; Moriyama, M.; Oh, J. E.; Park, A.; Silva, J.; Song, E.; Takahashi, T.; Taura, M.; Weizman, O.-E.; Wong, P.; Yang, Y.; Bermejo, S.; Odio, C.; Omer, S.; Dela Cruz, C.; Farhadian, S.; Martinello, R.; Iwasaki, A.; Grubaugh, N.; Ko, A. Saliva Is More Sensitive for SARS-CoV-2 Detection in COVID-19 Patients than Nasopharyngeal Swabs. *medRxiv* **2020**. https://doi.org/10.1101/2020.04.16.20067835.

## Appendix D: Supporting Information Chapter 5

**Table S1.** DNA sequences, primers, and probes used in this study

| | |
|---|---|
| Wild type BRAF | 5'-<br>TATATTTCTTCATGAAGACCTCACAGTAAAAATAGGTGATTTTG<br>GTCTAGCTACAGTGAAATCTCGATGGAGTGGGTCCCATCAGTTT<br>GAACAGTTGTCTGGATCCATTTTGTGGATGGTAAGAATTGAGGC<br>TATTTTTCCACTGATTAAATTTTTGGCCCTGAGATGCTGCTGAGT<br>TAC TAGAAAGTCATTGAAGGTCTCAACTATAGT-3' |
| Mutant V600E BRAF | 5'-<br>TATATTTCTTCATGAAGACCTCACAGTAAAAATAGGTGATTTTG<br>GTCTAGCTACAG**A**GAAATCTCGATGGAGTGGGTCCC<br>ATCAGTTTGAACAGTTGTCTGGATCCATTT<br>TGTGGATGGTAAGAATTGAGGCTATTTTTCCACTGATTAAATTTT<br>TGGCCCTGAGATGCTGCTGAGTTACTAGAAAGTCATTGAAGGTC<br>T CAACTATAGT-3' |
| BRAF_FIP | 5'-TCCAGACAACTGTTCAAACTGATGGTGATTTTGGTCTAG-3' |
| BRAF_BIP | 5'-TTGTGGATGGTAAGAATTGAGGC-<br>TTTCTAGTAACTCAGCAGCA-3' |
| BRAF_F3 | 5'-TCTTCATGAAGACCTCACAG-3' |
| BRAF_B3 | 5'-CTATAGTTGAGACCTTCAATGAC-3' |
| BRAF_LB | 5'-biotin-TCCACTGATTAAATTTTTGGCCCTG-3 |
| BRAF MB | 5'-FAM-CGCGCCCACTCCATCGAGATTTCACTGGCGCG-IABKFQ-3' |
| BRAF_LF_FAM | 5'-FAM-CCCACTCCATCGAGATTTCACTG-3' |
| ompW | CCTAAATGTAGCAAATTGATTTCCTACAAGTTTGTGTGATTTTTG<br>TGTGCTACTGT<br>GCGCGCAACACAAAGATAACAACATAGCCCTACAAAAAAGGAA<br>AACGTCATGAA<br>ACAAACCATTTGCCTAGCCGTACTTGCAGCCCTACTAGCCGCTC<br>CTGTATTTGC<br>TCACCAAGAAGGTGACTTTATTGTGCGCGCGGGTATTGCCTCGG<br>TAGTACCTAA<br>TGAC |
| ompW_BIP | 5'-ACCATTTGCCTAGCCGTACTACAATAAAGTCACCTTCTTGG-3' |

**Table S1.** Continued

| | |
|---|---|
| ompW_FIP | 5'-TCCTTTTTTGTAGGGCTATGTTGTTGTTTGTGTGATTTTTGTGTGC-3' |
| ompW_B3 | 5'-GTCATTAGGTACTACCGAGG-3' |
| ompW_F3 | 5'-CCTAAATGTAGCAAATTGATTTCCT-3' |
| ompW_LF | 5'-biotin-TGTGTTGCGCGCACAGTA-3' |
| ompW_MB | 5'-FAM-AGCGGCTGCAGCCCTACTAGCCGCT-Dabcyl-3' |
| ompW_LB_FAM | 5'-FAM-TGCAGCCCTACTAGCCGCT-3' |
| ORF1a | CCCTATGTGTTCATCAAACGTTCGGATGCTCGAACTGCACCTCATGGTCATGTTATGGTTGAGCTGGTAGCAGAACTCGAAGGCATTCAGTACGGTCGTAGTGGTGAGACACTTGGTGTCCTTGTCCCTCATGTGGGCGAAATACCAGTGGCTTACCGCAAGGTTCTTCTTCGTAAGAACGGTAATAAAGGAGCTGGTGGCCATAGTTACGGCGCCGATCTAAAGTCATTTGACTTAGGCGACGAGCTTGGCACTGATCCTTATGAAGA |
| ORF1a_BIP | 5'-CCAGTGGCTTACCGCAAGGTTTTAGATCGGCGCCGTAAC-3' |
| ORF1a_FIP | 5'-GAGGGACAAGGACACCAAGTGTATGGTTGAGCTGGTAGCAGA-3' |
| ORF1a_F3 | 5'-CTGCACCTCATGGTCATGTT-3' |
| ORF1a_B3 | 5'-AGCTCGTCGCCTAAGTCAA-3' |
| ORF1a_LB | 5'-biotin-TTCGTAAGAACGGTAATAAAGGAGC-3' |
| ORF1a_6-nt_stemMB | 5'-FAM-CGGCCG TAC TGA ATG CCT TCG AGT CGGGCG-IABKFQ-3' |
| ORF1a_5nt_stemMB | 5'-FAM-CGCCG TAC TGA ATG CCT TCG AGT CGGCG-IABKFQ-3' |
| ORF1a_MB_complement | 5'-ACTCGAAGGCATTCAGTACGG-3' |

Bolded letter denotes the location of the BRAF V600E mutation

**Table S2.** Summary of MB-LAMP-LFIA results following SPME from human plasma, pond water, and artificial saliva.

| BRAF from Human Plasma | |
|---|---|
| DNA concentration | Positive Samples |
| $10^7$ copies $mL^{-1}$ | 3/3 |
| $10^6$ copies $mL^{-1}$ | 2/3 |
| $10^5$ copies $mL^{-1}$ | 0/0 |
| ompW from Pond Water | |
| DNA concentration | Positive Samples |
| $10^7$ copies $mL^{-1}$ | 3/3 |
| $10^6$ copies $mL^{-1}$ | 3/3 |

**Table S2.** Continued

| | |
|---|---|
| $10^5$ copies $mL^{-1}$ | 0/3 |
| ORF1a from Artificial Saliva | |
| DNA concentration | Positive Samples |
| $10^7$ copies $mL^{-1}$ | 3/3 |
| $10^6$ copies $mL^{-1}$ | 3/3 |
| $10^5$ copies $mL^{-1}$ | 0/3 |

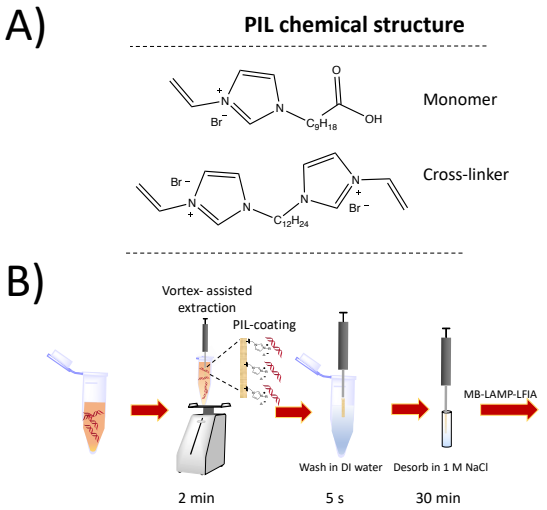


**Figure S1.** A) Chemical structure of polymeric ionic liquid sorbent phase used for SPME analysis. B) Representative schematic of SPME

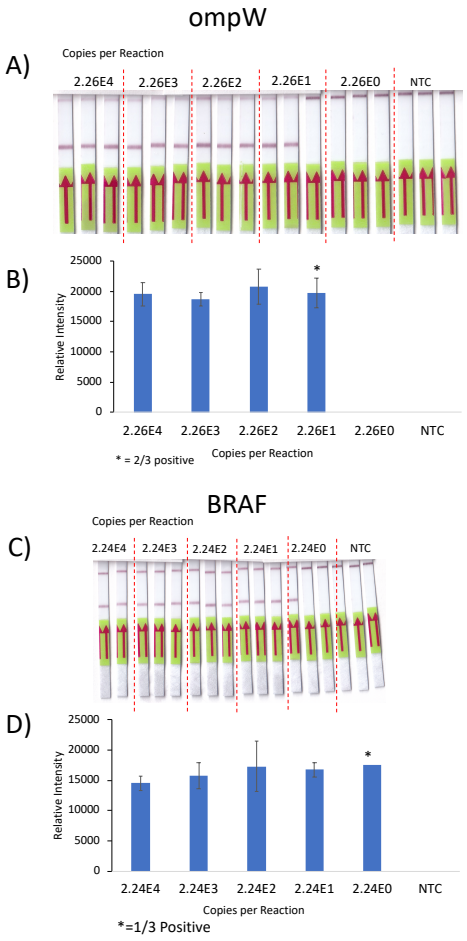


**Figure S2.** Images demonstrating the sensitivity of the MB-LAMP-LFIA method for the (A) ompW sequence and (C) BRAF sequences and resulting test-band intensities obtained from ImageJ analysis (B, D).

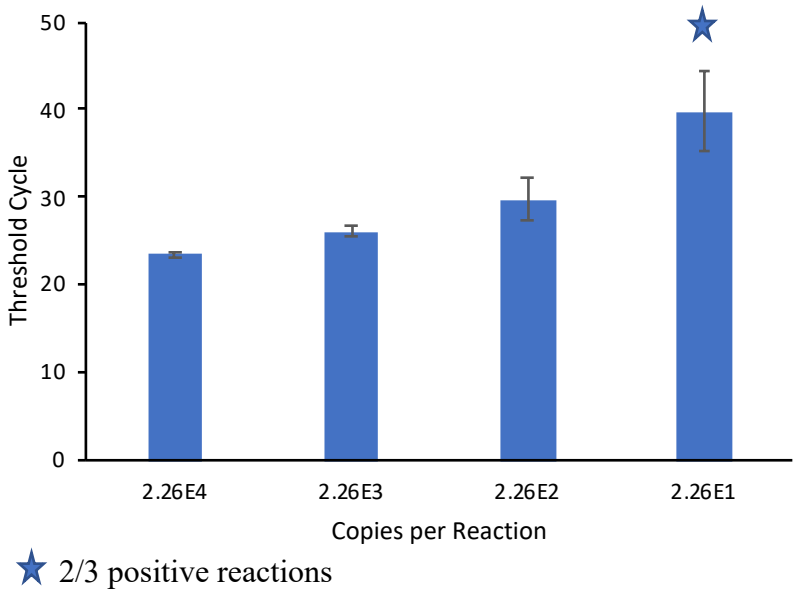


**Figure S3.** Sensitivity results obtained from real-time fluorescence plots following MB-LAMP of the ompW sequence.

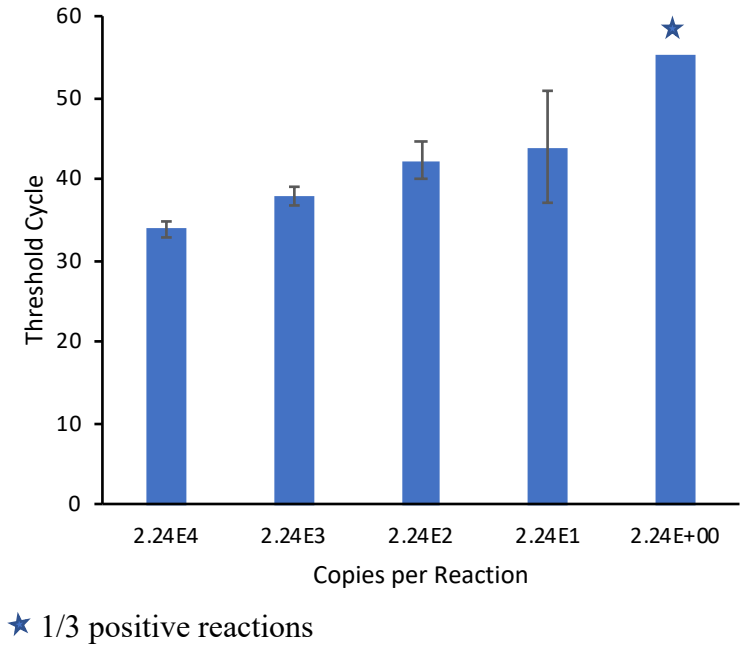


**Figure S4.** Sensitivity results from the BRAF sequence after MB-LAMP amplification obtained from the real-time fluorescence plots.

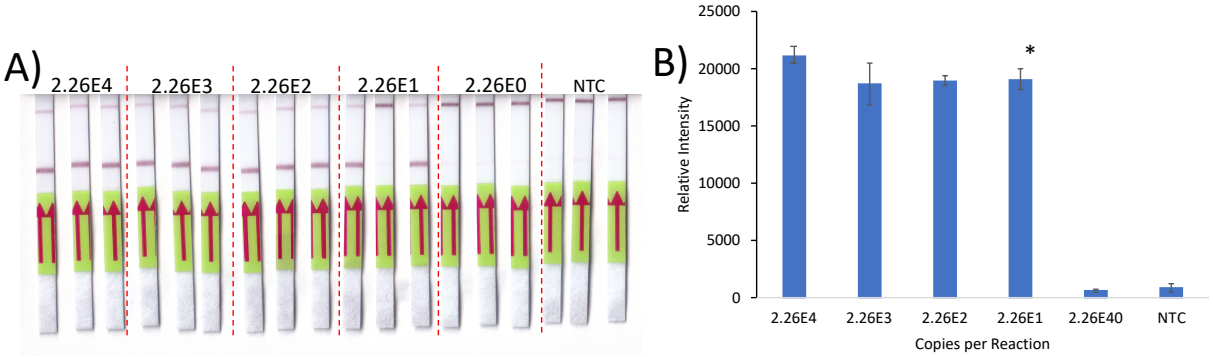


**Figure S5**. A) Sensitivity results derived from using the labeled primer strategy for the ompW sequence. B) ImageJ analysis of the test-bands derived from the sensitivity experiment.

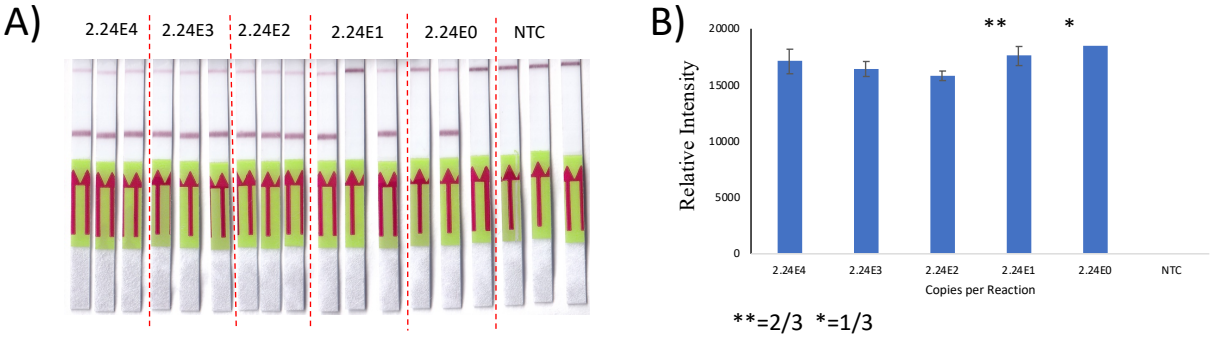


**Figure S6.** A) Image of the sensitivity results when the labeled primer strategy for the BRAF sequence was employed. B) ImageJ analysis of the test-bands derived from the sensitivity experiment.

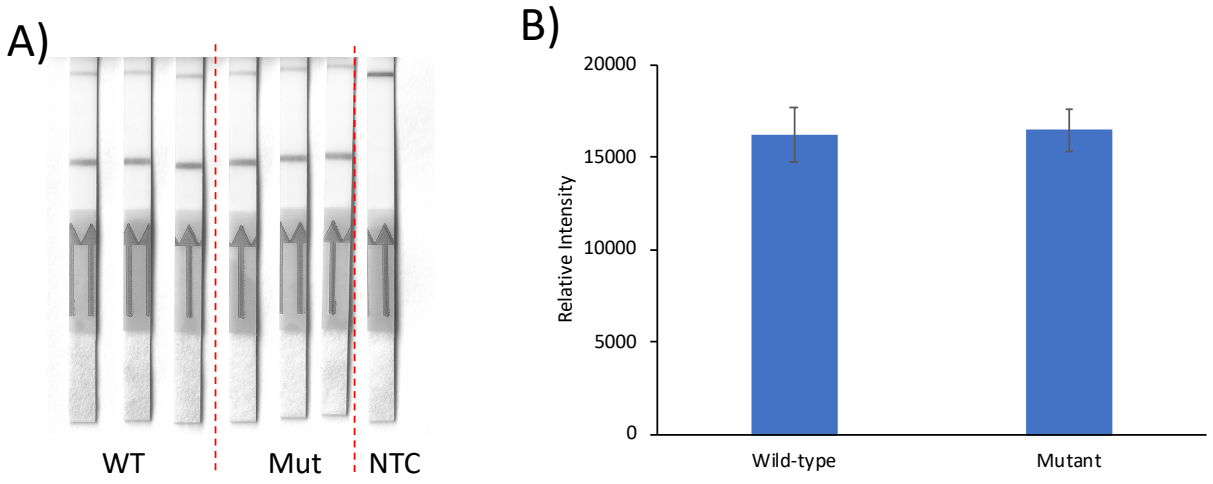


**Figure S7.** Detection of wild-type or mutant BRAF V600E using the labeled primer strategy. A) Image of LFIA strips following LAMP and (B) subsequent analysis using ImageJ.

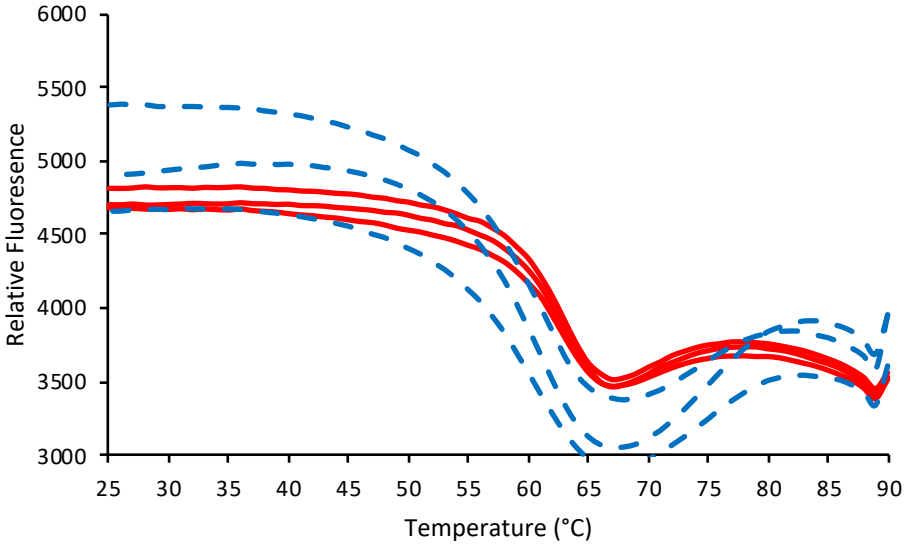


**Figure S8.** Fluorescence plots of annealing profiles performed with the ORF1a 5-nt stem MB (red) and 6-nt stem MB (blue).

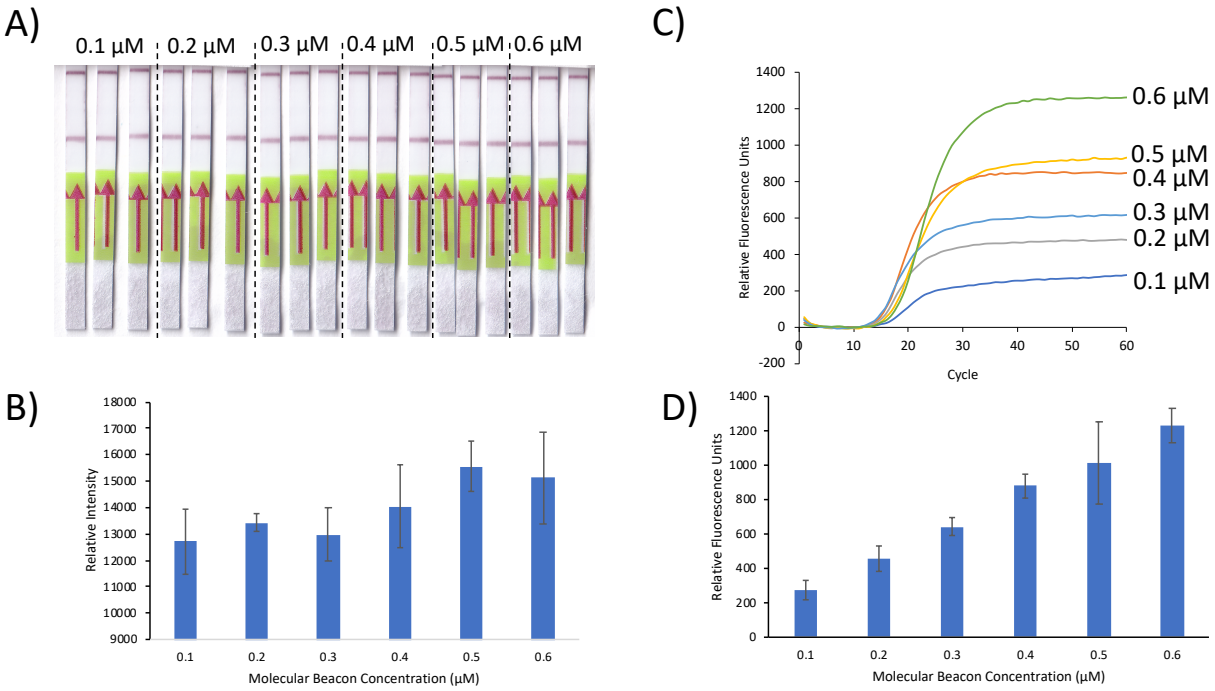


**Figure S9.** (A) Effect of MB concentration on the intensity of the test bands. B) Image J analysis of the test band intensity for each of the MB concentrations tested. Representative real-time fluorescence curves (C) and comparison of the endpoint relative fluorescence values for each concentration tested (D).

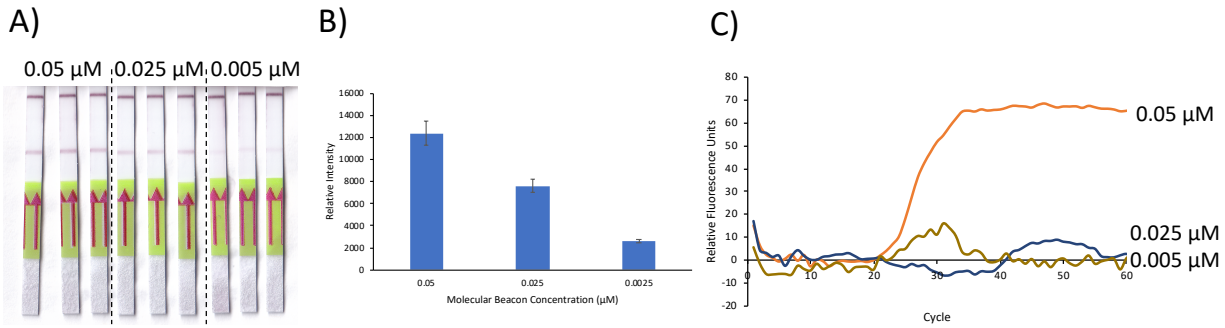


**Figure S10.** (A) Effect of lowering MB concentration on the intensity of the test bands. B) Image J analysis of the test band intensity for each of the MB concentrations tested. (C) Representative real-time fluorescence curves for the concentrations tested.

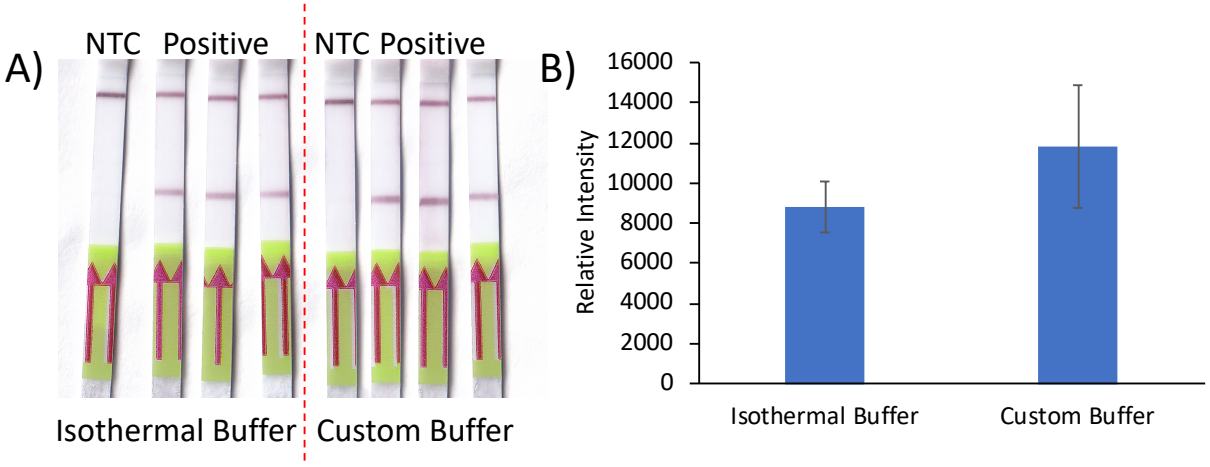


**Figure S11**. A) Image and B) ImageJ analysis of MB-LAMP-LFIA with Isothermal Buffer and Custom Buffer for ORF1a analysis.

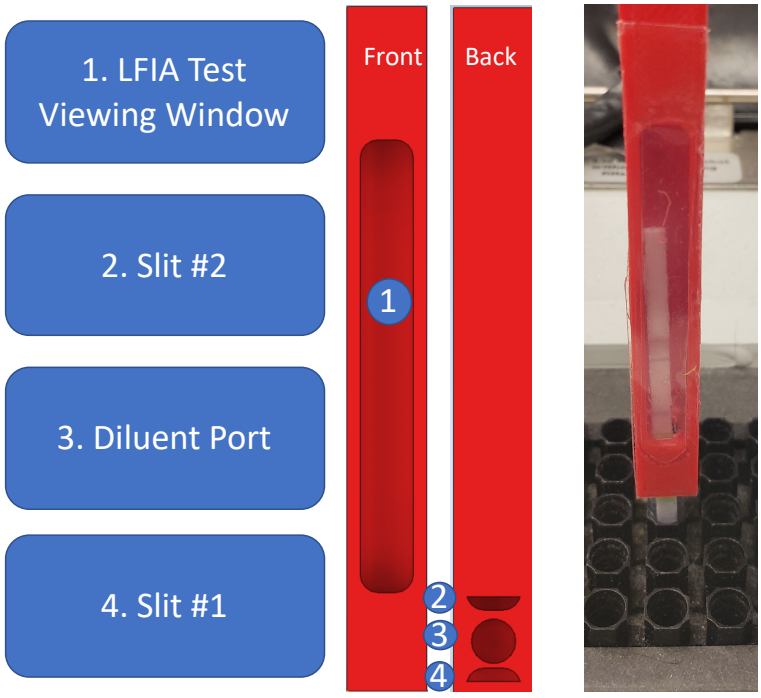


**Figure S12.** Representative front and back model and image of the 3D printed device used to prevent contamination upon opening the reaction vessel to add assay diluent.

**Reagents**

Three plasmids containing different inserts of 210 bp (BRAF wild-type), 210 bp (BRAF mutant), and 222 bp (ompW) were obtained from Eurofin Genomics (Louisville, KY, USA). A plasmid containing a 269 bp insert (ORF1a) as well as all primers and MBs were obtained from Integrated DNA Technologies (Coralville, IA, USA). Sequences of the inserts, primers, and probes used in this study are shown in Table S1. Pond water was collected from Lake Laverne (Ames, IA, USA) and stored at 4 °C until use. Human plasma was acquired from Innovative Research (Novi, MI, USA) and artificial saliva for pharmaceutical research was obtained from Pickering Test Solutions (Mountain View, CA, USA) and stored at 4 °C.

**Standard LAMP with Labeled Primers**

Standard LAMP reactions were performed for the ompW and BRAF sequences. 10 µL reaction mixtures were prepared with the following components: 1.4 mM of each dNTP (New England Biolabs, Ipswich, MA), 10× Isothermal Buffer (NEB), 6 mM MgSO4 (NEB), 1.6 µM FIP and BIP primers, 0.2 µM F3 and B3 primers, 0.4 µM of labeled loop forward and labeled loop backward primer , 3.2 U Bst 2.0 WarmStart DNA polymerase (NEB), and 1 µL of template DNA solution. Amplification of the BRAF sequence was performed by heating at 60.5 °C for 1 h while the ompW sequence was heated at 65 °C on a Bio Rad CFX96 Touch real-time PCR detection system (Hercules, CA, USA) with fluorescence measurements being recorded every 30 seconds.

**MB-LAMP of ompW**

Reaction mixtures (10 µL) were prepared with the following components: 1.4 mM of each dNTP, 10× Isothermal Buffer, 6 mM $MgSO_4$, 1.6 µM FIP and BIP primers, 0.2 µM F3 and B3 primers, 0.5 µM MB, 0.4 µM biotinylated loop forward primer , 3.2 U Bst 2.0 WarmStart DNA polymerase, and 1 µL of template DNA solution. Reaction containers were heated at 65 °C for 1 h on a CFX96 Touch real-time PCR detection system with fluorescence measurements being recorded every 30 seconds.

**MB-LAMP of BRAF**

Reaction mixtures (10 µL) were prepared with the following components: 1.4 mM of each dNTP, 10× Isothermal Buffer, 6 mM $MgSO_4$, 1.6 µM FIP and BIP primers, 0.2 µM F3 and B3 primers, 0.5 µM of MB, 0.4 µM of biotinylated loop backward primer, 3.2 U Bst 2.0 WarmStart DNA polymerase, and 1 µL of template DNA solution. Amplification was performed by heating at 60.5 °C for 1 h on a CFX96 Touch real-time PCR detection system with fluorescence measurements being recorded every 30 seconds.

**MB-LAMP of ORF1a**

Reaction mixtures (10 µL) were prepared with the following components: 1.4 mM of each dNTP, 10× Isothermal Buffer, 6 mM $MgSO_4$, 1.6 µM FIP and BIP primers, 0.2 µM F3 and B3 primers, 0.5 µM of MB, 0.4 µM of biotinylated loop backward primer, 3.2 U Bst 2.0 WarmStart DNA polymerase, and 1 µL of template DNA solution. Amplification was performed by heating at 60.5 °C for 1 h on a CFX96 Touch real-time PCR detection system with fluorescence measurements being recorded every 30 seconds.

**LFIA Detection and Analysis**

Following amplification, 100 µL of assay buffer was added to each reaction container and a lateral-flow strip was inserted. After 10 minutes, the lateral-flow strips were taped to white paper and scanned with a Canon LiDE scanner (Tokyo, Japan). Image analysis was performed on ImageJ using the gel analysis package. Comparison of intensity values was only performed within single images acquired. No comparisons were made using intensity values acquired from different images taken.

# CHAPTER 6. MODIFICATION OF POLYACRYLATE SORBENT COATINGS WITH CARBODIIMIDE CROSSLINKER CHEMISTRY FOR SEQUENCE-SELECTIVE DNA EXTRACTION USING SOLID PHASE MICROEXTRACTION

Reprinted with permission from *Analytical Methods* 2020, 12, 3200-3204



Marcelino Varona, Olga I. Shimelis and Jared L. Anderson

## Abstract

Selective DNA extraction is immensely useful for the isolation and detection of low-abundance sequences. Oligonucleotide-modified substrates are often used to capture sequences of interest for downstream analysis. In this study, we explore the chemical modification of commercial- available polyacrylate solid-phase microextraction fibers for selective DNA analysis using carbodiimide crosslinker chemistry. Reproducible modification conditions are found and the fibers were subsequently applied for selective DNA analysis. Several experimental parameters such as stir-rate, desorption time, and buffer-type are optimized. The developed method was able to selectively extract the target DNA sequence (260 bp) in the presence of 100-fold excess interfering salmon testes DNA.

## Introduction

Nucleic acids are essential biopolymers responsible for the storage, transfer, and regulation of genetic information within biological systems. In addition, nucleic acids represent valuable diagnostic molecules for the detection and identification of diseases.[1,2] Biomolecular techniques such as quantitative polymerase chain reaction (qPCR) can provide detailed information regarding nucleic acid sequences present within a sample. However, these methods use highly sensitive enzymes that are susceptible to inhibition by molecules native to biological matrices.[3] Therefore,

to enable successful analysis of these essential biomarkers, they must first be isolated in sufficient quantity and purity.

Total nucleic acid extraction methods typically rely on adsorption to silica particles[4] or liquid-liquid extraction (phenol/chloroform extraction).[5] While these methods can isolate large amounts of nucleic acid, they fall short in applications targeting specific and/or low-copy number sequences. In circulating tumor DNA analysis, these valuable sequences often comprise a small percentage of the total nucleic acid present (<1%) within a sample.[6] Moreover, traditional detection methods such as qPCR can suffer from amplification bias, where the most abundant sequence is preferentially amplified leading to false negatives and inconsistent quantification.[7] These issues can be overcome through the use of digital PCR,[8] which is expensive and not easily accessible, or through the upstream enrichment of target sequences.[9,10]

Methods for the isolation of specific sequences leverage the natural ability of nucleic acids to recognize complementary sequences through Watson-Crick base pairing interactions. A popular platform for this process is performed using biotin-modified oligonucleotides.[11] These probes can hybridize to their complementary sequence and be subsequently enriched using streptavidin-coated magnetic beads. However, beads are expensive, notoriously prone to aggregation,[12,13] and require an external magnetic field for their recovery.

An alternative preconcentration technique to magnetic beads is solid-phase microextraction (SPME).[14] Several studies have utilized SPME for the isolation of DNA and RNA from biological matrices.[15,16] In particular, Nacham et al. demonstrated the ability to use carbodiimide coupling chemistry to functionalize commercially-available polyacrylate fibers (PA) with amine-functionalized oligo deoxythymine 20 ($dT_{20}$) to develop a selective sorbent for mRNA extraction.[17] However, it was observed that significant fiber-to-fiber differences existed when the

modification chemistry was performed. The fibers were found to contain between 20 and 40 ng of oligo $dT_{20}$ following the modification procedure.[17]

In this study, we optimize the coupling chemistry in order to increase the fiber-to-fiber reproducibility of modified PA fibers. We also apply for the first time modified PA fibers for the selective extraction of DNA. Experimental parameters such as stir speed, buffer composition, and desorption time were optimized. The modified PA fibers were found to selectively extract the target DNA sequence while maintaining selectivity in the presence of 100-fold excess interfering DNA.

The coupling reaction and quantification assay were performed as previously described.[17] Further experimental details can be found in the supporting information. Conditions and a representative illustration of the quantification assay are shown in Figure 1. In brief, a dual-labeled oligonucleotide containing an amine group and a fluorescein (FAM) fluorophore was reacted with the PA fibers, washed multiple times with deionized water to remove unreacted oligo, and subjected to DNase I treatment. The resulting solution was analyzed with a plate reader and the amount of fluorophore in free solution quantified using an external calibration curve (Figure S1). All DNA sequences used in this study can be found in table S1 within the supporting information.

## Results and Discussion

Initially, the effect of conditioning fibers at 280 °C for 30 min on the loading of the oligo was explored. Two previously conditioned and two unconditioned fibers were subjected to carbodiimide crosslinker chemistry, multiple wash steps to remove unreacted oligo, and then the DNase assay. Table S2 shows that multiple washes over a 24 h period of time were required to remove residual oligo not bound to the fibers. Results showing the mass of bound DNA on the fibers obtained after modification and DNase treatment are shown in Table 1. These results indicate that fiber conditioning did not improve the reproducibility of the modification. It was

previously hypothesized that the loading efficiency was inconsistent due to lot-to-lot variation in the PA fibers.[17] This variation could result in a different number of acid groups available for the coupling reaction.

A)

| | Wash (1.5 mL) | Activation (1.5 mL) | Modification (30 µL) |
|---|---|---|---|
| Time | 5 h | 2 h | 12 h |
| Reagents | 1 M MES Buffer pH 6.0 | 200 mM NHS/100 mM EDC<br>0.1 M MES Buffer pH 6.0 | 0.1 mM Dual-labeled oligo<br>0.1 M $Na_2CO_3$/$NaHCO_3$ Buffer pH 9.0 |

B)

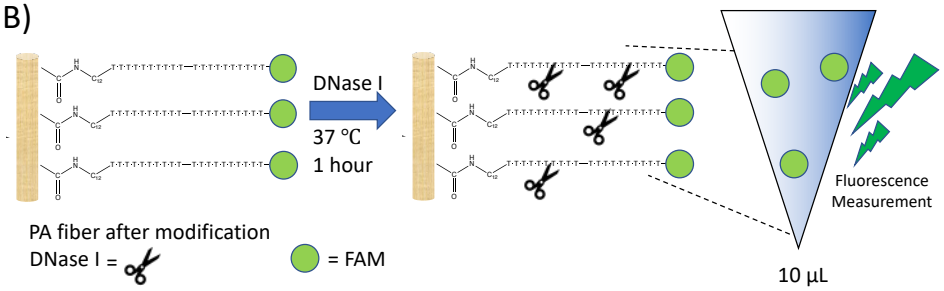


**Figure 1.** (A) Reaction conditions for the NHS/EDC modification of PA fibers and (B) representative schematic of the DNase assay used for quantification.

To test the reproducibility of the coupling reaction and DNase assay, a well-characterized support containing carboxylic acid groups (Supelco DSC-WCX ion exchange resin) was used. The reaction was performed as previously described on 1.2 mg of the particles. Following the DNase assay and fluorescence quantification, a total of 98.5 ng of oligo was able to be loaded onto the particles. Several more reactions were performed under the same conditions and the loading efficiency was found to have a relative standard deviation (RSD) >23%. (Table 2). This result indicated that reproducibility issues could be due to the employed reaction conditions. In particular, the pH of the coupling solution (pH 9) may affect reproducibility, as previous reports have utilized 2-(N-morpholino)ethanesulfonic acid (MES) buffer (pH 6) in all steps. Once the coupling reaction was performed in MES buffer, reproducibility was observed to increase substantially. The RSD of triplicate reactions performed in MES dropped significantly to 1.2%

(Table 2). These results indicated that the reaction must be performed under the appropriate conditions in order to achieve high reproducibility

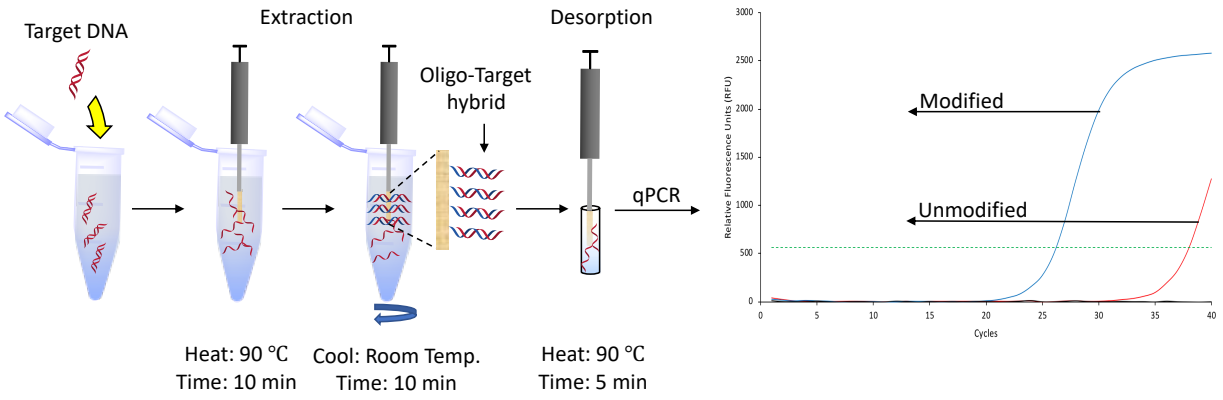


**Figure 2.** Representative schematic of the selective SPME process coupled to qPCR.

Using the previously optimized conditions, reactions were performed on six PA fibers from two different lots, as indicated by the manufacturer. Fiber-to-fiber reproducibility was tested by performing extractions of a 260 bp model sequence, as illustrated in Figure 2. The extraction performance was monitored using quantitative polymerase chain reaction (qPCR) which amplifies the target DNA exponentially. An external calibration curve was prepared using the target DNA (Figure S2) and was found to have an amplification efficiency of 102.31%, within the acceptable limits set by the MIQE guidelines.[18] For reference, a quantification cycle (Cq) value difference of one is equal to a two-fold difference in the amount of DNA present. Higher Cq values indicate lower amounts of DNA. Figure S3 demonstrates the results obtained following DNA extractions and reveal consistent extraction performance within the same lot. However, there was lot-to-lot variability observed, as previously shown.[17]

One important aspect of the method workflow is the desorption step, as it is necessary to maximize the amount of DNA recovered and to also reduce carryover effects. To determine the optimal desorption time, serial desorptions were performed in 10 µL of water in different time

intervals over a period of 20 min. A shown in Figure 3A, 95% of the extracted DNA could be desorbed after 10 minutes, with 99% desorption efficiency being attained by 15 min. However, some DNA could still be detected by qPCR after 20 min (213 copies of target DNA).

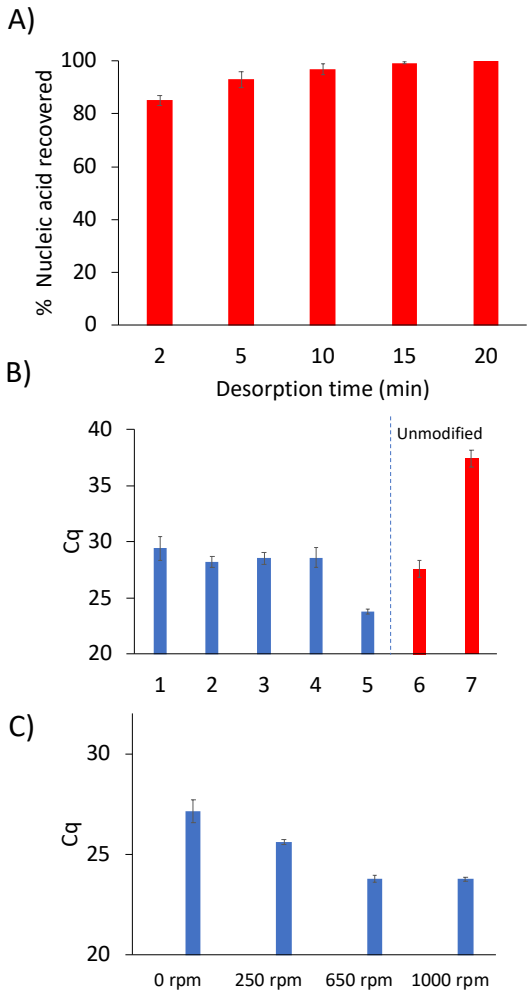


**Figure 3.** A) Desorption time analysis following sequence-specific DNA extractions showing the percent DNA recovered during each time period. B) Effect of buffer composition on the extraction efficiency (**1**: 25 mM NaCl, **2,7**: 250 mM NaCl, **3**: 20 mM Tris pH 8.0, **4**: 20 mM phosphate buffer pH 8.0, **5,6**: citric acid-phosphate buffer pH 6. C) Optimization of stir-rate during the annealing step on the extraction of DNA. For reference, a decrease of 1 in Cq value indicates a doubling of the DNA present in the qPCR reaction.

It was hypothesized that the use of a nuclease could permit the removal of undesorbed DNA as a means to prevent carryover. To test this, Exonuclease III was chosen to selectively remove the remaining DNA from the fiber. To prevent hydrolyzation of the probe, a spacer was

added to the 3' end to act as a protecting group. Figure S4 shows a schematic that demonstrates the proposed mechanism of action of the enzyme within the system. The process was tested by performing an extraction and an initial desorption followed by treatment with Exonuclease III and a subsequent desorption step. This result was compared with performing the second desorption without any previous enzyme treatment. Table S3 shows the ratio of DNA in the first desorption:second desorption. These results show that treating the fibers with Exonuclease III was able to significantly decrease carryover.

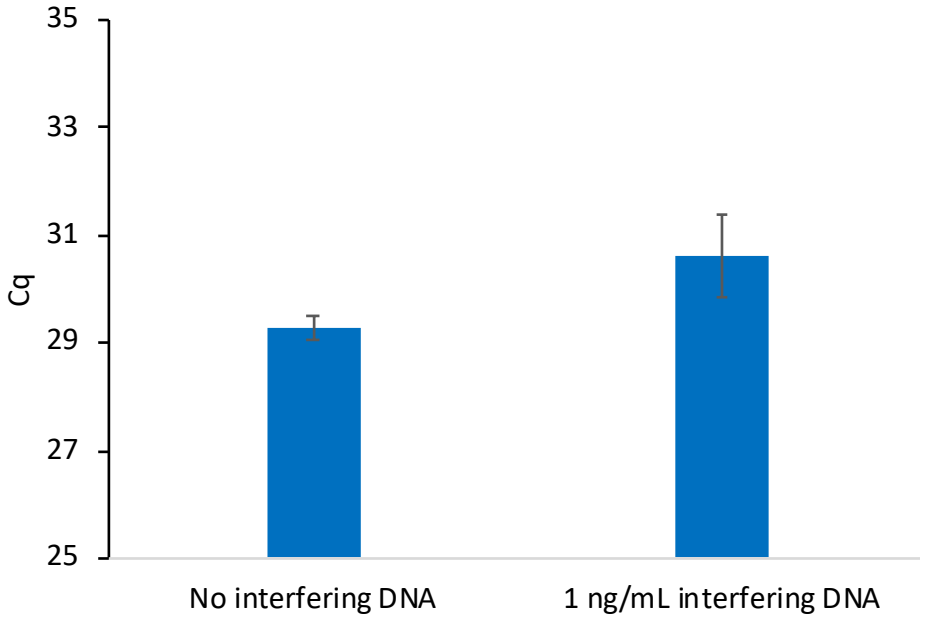


**Figure 4.** Extraction performance of modified PA fibers with and without interfering salmon testes DNA present.

Nucleic acid hybridization has been shown to be highly dependent on the surrounding environment.[19] Therefore, the buffer composition of the sample solution would be expected to play a role in the selective extraction of the target sequence. Extractions were performed from five different buffers to determine the composition that yielded the highest capture of target sequence (Figure 3B). As expected, the 250 mM NaCl solution yielded higher extraction of DNA compared to the 25 mM NaCl solution. This is due to higher DNA-duplex stability at increased ionic strength, resulting in higher melting temperatures of the probe-target complex.[19] In contrast, the Tris and

phosphate buffers did not yield different extraction results from each other or from the 25 mM NaCl solution. However, a disadvantage to using phosphate buffers is the chelation of magnesium by the phosphate groups which can cause PCR inhibition.[20]

**Table 1.** Mass of dual-labeled oligo bound to conditioned and unconditioned PA fibers following NHS/EDC modification and DNase treatment. Modification measurements were performed on two unconditioned and two conditioned fibers.

| PA Fiber | Total Mass (ng) |
|---|---|
| 1[a] | 50.8 |
| 2[a] | 113.2 |
| 3[b] | 57.2 |
| 4[b] | 0 |

[a] Conditioned [b] Unconditioned

Interestingly, the extractions from citric acid-phosphate buffer yielded much higher quantity of captured DNA compared to the 250 mM NaCl solution (Figure 3B). Extractions from the citric acid-phosphate buffer were approximately 16-fold higher than those from the NaCl solution. However, when extractions were performed with an unmodified fiber from the citric acid-phosphate buffer, a significant amount of DNA was still detected (approximately 18,000 copies). In contrast, the unmodified fiber in 250 mM NaCl extracted ≈ 18 copies, indicating 1000-fold lower non-specific DNA extraction than in citric acid-phosphate buffer. These results will be further explored in future studies, as previous work showed very low nonspecific extraction of DNA by PA fibers when extractions were performed from a Tris buffer.

The stir-rate was the final parameter optimized. In traditional SPME, the analysis time can often be decreased through the use of agitation. However, stirring had not previously been explored using hybridization-based SPME. In order to evaluate the effect of the stir-rate on the extraction of DNA, stirring was introduced into the hybridization step and varied between 0-1000 rpm. As shown in Figure 3C, the amount of captured DNA can be observed to increase from 0-650 rpm.

No difference in the amount of DNA extracted was observed when the agitation speed was increased from 650 to 1000 rpm.

**Table 2.** Mass of oligo $dT_{20}$ bound to DSC-WCX particles following NHS/EDC modification and DNase I treatment using either MES or carbonate buffer for the coupling solution.

| Buffer in Coupling Step | Mass (n =3) | RSD (n =3) |
|---|---|---|
| Carbonate Buffer | 89.11 | 23.44 |
| MES | 110.36 | 1.25 |

Sequence-specific nucleic acid extraction methods are highly desirable when non-target DNA is present in large amounts relative to the target sequence. Therefore, these methods must possess high enough selectivity to isolate the target when interfering sequences are present. As a proof-of-concept, extractions were performed as previously described with salmon testes DNA (average length = 2,000 base pairs) present as the interfering sequence at a concentration of 10 ng $mL^{-1}$. This concentration is 100 times higher than the target DNA concentration (10 pg $mL^{-1}$). The extraction results in Figure 4 show little difference in the amount of DNA extracted when the salmon testes DNA is present and compared to an extraction without interfering DNA. These results demonstrate the high selectivity of the developed method.

## Conclusion

In conclusion, the modification of PA fibers and their application for selective DNA analysis was explored. Reproducible NHS/EDC reaction conditions were studied in order to decrease the fiber-to-fiber variability. Carryover DNA from previous extractions was able to be minimized using Exonuclease III after the extraction procedure. A blocking group was added to the DNA probe bound to the fiber to prevent degradation by the exonuclease. The optimal extraction buffer and stir speed were also determined. Extractions of the target DNA were able to be performed in 100-fold excess interfering DNA. Subsequent studies will focus on further studying the selectivity of the sorbents for the extraction of single-nucleotide polymorphisms and

the performance of the modified fibers in biological matrices. In addition, this study allows for reproducible modification of PA fibers with other bioactive molecules such as proteins or antibodies for the future development of selective sorbents.

**Acknowledgements**

The authors acknowledge funding from the Chemical Measurement and Imaging Program at the National Science Foundation (Grant No. CHE-1709372).

**References**

1 E. Heitzer, P. Ulz and J. B. Geigl, *Clin. Chem.*, 2015, 61, 112–123.

2 D. Helb, M. Jones, E. Story, C. Boehme, E. Wallace, K. Ho, J. Kop, M. R. Owens, R. Rodgers, P. Banada, H. Safi, R. Blakemore, N. T. N. Lan, E. C. Jones-López, M. Levi, M. Burday, I. Ayakaka, R. D. Mugerwa, B. McMillan, E. Winn-Deen, L. Christel, P. Dailey, M. D. Perkins, D. H. Persing and D. Alland, *J. Clin. Microbiol.*, 2010, **48**, 229–37.

3 P. Rådström, R. Knutsson, P. Wolffs, M. Lövenklev and C. Löfström, *Appl. Biochem. Biotechnol. - Part B Mol. Biotechnol.*, 2004, 26, 133–146.

4 R. Boom, C. J. A. Sol, M. M. M. Salimans, C. L. Jancen, P. M. E. Wertheim-van-Dillen and V. der N. J, *J Clin Microbiol*, 1990, **28**, 495–503.

5 R. Patel, J. T. Kvach and P. Mounts, *J. Gen. Microbiol.*, 1986, **132**, 541–551.

6 S. O. Kelley, *ACS Sensors*, 2017, **2**, 193–197.

7 P. M. Warnecke, C. Stirzaker, J. R. Melki, D. S. Millar, C. L. Paul and S. J. Clark, *Nucleic Acids Res.*, 1997, **25**, 4422–4426.

8 B. Vogelstein and K. W. Kinzler, *Proc. Natl. Acad. Sci. U. S. A.*, 1999, **96**, 9236–9241.

9 M. Lovett, *Curr. Protoc. Hum. Genet.*, 1994, **00**, 3–6.

10 A. B. Schrock, D. Pavlick, S. J. Klempner, J. H. Chung, B. Forcier, A. Welsh, L. Young, B. Leyland-Jones, R. Bordoni, R. D. Carvajal, J. Chao, R. Kurzrock, J. K. Sicklick, J. S. Ross, P. J. Stephens, C. Devoe, F. Braiteh, S. M. Ali and V. A. Miller, *Clin. Cancer Res.*, 2018, **24**, 1881–1890.

11 A. Holmberg, A. Blomstergren, O. Nord, M. Lukacs, J. Lundeberg and M. Uhlén, *Electrophoresis*, 2005, **26**, 501–510.

12 D. C. Leslie, J. Li, B. C. Strachan, M. R. Begley, D. Finkler, L. A. L. Bazydlo, N. S. Barker, D. M. Haverstick, M. Utz and J. P. Landers, *J. Am. Chem. Soc.*, 2012, **134**, 5689–5696.

13 D. Liu, G. Liang, Q. Zhang and B. Chen, , DOI:10.1021/ac400412m.

14 C. L. Arthur and J. Pawliszyn, *Anal. Chem.*, 1990, **62**, 2145–2148.

15 O. Nacham, K. D. Clark and J. L. Anderson, *Anal. Chem.*, 2016, **88**, 7813–7820.

16 M. Varona, X. Ding, K. D. Clark and J. L. Anderson, *Anal. Chem.*, 2018, **90**, 6922–6928.

17 O. Nacham, K. D. Clark, M. Varona and J. L. Anderson, *Anal. Chem.*, 2017, **89**, 10661–10666.

18 J. F. Huggett, C. A. Foy, V. Benes, K. Emslie, J. A. Garson, R. Haynes, J. Hellemans, M. Kubista, R. D. Mueller, T. Nolan, M. W. Pfaffl, G. L. Shipley, J. Vandesompele, C. T. Wittwer and S. A. Bustin, *Clin. Chem.*, 2013, **59**, 892–902.

19 J. Fuchs, J. B. Fiche, A. Buhot, R. Calemczuk and T. Livache, *Biophys. J.*, 2010, **99**, 1886–1895.

20 S. R. Johnson, D. H. Martin, C. Cammarata and S. A. Morse, *J. Clin. Microbiol.*, 1995, 33, 1036–1038.

## Appendix E: Supporting Information Chapter 6

**Table S1.** Sequences of oligonucleotides used in this study.

| | Sequence |
|---|---|
| FAM labelled Oligo | 5'-/5AmMC12/TTT TTT TTT TTT TTT TTT TT-36-FAM/-3' |
| Extraction Probe | 5'-/5AmMC12/GAGGCCCACTCCCATAGGTT-3' |
| Extraction Probe with Blocker | 5'-/5AmMC12/GAGGCCCACTCCCATAGGT/3SpC3-3' |

**Table S1**. Continued

| | |
|---|---|
| Forward Primer | 5'-AAA ACG CCG CAG ACA CAT CC -3' |
| Reverse Primer | 5'-GAGGCCCACTCCCATAGGTT-3 |
| Target | GGATGTGTCTGCGGCGTTTTATCATCTTCCTCTTCATCCTGCTGCTAT GCCTCATCTTCTTGTTGGTTCTTCTGGACTATCAAGGTATGTTGCCC GTTTGTCCTCTAATTCCAGGATCATCAACAACCAGCACCGGACCAT GCAAAACCTGCACAACTCCTGCTCAAGGAACCTCTATGTTTCCCTCA TGTTGCTGTACAAAACCTACGGACGGAAACTGCACCTGTATTCCCA TCCCATCATCTTGGGCTTTCGCAAGTAACCTATGGGAGTGGGCCTC |

**Table S2.** Fluorescence results of the washes following NHS/EDC coupling with FAM-labeled oligo

| | Fluorescence Results | | | |
|---|---|---|---|---|
| Wash Number | Fiber 1 | Fiber 2 | Fiber 3 | fiber 4 |
| 1 (24 hr) | 3500 | 1740 | 1362 | 3 |
| 2 (2 hr) | 2828 | 1702 | 2246 | 8 |
| 3 (30 min) | 1098 | 686 | 987 | 5 |
| 4 (1.5 hr) | 120 | 58 | 81 | 2 |

**Table S3.** Results showing the relative ratio of DNA in the first:second desorption with and without Exonuclease III treatment. Ratios were obtained using the average DNA desorbed in the first and second desorption from 3 different extractions for each treatment.

| | DNA first desorption:second desorption |
|---|---|
| Without Enzyme | 12 |
| With Enzyme | 8810 |

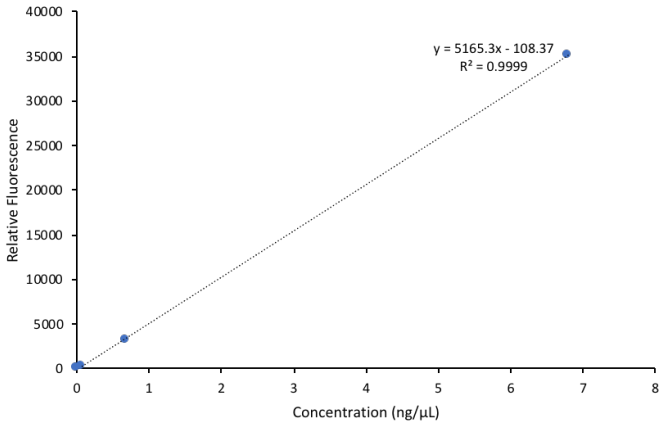


**Figure S1.** 4-point calibration curve of dual-labeled (amine and FAM) oligonucleotide used to quantify loading following DNase treatment of the fibers. Triplicate measurements were recorded for each point.

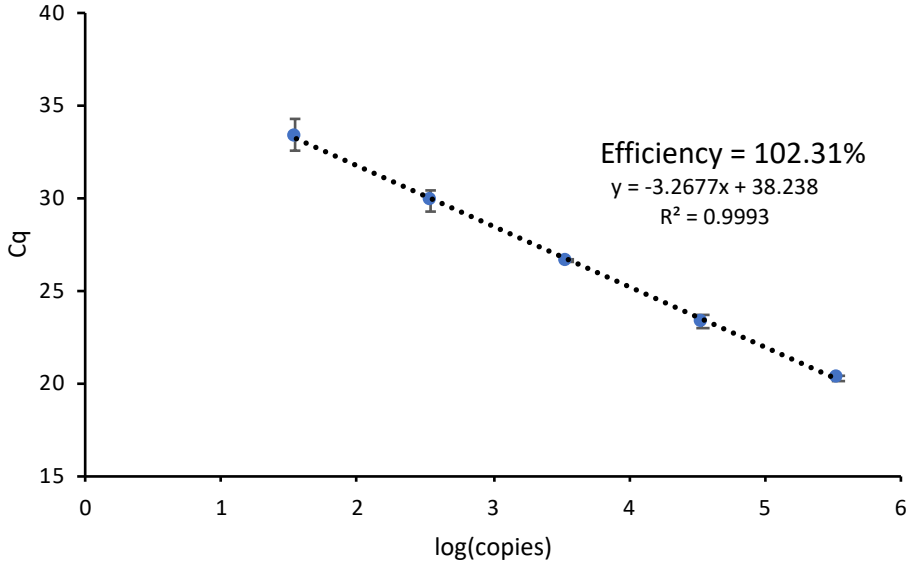


**Figure S2**. Five-point qPCR calibration curve of the target DNA sequence. Each point was measured in triplicate.

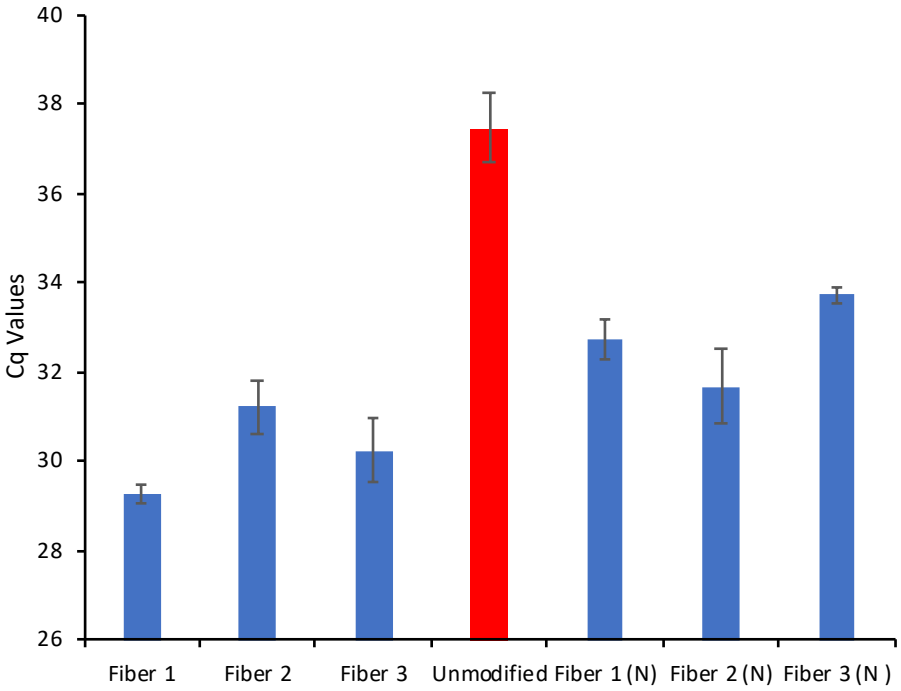


**Figure S3.** Extraction results from 6 different PA fibers following NHS/EDC modification chemistry. The modification and extraction performance is compared from two separate lots of fibers.

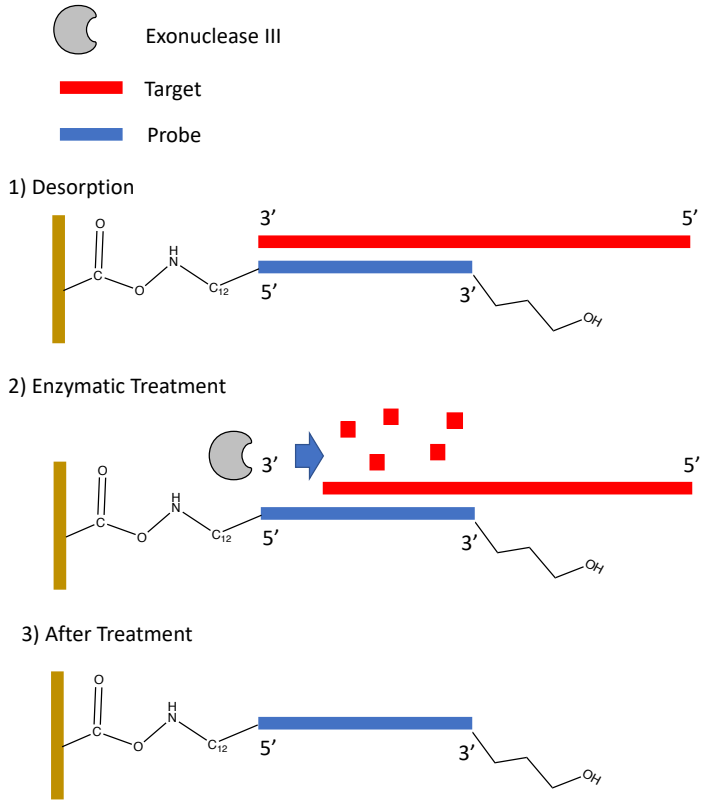


**Figure S4.** Representative schematic of the effect of using Exonuclease III to reduce carryover by hydrolyzing the target sequence after an initial desorption.

**Reagents and Instrumentation**

All primers and oligonucleotides used in this study were obtained from Integrated DNA Technologies (Coralville, IA, USA). The SPME fibers were obtained from Supelco (Bellefonte, PA, USA). For the coupling chemistry, 1-ethyl-3-(3-dimethylaminopropyl) carbodiimide hydrochloride (EDC.HCl, >97.0%), N-hydroxysuccinimide (NHS, +98%), citric acid >99.5%, salmon testes DNA, and 2-(N-morpholino)ethanesulfonic acid were obtained from Sigma Aldrich (St. Louis, MO, USA). Tris(hydroxymethyl)aminomethane (Tris) was obtained from P212121 (Ypsilanti, MI, USA). Sodium chloride 99%, disodium phosphate ≥99%, sodium carbonate ≥99.5%, and sodium bicarbonate ≥99.7% were purchased from Thermo Fisher Scientific (Waltham, MA, USA). Exonuclease III was obtained from New England Biolabs (Ipswich, MA, USA). RQ1 RNase-Free DNase and 10X reaction buffer were obtained from Promega (Madison, WI, USA). Deionized water (18.2 MΩ cm) was used throughout the study and it was obtained from a Millipore Milli-Q water purification system. qPCR assays were performed on a CFX96 Touch qPCR instrument using SsoAdvanced Universal SYBR Green supermix from Bio-Rad Laboratories (Hercules, CA, USA). Fluorescence measurements were performed using a BioTek Synergy Hybrid H1 microplate reader using a black, flat bottom, Greiner Bio 384-well microplate. Fibers were conditioned using the inlet of an Agilent Technologies 6850 gas chromatograph (Santa Clara, CA, USA).

**Selective extraction of DNA with oligo-functionalized PA fibers**

A 1.5 mL, 10 pg $mL^{-1}$ (34,800 copies $mL^{-1}$) DNA solution was prepared in a 2 mL Eppendorf LoBind tube. A small stir-bar was added into the tube to enable stirring. The cap was pierced to allow the PA fiber through the tube and into the extraction solution. The tubes with the fibers were immediately placed in a 90 °C water bath for 10 min. Following the heating process, the tubes were transferred to a room temperature water bath placed over a magnetic stir-plate.

Following the hybridization process, the fiber was retracted and removed from the extraction solution. The fiber was subsequently washed with water to removed nonspecifically adsorbed DNA and subjected to a desorption in 10 µL of water at 90 ℃ for 5 min. After the desorption process, a 1 µL aliquot from the desorption solution was subjected to qPCR analysis.

**Serial desorption experiment**

The serial desorption experiments were performed as follows. Five desorption containers containing 10 µL of water were prepared and placed in a 90 ℃ water bath. After the sequence-selective extraction, the fiber was placed in a desorption container for 2 min and subsequently moved to another desorption container. This was done in intervals of 2, 3, 5, 5 and 5 min, giving a total of 20 min. A 1 µL aliquot was collected from each desorption container and subjected to qPCR. The percent desorbed was calculated in the following way. The amount recovered at each time interval was calculated and added to the amount recovered in any previous interval. This was divided by the total DNA recovered after the 5 intervals.

Let $t1 - t5$ be the amount of DNA recovered in each time interval.

$$\frac{t1}{(t1+t2+t3+t4+t5)} \times 100 = \% \text{ recovered at 2 min}$$

$$\frac{t1+t2}{(t1+t2+t3+t4+t5)} \times 100 = \% \text{ recovered at 5 min}$$

$$\frac{t1+t2+t3}{(t1+t2+t3+t4+t5)} \times 100 = \% \text{ recovered at 10 min}$$

$$\frac{t1+t2+t3+t4}{(t1+t2+t3+t4+t5)} \times 100 = \% \text{ recovered at 15 min}$$

$$\frac{t1+t2+t3+t4+t5}{(t1+t2+t3+t4+t5)} \times 100 = \% \text{ recovered at 20 min}$$

# CHAPTER 7. MAGNETIC IONIC LIQUIDS: INTERACTIONS WITH BACTERIAL CELLS, BEHAVIOR IN AQUEOUS SUSPENSION AND BROADER APPLICATIONS

Reprinted with permission from *Analytical and Bioanalytical Chemistry* 2020, 412, 1741-1755



Stephanie A. Hice, Marcelino Varona, Allison Brost, Fan Dai, Jared L. Anderson, and Byron F. Brehm-Stecher

## Abstract

Previously, we demonstrated capture and concentration of *Salmonella enterica* subspecies *enterica* ser. Typhimurium using magnetic ionic liquids (MILs), followed by rapid isothermal detection of captured cells *via* recombinase polymerase amplification (RPA). Here, we report work intended to explore the broader potential of MILs as novel pre-analytical capture reagents in food safety and related applications. Specifically, we evaluated the capacity of the ($[P_{66614}^+][Ni(hfacac)_3^-]$) ("Ni(II)") MIL to bind a wider range of human pathogens using a panel of *Salmonella* and *Escherichia coli* O157:H7 isolates, including a "deep rough" strain of *S.* Minnesota. We extended this exploration further to include other members of the family *Enterobacteriaceae* of food safety, clinical or agricultural significance. Both the Ni(II) MIL and the ($[P_{66614}^+][Dy(hfacac)_4^-]$) ("Dy(III)") MIL were evaluated for their effects on cell viability and structure-function relationships behind observed antimicrobial activities of the Dy(III) MIL were determined. Next, we used flow imaging microscopy (FIM) of Ni(II) MIL dispersions made in model liquid media to examine the impact of increasing ionic complexity on MIL droplet properties as a first step towards understanding the impact of suspension medium properties on MIL dispersion behavior. Finally, we used FIM to examine interactions between the Ni(II) MIL and *Serratia marcescens*, providing insights into how the MIL may act to capture and concentrate

Gram-negative bacteria in aqueous samples, including food suspensions. Together, our results provide further characterization of bacteria-MIL interactions and support the broader utility of the Ni(II) MIL as a cell-friendly capture reagent for sample preparation prior to cultural or molecular analyses.

## Introduction

The family *Enterobacteriaceae* is a related grouping of Gram-negative, facultatively anaerobic rod-shaped bacteria. The family contains several genera of importance to agriculture, food safety and human health, including *Cronobacter*, *Enterobacter*, *Erwinia*, *Escherichia*, *Klebsiella*, *Pantoea*, *Pectobacterium*, *Salmonella*, *Serratia*, *Shigella* and *Yersinia* (1). From a food safety perspective alone, four of these groups or species - nontyphoidal *Salmonella* spp., *Escherichia coli* O157:H7, *Shigella* spp. and *Yersinia enterocolitica* are estimated to be responsible for a combined 1,319,624 foodborne illnesses each year in the US, resulting in 23,463 hospitalizations and 437 deaths (2) (Electronic Supplementary Material Table S1). Apart from the human suffering caused, foodborne disease also has very real economic impacts stemming from lost wages, lost productivity and the costs of hospitalization, product recalls and litigation. The estimated economic burden of foodborne disease caused each year by *Salmonella* spp. in the US alone is $3.4 billion; for *E. coli* O157:H7 it is $271 million (3). These figures highlight the need for detection of enterobacterial pathogens such as *Salmonella* and *E. coli* O157:H7 in foods, and by extension, detection of agricultural pests and clinically important members belonging to this family in crop and soil matrices or in clinical samples across the farm-to-fork-to-physician continuum (4, 5).

Because problematic bacteria may be present at low levels in foods or other samples, environmental, food and clinical microbiologists rely heavily on the use of growth-based enrichment steps prior to downstream analysis. Selective media for enrichment and identification

of *Enterobacteriaceae* exist, primarily for their detection in foods as indicators of proper hygienic practices or in nonsterile pharmaceutical products for ensuring compliance with quality or regulatory standards (6). Unfortunately, growth-based enrichment of bacteria is extremely time-consuming and therefore represents a major hurdle to moving quickly from sample to answer (4).

Approaches for growth-independent, physical enrichment of bacteria include "brute force" methods such as centrifugation and filtration, but these often result in co-extraction of matrix-associated debris, which can interfere with downstream detection assays. To circumvent this, magnetic separation technologies can be used for rapid preconcentration and isolation of bacteria. For example, functionalized magnetic particles can be added to complex samples and allowed to bind to bacteria *via* electrostatic interactions, glycan binding, antigen-antibody pairing or other capture modalities of varying specificities. Subsequent application of a magnetic field allows manipulation of particle-bound bacteria, enabling their concentration and separation from matrix-associated contaminants (4, 7, 8). Although this approach is selective, drawbacks include the high cost of particle functionalization and issues such as particle aggregation or limited physical access to microniches occupied by target bacteria (8).

Magnetic ionic liquids (MILs) are magnetoactive solvents comprised of organic/inorganic cation and anion pairs. A paramagnetic component is integrated into either the cation or anion moiety, conferring susceptibility to magnetic fields (9, 10). MILs may also have the additional advantages of being nonvolatile and nonflammable, with tunable physicochemical properties. The hydrophobic and fluid nature of MILs allows for their distribution throughout aqueous samples as liquid microdispersions, which facilitates interactions with and capture of biochemical or cellular analytes. Due to these novel properties, MILs are emerging as a powerful and versatile reagent platform for extraction of a wide variety of bioanalytes, including hormones, nucleic acids and

viable bacterial cells (11-13). In bacterial applications, MILs have enabled preconcentration of viable, nonpathogenic *E. coli* from fluid milk, followed by downstream detection *via* microbiological culture or quantitative polymerase chain reaction (qPCR) (9). More recently, MILs have been paired with recombinase polymerase amplification (RPA) for the rapid preconcentration and detection of *Salmonella* Typhimurium from 2% milk, almond milk and liquid egg product (8). However, despite the success to date of MILs in microbiological applications, little is known about MIL-bacterial interactions and the physicochemical principles responsible for capture and concentration of viable cells. In order to further the development of MILs as whole-cell sample preparation agents, a greater understanding is needed of how they behave in aqueous suspensions both alone and in the presence of bacteria, whether or not they possess intrinsic antibacterial activities that might limit their use in applications where maintaining cell viability is critical, and how broadly they may be applied for capture of bacteria of concern across the farm-to-fork-to-physician continuum.

In this study, we evaluated the capacity of the Ni(II) MIL to capture a broad range of Gram-negative bacteria, including *Salmonella* serovars, *E. coli* O157:H7 and other representatives of the family *Enterobacteriaceae* of importance to global agriculture, food safety and human health. We also plated MIL-exposed cells in parallel onto selective and non-selective agars to explore whether or not MIL-based capture causes cellular injury in either *Salmonella* or *E. coli* O157:H7. We determined extent of and the chemical and structural bases of observed antibacterial activity of the Dy(III) MIL, and we directly compared the antimicrobial activities of the Ni(II) MIL and ($[EMIM^+][SCN^-]$), a non-magnetic IL used previously by others for extraction of *Salmonella* and other pathogens from foods (14). Finally, we used Flow Imaging Microscopy (FIM) to capture data on the physical properties of aqueous Ni(II) MIL suspensions under different ionic conditions

and to characterize the behavior of the Ni(II) MIL in the presence of the pigmented enterobacterial strain *S. marcescens*. This study underscores the promise of the Ni(II) MIL as an emerging sample preparation reagent by providing a more complete picture of its utility for capture of various enterobacterial pathogens, demonstrating its generally non-injurious nature and offering new insight into potential mechanisms behind its ability to physically enrich bacteria from complex samples.

## Materials and Methods

### Reagents and Magnetic Ionic Liquid Preparation

Chemical structures of the two MIL solvents examined in this study are shown in Figure 1a. Synthesis and characterization of the MILs was performed as previously described (15). A brief description of MIL synthesis is also included in the accompanying Electronic Supplementary Material. MIL solvents were purified by liquid-liquid extraction with acetonitrile/hexane and dried *in vacuo*. Prior to all experiments, MILs were stored in a desiccator for at least 24 h.

### Bacteria and Culture Conditions

All of the bacterial strains used in this study belong to the family *Enterobacteriaceae*, and are listed in Table 1. All growth media were from Becton, Dickinson and Company (Franklin Lakes, NJ, USA). Cultures of *S. marcescens* were grown as previously described (8). *Salmonella* and *E. coli* were grown 24 h in 10 mL volumes of Tryptic Soy Broth (TSB) at 37 °C. *K. aerogenes* and *C. sakazakii* were grown in 5 mL volumes of TSB at 30 °C and *Y. enterocolitica* strains were grown at 37 °C, with shaking (190 rpm) on a Shel Lab Shaking incubator (Sheldon Manufacturing, Inc., Cornelius, OR, USA). Plant pathogens were grown in 10 mL volumes of Columbia Broth (CB) at 28 °C with shaking at 190 rpm. Depending on the experiment, bacteria were enumerated using Tryptic Soy Agar (TSA), Columbia Agar (CA), Bismuth Sulfite Agar (BSA) or Violet Red Bile Glucose Agar (VRBGA) plates as described below under “Plating and Enumeration”.

**Table 1** Enterobacterial strains used in this study

| Organism | Source |
|---|---|
| *Cronobacter sakazakii* 01088P (derived from ATCC 29544) | Microbiologics[a] |
| *Erwinia amylovora* Ea935 | ISU PP[b] |
| *Escherichia coli* O157:H7 N886-71 | OHA[c] |
| *Escherichia coli* O157:H7 N366-2-2 | OHA |
| *Escherichia coli* O157:H7 N549-3-1 | OHA |
| *Escherichia coli* O157:H7 N317-3-1 | OHA |
| *Escherichia coli* O157:H7 N192-5-1 | OHA |
| *Escherichia coli* O157:H7 N192-6-1 | OHA |
| *Escherichia coli* O157:H7 N336-4-1 | OHA |
| *Escherichia coli* O157:H7 N405-5-8 | OHA |
| *Klebsiella aerogenes* ATCC 29940 | ISU PP |
| *Pantoea eucalypti* 299R (formerly *Pantoea agglomerans* 299R) | ISU PP |
| *Pantoea stewartii* Rif9A | ISU PP |
| *Pectobacterium carotovorum* pv. *carotovorum* | ISU PP |
| *Salmonella bongori* SA4410 | SGSC[d] |
| *Salmonella enterica* subsp. *arizonae* SA4407 | SGSC |
| *Salmonella enterica* subsp. *diarizonae* SA4408 | SGSC |
| *Salmonella enterica* subsp. *enterica* ser. Minnesota SLH 157 | SLH[e] |
| *Salmonella enterica* subsp. *enterica* ser. Minnesota mR613 | SGSC |
| *Salmonella enterica* subsp. *enterica* ser. Typhimurium ATCC 14028 | ATCC[f] |
| *Salmonella enterica* subsp. *houtenae* SA4409 | SGSC |
| *Salmonella enterica* subsp. *indica* SA4411 | SGSC |
| *Salmonella enterica* subsp. *salamae* SA4406 | SGSC |
| *Serratia marcescens* | CBS[g] |
| *Yersinia enterocolitica* subsp. *enterocolitica* ATCC 9160 | ATCC[f] |
| *Yersinia enterocolitica* subsp. *enterocolitica* ATCC 23715 | ATCC |

[a]Microbiologics (St. Cloud, MN); ISU PP, [b]Iowa State University Plant Pathology; [c]OHA, Oregon Health Authority, Public Health Division (Portland, OR, USA); [d]SGSC, *Salmonella* Genetic Stock Centre (Calgary, Alberta, Canada); [e]SLH, Wisconsin State Laboratory of Hygiene (Madison, WI, USA); [f]ATCC, American Type Culture Collection (Manassas, VA, USA); [g]CBS, Carolina Biological Supply (Burlington, NC)

**MIL-Based Whole-Cell Extraction**

A universal schematic for MIL-based cell extraction is depicted in Figure 1b. A 1 mL volume of diluted cell suspension was added to a flat-bottomed 4-mL screw cap glass vial. Fifteen microliters of either the Ni(II) or Dy(III) MIL was added and dispersed into microdroplets by vortex agitation for 30 s (9). The aqueous phase was decanted following dispersive extraction, and the MIL was subjected to a brief wash step using 1 mL of nuclease-free water (Integrated DNA

Technologies, Coralville, IA, USA) to ensure adequate removal of loosely or incidentally bound cells (9). After washing, release of viable cells from the MIL extraction phase was carried out using a "back-extraction" step accomplished through addition of 1 mL of an ionically-rich nutritive medium comprised of 20 g $L^{-1}$ tryptone and 10 g $L^{-1}$ NaCl, followed by a 120 s vortex step (8). After back-extraction, aliquots of the cell-enriched back-extraction medium were enumerated using the track dilution method described by Jett et al. (16) using 100 x 100 mm square, gridded TSA, BSA, CA or VRBGA plates.

**Plating and Enumeration:**

Following back-extraction, aliquots of the cell-enriched back-extraction medium were serially diluted in 0.1% peptone water and a 10 µL aliquot of each dilution was applied to a separate lane on square plates containing an appropriate agar medium. The plates were then tilted at an ~80° angle for 15 min to allow the droplets to travel toward the opposite end of the plate (16). The plates were incubated for 24 h at 37 °C (TSA, VRBGA), for 48 h at 37 °C (BSA) or for 24 h at 37 °C (CA). Colonies were counted and colony forming units (CFU) were determined. The enrichment factor ($E_F$) for MIL-based extraction was calculated using Equation 1, where $C_{MIL}$ represents the concentration of bacteria in suspension following extraction using the MIL and $C_S$ is the initial concentration of bacteria in the sample.

$$E_F = \frac{C_{MIL}}{C_S} \quad \text{(Equation 1)}$$

**Exposure to Ni(II) MIL as a Function of Time and Evaluation of [EMIM+][SCN-] IL Toxicity**

To examine whether exposure time to the Ni(II) MIL affected cell viability, MIL-based whole-cell extraction was performed using the Ni(II) MIL, and cell-enriched back-extraction media were enumerated at 0, 5, 10 and 15 min on both TSA and BSA. To evaluate toxicity of the

[$EMIM^+$][$SCN^-$] IL, one milliliter of diluted *S.* Typhimurium ATCC 14028 cell suspension was added to a 4-mL screw cap glass vial. A 5% (vol/vol) or 50% (vol/vol) aqueous solution of 1-ethyl-3-methylimidazolium thiocyanate ("[$EMIM^+$][$SCN^-$]") (IoLiTec, Tuscaloosa, AL, USA) was added and mixed by vortexing for 30 s (14). Aliquots were enumerated at 0, 5, 10 and 15 min using TSA and BSA.

**Comparison of Air-Displacement and Positive-Displacement Pipettes for MIL Handling**

A 1 mL volume of diluted *S.* Typhimurium ATCC 14028 cell suspension was added to a 4-mL screw cap glass vial. Fifteen microliters of the Ni(II) MIL was added using either a Pipetman Classic P20 air-displacement pipette (Gilson, Middleton, WI, USA), or a Microman E M25E positive-displacement pipette (Gilson) and dispersed into microdroplets by vortex agitation for 30 s. MIL-based extraction and enumeration was carried out as previously described.

**Exposure to Dy(III) MIL, DyCl3 and ([NH4+][Dy(hfacac)4-])**

One milliliter of diluted *S.* Typhimurium ATCC 14028 cell suspension was added to a 4-mL screw cap glass vial. Fifteen microliters of either the Dy(III) MIL or 2-10 µL of 100 mM $DyCl_3$ solution or 10 mg of the ammonium tetra(hexafluoroaceto)dysprosium salt (15) ([$NH_4^+$][$Dy(hfacac)_4^-$]) ("Dy(III) ammonium salt") was added and dispersed by vortex agitation for 30 s. Aliquots of the Dy(III) MIL- or Dy(III) ammonium salt-exposed cell suspension were enumerated using square TSA or BSA plates (BD).

**Impact of Ionic Environment on Ni(II) MIL Dispersion Properties and Bacteria-MIL Interactions by Flow Imaging Microscopy**

For analysis of MIL dispersion properties as a function of ionic environment, microdroplet suspensions of the Ni(II) MIL were generated as above for whole-cell extraction of bacteria and analyzed with a FlowCam 8000 instrument (Fluid Imaging Technologies, Inc., Scarborough, ME). Briefly, three peptone water (PW) formulations representing multiples of the manufacturer's basal

formulation for this medium were added to 4-mL screw cap glass vials. Fifteen microliters of the Ni(II) MIL were added to each PW formulation and the mixture dispersed with vortexing for 30 s for microdroplet formation. Samples were analyzed immediately using the FlowCam instrument using the 10x objective (100 µm field of view). Samples (20 µL) were taken from the top portion of each tube with a ~25 s collection time. PW formulations evaluated were 1x (0.5% NaCl/1% peptone), 5x (2.5% NaCl/5% peptone) and 10x (5% NaCl/10% peptone). Data were analyzed with VisualSpreadsheet® software (v. 5.0, Fluid Imaging Technologies, Inc.). A basic size filter of 5 µm (minimum droplet size) to 10,000 µm (maximum droplet size) was applied, and droplet distributions were plotted as volume (%) vs. equivalent spherical diameter (ESD). Key measurements tabulated for each ionic condition include mean droplet diameter (ESD), maximum droplet size, $D_{50}$ (median droplet size; 50% are smaller and 50% are larger than this value), $D_{90}$ (90% of droplets are smaller than this value) and number of droplets $mL^{-1}$. The same settings were used for analysis of bacteria-MIL interactions, with high concentrations (~$10^7$ – $10^8$ CFU $mL^{-1}$) of *S. marcescens* suspended in 1x PW prior to addition of the MIL and sampling.

**Statistical analysis**

The following statistical analysis was performed in SAS 9.4. Four master suspensions of bacteria were prepared for four *Salmonella enterica* serovars: subsp. Typhimurium, subsp. *arizonae*, subsp. *diarizonae* and subsp. *houtenae*. Two master suspensions were made for the remaining three *Salmonella* serovars or species: *S. enterica* subsp. *indica*, subsp. *salamae* and *S. bongori*. For *E. coli* O157:H7, two master suspensions of bacteria were prepared for each of the eight strains studied. For all bacteria tested, two replicate extractions from the same master suspension were performed, using the $10^{-3}$ dilution. Following MIL-based capture, back-extraction solutions were plated to non-selective agar (TSA) and selective agar (BSA) for

*Salmonella* and SMAC for *E. coli*. To identify whether significant differences existed for the capture of *Salmonella* and *E. coli* O157:H7, we applied a linear mixed model for the response variable (enrichment factor) with log transformation in order to reduce skewness. We treat both the strain and the medium as fixed effects and the suspension of bacteria as the random block.

In order to compare potential injury caused by the MIL across genera (*Salmonella* serovars and STEC *Escherichia*), a medium suitable for growth of both organisms (VRBGA) was used in parallel with TSA and resulting counts were compared in experimental settings repeated across five different days. In each experiment, three *Salmonella* serovars were tested: *S.* Typhimurium ATCC 14028, *S.* Minnesota SLH 157, and deep rough mutant *S.* Minnesota mR613. Two *E. coli* strains were also tested: *E. coli* O157:H7 N192-6-1 and *E. coli* O157:H7 N192-5-1. We applied the linear mixed model for the log-transformed enrichment factors with fixed strain and agar effects and random blocks of the experiment days as samples from a population of days. Additional statistical analyses regarding precision measurements and CFU counts vs. time for the MIL capture experiments depicted in Figure 2 are also provided in the accompanying Electronic Supplementary Material, including Electronic Supplementary Material Table S2.

## Results

### Exposure to Ni(II) MIL as a Function of Time and Evaluation of [EMIM$^+$][SCN$^-$] IL Toxicity

Because culture-based methods depend on sample preparation steps that preserve bacterial viability, potential deleterious cytotoxic effects imparted by MIL extractants must be considered. To begin our further study of MIL-bacterial interactions, we selected *S.* Typhimurium ATCC 14028 as a model Gram-negative pathogen and the Ni(II) MIL as extractant, as most of our work to date has used this combination (8). Briefly, a 1 mL aliquot of TSB was inoculated with $1x10^5$ CFU mL$^{-1}$ of bacteria and spiked with 15 µL of the Ni(II) MIL, and the general schematic for MIL-

based extraction and recovery followed as shown in Figure 1b. After extraction, 10 µL aliquots of the back-extraction solution were enumerated at 0, 5, 10 and 15 min using TSA and BSA. Average CFU counts were compared to a standard that was not exposed to the Ni(II) MIL. As shown in Figure 2, average CFU counts for *S.* Typhimurium exposed to the Ni(II)-based MIL appeared to be similar on both TSA and BSA for exposure periods ranging from 0 to 15 min. To better understand the data in Figure 2, statistical analyses of Ni(II) MIL capture precision and CFU count variation as a function of MIL exposure time were performed and are provided in the Electronic Supplementary Material. Variation in MIL capture may stem from inherent randomness of MIL dispersion and coalescence behaviors.

**Table 2** Enrichment factors for *S.* Typhimurium as a function of exposure time to the Ni(II) MIL

| Time (min) | Enrichment Factor (TSA) | Enrichment Factor (BSA) |
|---|---|---|
| 0 | 8 | 7 |
| 5 | 7 | 8 |
| 10 | 6 | 8 |
| 15 | 8 | 9 |

Enrichment factors were calculated as a function of time and are reported in Table 2. For TSA, the resulting average $E_F$ value was 7.2±0.6 (n=4); for BSA, the average $E_F$ value was 8.2±1.0 (n=4).

The effects of 5% or 50% (vol/vol) aqueous solutions of the $[EMIM^+][SCN^-]$ IL on the viability of the cells were also evaluated (14). Average CFU counts were compared to a standard not exposed to $[EMIM^+][SCN^-]$. In our hands, when *S.* Typhimurium was exposed to 50% (vol/vol) solutions of $[EMIM^+][SCN^-]$, no recovery was observed on either TSA or BSA after 5 min of exposure.

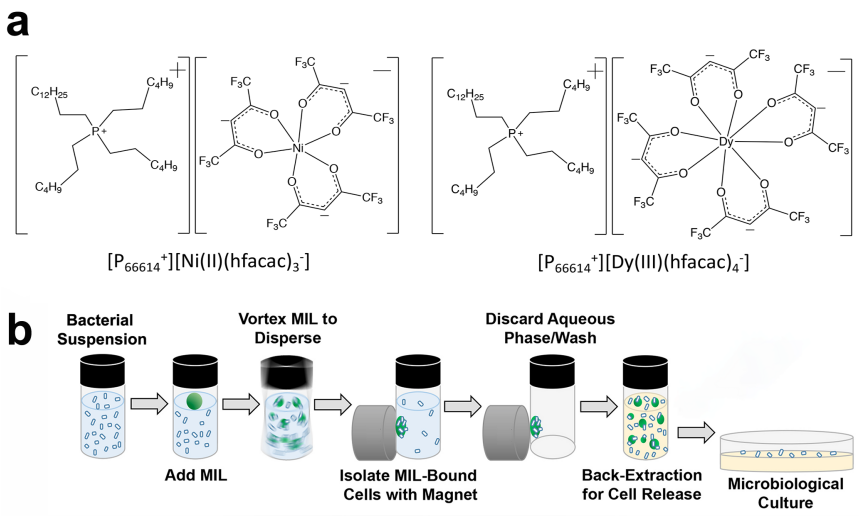


**Figure 1.** (a) Structures of the MILs used in this study. (b) Schematic for the capture, concentration and recovery of enterobacteria from aqueous samples, followed by downstream analysis by microbial culture using non-selective and/or selective media. Figure 1b adapted from Hice et al., 2019

**Evaluation of Capture and Recovery of Wild Type and Mutant *Salmonella* Minnesota Strains Using the Ni(II) MIL**

To further evaluate the importance of the OM to serve as a surface to which the MIL can bind and as a protective layer from potentially deleterious activities of the Ni(II) MIL, capture and recovery of two physiological variants of *S.* Minnesota was performed. The strains compared were *S.* Minnesota SLH 157 (wild type, functional OM) and *S.* Minnesota mR613 (OM mutant). *S.* Minnesota mR613 is considered a "deep rough" mutant, possessing a truncated OM core. Compared to the wild type, cells with a truncated OM are dramatically more susceptible to damage from antimicrobial agents or chemically harsh environments (17). To study the effect of the Ni(II) MIL exposure on the recovery of wild type and mutant strains of *S.* Minnesota, a 1 mL aliquot of TSB was inoculated with $1x10^5$ CFU $mL^{-1}$ of bacteria and spiked with 15 µL of the Ni(II) MIL. MIL-based extraction was performed and 10 µL aliquots of the back-extraction solution were enumerated using TSA and BSA plates. Average CFU counts were compared to a standard that was not exposed to the Ni(II) MIL. Extraction and recovery of *S.* Typhimurium was also assessed. Enrichment factors were calculated and are reported in Table 3.

While the extraction efficiency using the Ni(II) MIL was greatly reduced for *S.* Minnesota mR613, capture and recovery of viable cells was observed on TSA. As expected, no growth of mR613 was seen on BSA due to the inherent susceptibility of this OM mutant to selective agents. Likewise, growth of the *S.* Minnesota mR613 standard was observed on TSA but not on BSA.

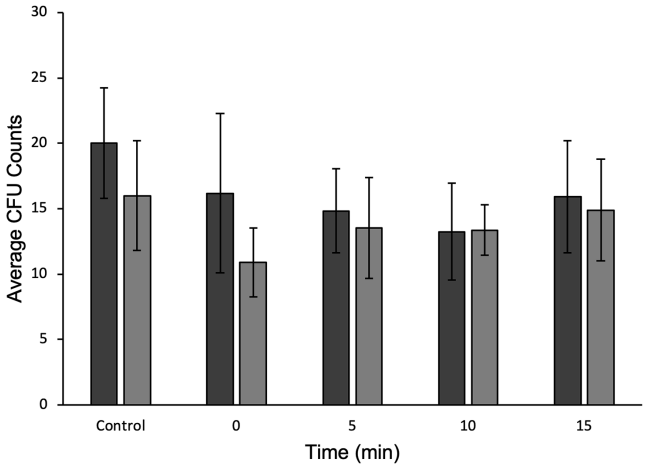


**Figure 2.** Recovery of *Salmonella* Typhimurium extracted with Ni(II) MIL as a function of time (min). Average colony forming unit (CFU) counts recovered from the aqueous Ni(II) MIL back-extraction phase over time (0 - 15 min). A suspension of *S.* Typhimurium ATCC 14028 was prepared and captured with the Ni(II) MIL as described in the text, back-extracted using modified LB broth containing 20 g $L^{-1}$ tryptone and 10 g $L^{-1}$ NaCl, then plated on TSA (dark bars) and BSA (light bars). Also shown are results for a standard not treated with the MIL (Control). Statistical analyses of these data (precision, variation over time) are provided in Electronic Supplementary Materials.

## Capture and Recovery of Seven Representative DNA Subgroups of *Salmonella* and Eight Strains of *E. coli* O157:H7

Previous work has demonstrated successful capture of *E. coli* K12, *Serratia marcescens* and *Salmonella* Typhimurium using MILs (8, 9). In order to explore the broader utility of our approach, evaluation of additional cell types is needed. We began this extended evaluation of the Ni(II) MIL with seven representative DNA subgroups of *Salmonella* and eight strains of *E. coli* O157:H7. Briefly, a 1 mL aliquot of TSB was inoculated with $1x10^6$ CFU $mL^{-1}$ of bacteria, and spiked with 15 µL of the Ni(II) MIL. MIL-based extraction was performed and 10 µL aliquots of the back-extraction solution were enumerated using TSA and BSA plates (*Salmonella*) or TSA

plates (*E. coli* O157:H7). Initially, we examined MacConkey Agar with Sorbitol (SMAC) as a common selective medium for parallel evaluation of injury in *Salmonella* and *E. coli* O157:H7, but *Salmonella* did not grow well on this medium (data not shown). We later determined that VRBGA was a suitable common medium for this purpose and used this in our statistical analysis. Average CFU counts were compared to standards that were not exposed to the Ni(II) MIL. Enrichment factors were calculated for *Salmonella* on both non-selective (TSA) and selective agars (BSA) and for *E. coli* O157:H7 on non-selective agar (TSA), as reported in Table 4.

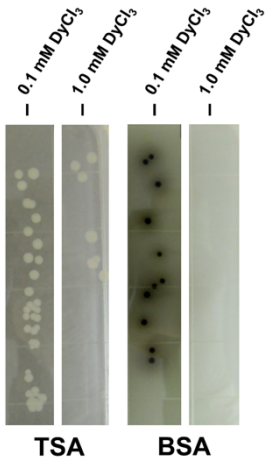


**Figure 3.** Recovery of *Salmonella* Typhimurium following 30 s exposure to 0.1 mM and 1.0 mM $DyCl_3$. Viable CFU counts recovered on non-selective TSA (left) and selective BSA (right) from the $DyCl_3$-exposed cells following a 30 s treatment

**Comparison of the Initial Wash and Full MIL Extraction Procedure on the Recovery of *S.* Typhimurium**

Although all of the strains assessed were capable of being enriched by the MIL, some species were physically enriched to greater extents than others with extraction. In order to further examine the cause for this finding, the number of captured cells lost to the wash solution was investigated. The wash step is performed after the MIL enrichment step in order to remove any incidentally-adsorbed bacteria prior to back-extraction. It is hypothesized that the cells with lower enrichment factors have lower affinities for the MIL and are therefore lost in greater number to the

wash solution than those having higher enrichment factors. To test this, five different *Salmonella* strains exhibiting varying degrees of enrichment in initial experiments were examined. The percent-loss during the wash step ranged from 47-79%. These data, along with inferred relative affinities for the MIL are shown in Table 5. $E_F$ data from Table 4 for three overlapping *Salmonella* strains are superimposed to highlight trends in percent-loss, relative affinity and $E_F$. The data for *S.* Minnesota mR613 (79% cell loss to wash) support the conclusion that the lower $E_F$ values observed for this strain result from lower affinity to the MIL, rather than from antimicrobial effects.

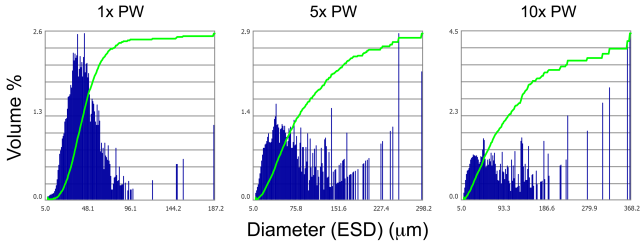


| Treatment | Mean Diameter (ESD) | Max Droplet Size | D50 | D90 | Droplets $mL^{-1}$ |
|---|---|---|---|---|---|
| **1x PW** | 22.44 µm | 187.19 µm | 20.29 µm | 41.45 µm | 392,896 |
| **5x PW** | 16.69 µm | 298.18 µm | 12.08 µm | 32.76 µm | 1,338,275 |
| **10x PW** | 14.41 µm | 368.20 µm | 10.46 µm | 26.53 µm | 1,370,130 |

**Figure 4.** Visualization of MIL-bacteria interactions *via* Flow Imaging Microscopy (FIM). Key metrics from FIM analyses of Ni(II) MIL suspension characteristics under three different concentrations of peptone water (PW) are shown. VisualSpreadsheet® software (v. 5.0, Fluid Imaging Technologies) was used for to analyze sample data. A trend toward smaller droplet size and greater extremes of maximum droplet size was seen as the ionic complexity of the medium increased.

### Capacity of the Ni(II) MIL for Capture of other Members of the Family *Enterobacteriaceae* of Food Safety, Clinical or Agricultural Significance

Our results show that all of the additional *Enterobacteriaceae* examined here could be concentrated from aqueous suspension using the Ni(II) MIL. These bacteria are ranked in descending order according to $E_F$, with *P. eucalypti*, *K. aerogenes* and *P. carotovorum* pv. *carotovorum* yielding much higher $E_F$ than seen with other bacteria tested, either here or in our previous work (8, 9).

**Investigating Mechanisms for Observed Antimicrobial Activities of the Dy(III) MIL**

Incorporation of a rare-earth metal into the MIL structure is of significant interest as these metals possess greater magnetic moments. In principle, this should allow for improved magnetic manipulation compared to transition metal-based MILs. However, when the Dy(III) MIL was previously examined for the capture of bacteria, recovery of viable cells was not observed (9). To further explore these results and to determine if they result from intrinsic antimicrobial activity of this MIL, bacterial suspensions of *S.* Typhimurium were exposed to various structural components of the MIL.

Within 30 s of vortexing a cell suspension to which 15 µL of the Dy(III) MIL was added, we observed extensive flocculation and no growth after plating, suggesting that this MIL may have intrinsic antimicrobial activity, resulting in rapid cell lysis.

To gain further insight into this phenomenon, the effect of free elemental dysprosium was evaluated by subjecting the cells to 0.1 mM and 1.0 mM solutions of $DyCl_3$. The cells were exposed to the metal salt solutions for 30 s and subsequently plated on selective and non-selective media. Results shown in Figure 3 demonstrate that growth can be observed on both types of plates. However, substantially lower counts were observed on BSA than TSA, particularly at the higher $DyCl_3$ concentration.

**Comparison of Positive- and Air-Displacement Pipettes for MIL Delivery**

We found that handling and delivery of the Ni(II) MIL was challenging when using traditional air-displacement (AD) pipettes, due to both MIL viscosity and incomplete delivery of aspirated MIL. We therefore sought to compare AD pipetting with piston-driven positive-displacement (PD) pipetting and the impact, if any, on bacterial extraction results. Briefly, 15 µL of MIL was delivered from each pipette and weighed using an analytical balance (n=3). The PD pipette was able to deliver a substantially greater mass of MIL (17.1±0.6 mg) compared to the AD

pipette (11.3±0.4 mg), with similar reproducibility (Electronic Supplementary Material Figure S1). To test whether or not this difference impacted extraction performance, extractions were performed, using each pipette to dispense 15 µL of MIL. The calculated $E_F$ did not differ according to the pipetting method used, despite the disparity in the amount pipetted (data not shown).

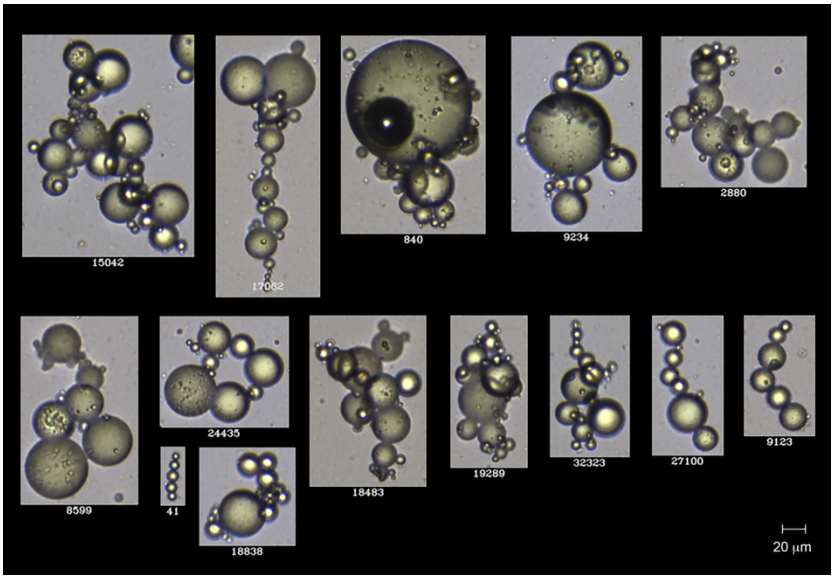


**Figure 5.** *Serratia marcescens*-Induced Aggregation of Ni(II) MIL Droplets**.** The presence of *S. marcescens* resulted in a dramatic shift in the presentation of Ni(II) MIL droplets in 1x peptone water (PW). In the presence of *S. marcescens*, MIL droplets formed large and complex aggregates, which may suggest a physical mechanism for MIL-based concentration of bacteria.

**Characterization of MIL Dispersions Under Differing Ionic Conditions Using Flow Imaging Microscopy**

As summed in Figure 4 below, FIM measurements of Ni(II) MIL dispersions in aqueous samples of increasing ionic complexity (1x, 5x and 10x PW) showed that as solute concentration increased, droplet size decreased. As would be expected, these trends towards smaller particle sizes were directly correlated to increasing numbers of total particles per unit volume (particles $mL^{-1}$). An additional trend towards larger outlier droplets (overall droplet heterogeneity) was seen as ionic complexity increased.

### *Serratia marcescens*-Induced Aggregation of Ni(II) MIL Droplets - Implications for MIL-Mediated Bacterial Concentration

In general, cell-free suspensions of Ni(II) MILs under various conditions of ionic complexity yielded distributions of individual or minimally-aggregated droplets (Electronic Supplementary Material Figure S2). In some cases, apparent surface granularity of MIL droplets suggested a MIL coalescence mechanism similar to oil-in-water emulsions through aggregation and merging of smaller particles. In the presence of *S. marcescens* cells, however, we observed a radically different presentation of MIL droplets (Figure 5), with the formation of multi-droplet aggregates and chains under the "food-like" conditions of 1x PW (0.5% NaCl, 1% peptone), which may suggest a physical mechanism for MIL-based concentration of bacteria.

**Table 3.** Enrichment factors for *S.* Typhimurium, *S.* Minnesota SLH 157 (wild type) and *S.* Minnesota mR613 (mutant)

| Strain | Enrichment Factor (TSA) | Enrichment Factor (BSA) |
|---|---|---|
| *S.* Typhimurium | 10 | 14 |
| *S.* Minnesota SLH 157 | 17 | 11 |
| *S.* Minnesota mR613 | 4 | * |

* For both the standard and the MIL-treated cells, no growth was observed on BSA using the *S.* Minnesota mR613 "deep rough" mutant strain.

## Discussion

### Exposure to Ni(II) MIL as a Function of Time and Evaluation of [EMIM$^+$][SCN$^-$] IL Toxicity

Cell injury can be detected by plating MIL-treated cells in parallel on both non-selective and selective media and evaluating growth under each condition (18). Gram-negative cells possess an outer membrane (OM), which protects them against the diffusion of otherwise toxic molecules into the cell. As a result, physiologically intact Gram-negative cells are able to tolerate exposure to toxic agents such as bile salts, crystal violet or brilliant green used in selective agars designed to limit the growth of Gram-positive cells. Injury to Gram-negative cells caused by exposure to

deleterious physical or chemical conditions is typically characterized by damage to the OM, which causes these cells to become "leaky" and show impaired growth on selective agars. Injury can therefore be detected by plating treated cells in parallel on both non-selective and selective agars and comparing the results (18). When we exposed suspensions of *S.* Typhimurium to the Ni(II) MIL for times ranging from 0 min (essentially our standard 30 s extraction protocol) to 15 min, the resulting average CFU counts on TSA and BSA appeared similar, regardless of exposure time. We explored these data further using the statistical analyses reported in the Electronic Supplementary Material. For TSA, no statistically significant differences were shown in the CFU counts over time. For cases that were plated to BSA, we did find significant evidence that the CFU counts at time 5 min, 10 min, and 15 min are statistically greater compared to time 0 counts. We hypothesize that if the Ni(II) MIL was chemically injurious to *S.* Typhimurium, counts on BSA would be lower than those observed on TSA, and further, that BSA counts would continue to fall as a function of exposure time. Although we found that CFU counts on BSA were statistically different from counts at time zero, the observation that counts at 5, 10 and 15 min were greater than those at time zero support our conclusion that the Ni(II) MIL did not cause detectable injury to *S.* Typhimurium with this media pairing, even after exposure periods thirty times longer than our standard 30 s extraction time.

The $[EMIM^+][SCN^-]$ IL has been previously investigated for solubilization of protein-rich food matrices as a means for sample preparation (14). The $[EMIM^+]$ cation potentially acts as a detergent, while the $[SCN^-]$ anion is chaotropic. The ability to essentially obliterate difficult food matrices with this IL, then collect released bacterial cells for analysis represents a novel advance in sample preparation. However, these authors have reported that $[EMIM^+][SCN^-]$ is injurious to *Salmonella* Typhimurium in this application, with only 34 – 45% of inoculated *S.* Typhimurium

recovered after IL-mediated matrix lysis when plated to a selective agar (14). In our hands, when *S.* Typhimurium was exposed to [$EMIM^+$][$SCN^-$] as originally described for IL-based extraction of this pathogen from foods (14), no recovery was observed on either TSA or BSA, confirming the injurious nature of this IL in stark contrast to and in direct comparison with our "cell-friendly" Ni(II) MIL.

It is possible that a major contributor to the innocuous behavior of our Ni(II) MIL with Gram-negative bacteria stems from the inherent capacity of the OM to exclude hydrophobic compounds – which the MIL clearly is. We therefore sought to further investigate the role of the OM 1) as a key cell structure of potential importance in mediating MIL-based binding and capture of cells and 2) in protecting Gram-negative cells against potential MIL toxicity, as discussed further below.

**Evaluation of Capture and Recovery of Wild Type and Mutant *Salmonella* Minnesota Strains Using the Ni(II) MIL**

Our ability to capture this mutant strain demonstrates two key points: 1) the Ni(II) MIL has the capacity to capture and concentrate a strain of *S.* Minnesota that displays a drastically different external surface than wild type cells, and 2) the post-capture growth behavior of this physiologically sensitive strain suggests that the Ni(II) MIL capture process is not overtly antimicrobial. Apparent absence of a toxic impact for the Ni(II) MIL on the "deep rough" mutant *S.* Minnesota strain may result from a lack of intrinsic chemical toxicity, from low diffusivity of the hydrophobic MIL across whatever remaining barrier is offered by this strain's truncated OM, the tendency of the insoluble, hydrophobic MIL to quickly sequester itself into large, non-diffusible aggregate structures in aqueous media, or any combination of these potential phenomena. These data suggest that Gram-negative cell surface molecular diversity and character are likely important factors mediating successful cell binding and capture by MILs. We expect that

other enterobacterial OM mutants, and possibly mucoid strains (see further discussion below) may also vary in their capacity for capture with the Ni(II) MIL.

**Capture and Recovery of Seven Representative DNA Subgroups of Salmonella and Eight Strains of E. coli O157:H7:**

Our results for capture of the various strains of *Salmonella* and *E. coli* O157:H7 (Table 4) show that all strains of both pathogens could be captured to some degree, when plated onto TSA. *Salmonella* strains representing the seven DNA subgroups belonging to this genus also showed very similar results when plated to BSA (Table 4), suggesting a lack of MIL-imparted injury. To delve beyond superficial visual interpretation of the data, we evaluated a subset of the strains thus far examined and applied statistical analyses to determine 1) whether capture of bacteria varied significantly as a function of strain and 2) if selective agars used revealed the presence of MIL-conferred injury. Our analysis confirmed significant serotype or strain effects for capture of *Salmonella* (p-value < 0.0001) and *E. coli* O157:H7 (p-value = 0.0721). Regarding MIL-conferred injury, no significant differences (p-value = 0.4491) were seen between TSA and VRBGA for recovery of *E. coli* O157:H7, indicating that for this agar pairing, no injury could be detected. Interestingly, while no statistically significant differences (p-value = 0.7248) were seen for *Salmonella* serovars on TSA or BSA (i.e. no detectable injury), recovery of *Salmonella* on VRBGA was significantly lower than on TSA (p-value = 0.0004). These results suggest that the choice of selective agar is important for both revealing the presence of injury and for informing practical application of MIL-based capture for cultural detection, especially if selective agars are to be used. Comparing the two selective agars, VRBGA contains two selective agents – crystal violet and bile salts, while the sole selective agent in BSA is brilliant green dye. Bile salts are generally agreed to be membrane-active amphiphilic “detergents”, and Gram-negative bacteria with an intact OM can exclude crystal violet from the cell, avoiding its deleterious effects. It is

possible that the barrier function of the OM is altered in some way through its interaction with the MIL during capture, that VRBGA's bile salts and crystal violet act cooperatively on the impaired OM and that *Salmonella* is more susceptible to these effects than *E. coli* O157:H7. It is important to note that BSA is a robustly selective agar. The fact that MIL-exposed *Salmonella* serovars were not impaired for growth on BSA indicates that MIL-based capture can be paired with selective plating onto this medium without interference from the capture process.

**Comparison of the Initial Wash and Full MIL Extraction Procedure on the Recovery of *S.* Typhimurium**

This experiment provides evidence that differences in $E_F$ values for the various bacteria tested could be due to intrinsic differences in affinity for the MIL extraction phase. If this is true, bacteria with lower affinities for the MIL may be weakly bound, and are therefore easily removed by the wash step compared to the strains with higher observed enrichment factors.

**Capacity of the Ni(II) MIL for Capture of other Members of the Family *Enterobacteriaceae* of Food Safety, Clinical or Agricultural Significance**

Our work with additional enterobacterial strains of concern clearly highlights the broader utility of the Ni(II) MIL for capture and concentration of these economically important bacteria. Of particular interest was the extremely high $E_F$ result seen Table 6 for *P. eucalypti* 299R (formerly *P. agglomerans* 299R), which yielded an $E_F$ of 169 - approximately 20x greater than that for many of the other enterobacteria examined in this study. The reason for this result is not yet known, although this strain was visually more pigmented than other enterobacteria tested, suggesting a possible connection between carotenoid content and higher binding. Another potential reason for this result may be the formation of "symplasmata" by this strain. Symplasmata are multicellular aggregates (hence this strain's previous epithet "*agglomerans*", meaning "forming into a ball") that confer competitive advantages to this bacterium. Symplasmata are comprised of many (potentially hundreds of) clonal cells bound within a thick polysaccharide envelope and are known

to form in laboratory media, as well as on plant surfaces (19). It is reasonable to suggest that our remarkable $E_F$ results for *P. eucalypti* 299R could be due to the presence of symplasmata in our culture of this organism – a possibility that we plan to investigate in the future. If this is the case, it would demonstrate the exciting potential of our MIL-based approach to capture and concentrate unique multicellular structures of importance to plant health in additional to individual bacterial cells.

**Table 4.** Enrichment factors for seven representative DNA subgroups of *Salmonella* and eight strains of *E. coli* O157:H7

| Strain | Enrichment Factor (TSA) | Enrichment Factor (BSA) |
|---|---|---|
| *S. enterica* subsp. *salamae* | 12 | 9 |
| *S. enterica* subsp. *diarizonae* | 7 | 11 |
| *S. enterica* subsp. *houtenae* | 8 | 8 |
| *S.* Typhimurium | 8 | 6 |
| *S. bongori* | 4 | 4 |
| *S. enterica* subsp. *arizonae* | 3 | 2 |
| *S. enterica* subsp. *indica* | 3 | 4 |
| | | |
| *E. coli* O157:H7 N192-6-1 | 9 | - |
| *E. coli* O157:H7 N549-3-1 | 8 | - |
| *E. coli* O157:H7 N192-5-1 | 7 | - |
| *E. coli* O157:H7 N886-71 | 4 | - |
| *E. coli* O157:H7 N366-2-2 | 4 | - |
| *E. coli* O157:H7 N317-3-1 | 4 | - |
| *E. coli* O157:H7 N336-4-1 | 3 | - |
| *E. coli* O157:H7 N405-5-8 | 2 | - |

The broad applicability of MIL-based capture and concentration to enterobacteria occurring across the production-to-consumption continuum underlines the potential value of this approach to rapid detection methods aimed at mitigating human disease and preventing crop loss. A brief overview of the significance of the bacteria included in this study to agriculture, food safety and human health is provided below. Foodborne and clinically-important enterobacteria include *Cronobacter sakazakii*, which is problematic in powdered infant formula, causing neonatal infections with mortality as high as 40% (1). Pathogenic *Escherichia coli* can be divided into

several important groups based on pathology, with *E. coli* O157:H7 and five other Shiga toxin-forming *E. coli* (STEC) forming the "Big Six" – bacteria regarded by regulatory agencies as "zero tolerance" food adulterants. In 2018 there were two multistate outbreaks of *E. coli* O157:H7 in Romaine lettuce; at the end of 2019, another such outbreak and recall of Romaine lettuce from the Salinas Valley occurred, affecting 167 people in 27 states (20). *Salmonella* spp. represent one of the most pervasive bacterial threats to the food system, in terms of the estimated number of infections (Electronic Supplementary Material Table S1) and breadth of foods affected. The genus *Yersinia* includes *Y. pestis* – the cause of the plague (the "Black Death") and *Y. enterocolitica*, which is transmitted through undercooked pork infections (Electronic Supplementary Material Table S1). On the clinical side, carbapenem-resistant *Enterobacteriaceae*, which includes some *Klebsiella* strains, has been prioritized as an "urgent threat" by the Centers for Disease Control and Prevention (CDC), meaning that urgent and aggressive action is required to counter this threat to public health (21). Enterobacterial plant pathogens include *Erwinia amylovora*, the cause of fire blight, which can decimate entire apple or pear orchards. *Pantoea* spp. cause infections in both humans and plants and, like *Cronobacter*, have been isolated from powdered infant formula (1). *P. eucalypti* is an epiphyte on many plants and causes disease in others, including pea, sweet corn and wheat, while *Pantoea stewartii* causes wilt in corn and seed rot in cotton, among others (22). *Pectobacterium carotovorum* pv. *carotovorum* is a ubiquitously distributed pathogen causing bacterial soft rot in various plants and blackleg disease in potato (1).

The family *Enterobacteriaceae* is a large group of genetically- and physiologically-related Gram-negative bacteria existing in a wide variety of niches of importance to and overlapping with human activities. Although there is considerable diversity within the family, these bacteria share several structural and biochemical features that are of importance in defining their surface

characteristics, and therefore, their potential to interact with MILs. These are discussed further below.

As Gram-negative bacteria, the *Enterobacteriaceae* all possess a lipopolysaccharide outer membrane (OM) comprised of a lipid element, a conserved oligosaccharide core and a highly variable polysaccharide sequence, termed the "O-antigen" (23-25). The OM serves as barrier to the diffusion of toxic compounds such as antibiotics, and the O-antigen plays roles in avoiding phagocytosis and protecting cells against complement-mediated cell lysis (24). There are two notable types of O-antigen variants in *Salmonella* and other enterobacteria – "rough" and "mucoid". Rough mutants have a truncated LPS and do not possess an O-antigen; mucoid variants have an O-antigen, but it is obscured by a capsule that obscures it from immunologic detection. The surface antigens displayed by the *Salmonella* strains representative of the seven DNA subgroups that comprise this genus are shown in Electronic Supplementary Material Table S3. This table highlights the considerable surface molecular diversity of the *Salmonella* strains used in this study. Despite this molecular diversity and its expected impact on diversity of cell surface charge, all of these salmonellae could be captured by the Ni(II) MIL, with 4 of the 7 strains displaying $E_F$ on par with what we have previously observed for *S.* Typhimurium and nonpathogenic *E. coli* (8). The lower $E_F$ values for *S. bongori*, *S. arizonae* and *S. indica* may be explored in future studies, using whole-cell ς-potential measurements to assess differences in cell surface charge.

Another feature common to the family, as suggested by the name, is the Enterobacterial Common Antigen (ECA), a polysaccharide repeat structure located in the cell envelope that is linked to maintenance of OM integrity and represents a useful target for detection of enterobacterial strains (23, 24). Additional cell surface structures that contribute to the molecular

and charge diversity of enterobacteria include porins - transmembrane transport proteins, which also act as receptors for bacteriophage, fimbriae (also referred to as adhesins or pili) - stiff, hair-like appendages uniformly distributed across the cell surface and that mediate bacterial binding to host cells, and flagella. Flagella (H-antigen) are whip-like structures that confer cell motility and whose number and surface arrangement may vary according to cell type (1).

**Table 5** Percent-loss of cells to wash, relative affinity for MIL and $E_F$ of select *Salmonella* spp.

| Strain | Percent-Loss[a] | Relative Affinity for MIL[b] | $E_F$ TSA/BSA[c] |
|---|---|---|---|
| *S. enterica* subsp. *diarizonae* | 47±7 | +++++ | 7/11 |
| *S.* Typhimurium | 53±3 | ++++ | 8/6 |
| *S.* Minnesota SLH 157 | 59±3 | +++ | - |
| *S.* Minnesota mR613 | 69±5 | ++ | - |
| *S. enterica* subsp. *arizonae* | 79±1 | + | 3/4 |

[a] Percent-loss was calculated by dividing the counts obtained from the wash solution by the sum of the counts of the wash and back-extraction solution, multiplied by 100. [b] Relative affinity (RA) for MIL assumes higher losses during wash step are due to lower cellular affinity for the MIL. [c] $E_F$ data from Table 4 for both TSA and BSA are provided here to show parity in RA- $E_F$ trends for select *Salmonella* spp.

**Investigating Mechanisms for Observed Antimicrobial Activities of the Dy(III) MIL**

The partially inhibitory effects of $DyCl_3$ indicates that the coordinated metal itself may be partially responsible for the observed deleterious effects of the MIL. While the metal did show cytotoxicity, it cannot be completely responsible for the Dy(III) MIL's effect on the cells, as no flocculation was seen and growth was still observed. Since both the Ni(II) and the Dy(III) MILs contain identical cations ($[P_{6,6,6,14}^+]$), the role of the anion structure was evaluated. The anion of the Dy(III) MIL contains one additional hexafluoroacetylacetonate ligand than the Ni(II) MIL (Figure 1), making the coordination geometry of the two complexes different. To test the effects of the anion structure, cells were subjected to 10 mg of the Dy(III) ammonium salt. After 30 s vortex, similar flocculation was observed as when the cells were exposed to the native Dy(III) MIL. After plating and 24 h incubation, no growth was seen on either TSA or BSA. These results,

combined with those from $DyCl_3$ exposure experiments, provide strong evidence that the anion structure is largely responsible for the antimicrobial effects of this MIL. Ongoing work is focused on the design and synthesis of a non-toxic Dy(III)-based MIL whose strong paramagnetism can be exploited.

**Comparison of Positive- and Air-Displacement Pipettes for MIL Delivery**

Although the PD pipette delivered substantially more of the target 15 µL volume of Ni(II) MIL, enrichment factors from bacterial extractions were not affected by this ~6 µL difference added to bacterial suspensions (data not shown). These results suggest that, for the number of bacteria present in standardized suspensions, the amount of MIL used is above the carrying capacity of the MIL (the amount at which it is saturated and cannot bind additional bacteria). Apart from the performance equivalence of the two methods, PD pipetting was faster, easier and did not result in loss of MIL due to adherence to the pipette tip, which could be economically advantageous, especially for high-throughput applications.

**Characterization of MIL Dispersions Under Differing Ionic Conditions Using Flow Imaging Microscopy**

As noted above in Results, as the ionic complexity of PW solutions increased, droplet size decreased, with trends toward smaller droplet size resulting in a commensurate trend towards higher droplet count (droplets $mL^{-1}$). The effect was not completely uniform, however, as overall sample heterogeneity, as characterized by increasing outlier particle size, increased along with increasing solute concentration. It is not clear how applicable the principles of traditional oil-in-water emulsion chemistry are to our consideration of MIL behavior in aqueous suspension, as the MILs, while hydrophobic, are not technically “oils”. Further, because they are comprised of ion pairs, they are chemically inhomogeneous. As such, the term “emulsion”, which also implies an

inherently stable structure, can only be loosely applied to their behavior when they are mechanically dispersed in aqueous media.

Of importance to their application as sample preparation reagents, mechanically dispersed MILs form a short-lived "cloud" of particles capable of interacting with different charged species within aqueous matrices such as foods, including solutes and suspended particles, followed by eventual density-based coalescence at the bottom of the sample vial. Because they are paramagnetic, their separation from the aqueous phase, along with any bound species, can be hastened in the presence of a magnet. Our results with differing concentrations of PW suggest that interactions with and partitioning of charged solutes, such as NaCl and the peptidic and amino acid components of this medium into the MIL phase affect droplet size, and subsequently, the number of droplets $mL^{-1}$.

These interactions of the MIL with sample components may have important impacts on the efficacy of the MIL as a bacterial capture reagent. On one hand, a trend towards smaller droplets and greater overall numbers of droplets per unit volume is expected to favor more efficient collision with colloidal particles such as bacteria. However, we also hypothesize that higher sample ionic complexity may compete with bacterial binding, if such binding is governed solely by electrostatic binding effects. The concentrations of PW used here include levels of NaCl beyond which we would expect the Ni(II) MIL to be effective as a bacterial capture reagent in foods. For example, we previously used a medium containing only 1% NaCl for desorption of captured bacteria from the MIL phase during our "back extraction" procedure (8). To contextualize these salt levels in terms of model food systems, we used nutritional content panel information from store-bought chicken broth, a perceivably salty food, to calculate its NaCl content as ~0.2% - well below the 1% we used for MIL-desorption. Still, the use of PW-based model matrix formulations

yielding NaCl concentrations ranging from 0.5% (food-like) to 5% provided new insights into MIL dispersion/medium composition trends that may inform applications of MILs in various sample types, including non-food samples.

It is not clear what the trend towards larger outlier droplets in the presence of higher ionic concentration indicates, as this could result from poorer initial MIL dispersion or from faster coalescence. In separate work, we have used nonionic polyoxyethylene detergents such as Brij 700 to modify dispersion characteristics of MILs. This approach may be useful for ensuring greater droplet homogeneity, although the impacts of these detergents on extraction characteristics of MILs is unknown. Presumably, because they are nonionic in nature and our working hypothesis is that charge-based interactions are important in governing the partitioning of bacterial surface structures into MILs, they would not interfere with extraction behavior. However, we are also exploring other potential modes through which MILs might interact with bacteria, such as hydrophobic interactions. If these also play a role, the hydrophobic aliphatic chains of such detergents could partition into the MIL and affect extraction behavior. In the absence of such information, purely physical approaches for promoting droplet homogeneity, which could help reduce inter-experimental variability, such as the use of conical or baffled vials for sample dispersion may also be valuable, as they would not result in or depend on chemical modification of the MIL. It is also worth noting that the intrinsic chemical properties of the aqueous food matrix itself may pose limitations to application of MILs - an additional topic for further exploration.

**Serratia marcescens-Induced Aggregation of Ni(II) MIL Droplets - Implications for MIL-Mediated Bacterial Concentration**

The dramatically different presentation of MIL particles in the presence of *S. marcescens* was an unexpected result. Although the FlowCam magnification used (10x) was not sufficient for visualizing individual cells, we interpret the formation of large aggregates and chains in the

presence of *S. marcescens* as the result of cell-mediated "bridging" of individual droplets. We expect that, although *S. marcescens* produces a hydrophobic pigment (prodigiosin) and is known to avidly partition into hydrocarbons such as *n*-hexadecane (26), as a bacterium, its native environment is largely aqueous and partitioning inside of MIL droplets would not be energetically favorable. We hypothesize that cells of *S. marcescens* are able to bind to and partition into MIL droplet surfaces, leaving one side of the organism in contact with the MIL and the other side exposed to the environment. Subsequent collision with and binding to suspended MIL particles creates a MIL-bacterium-MIL "sandwich" (Electronic Supplementary Material Figure S3), which, when repeated, results in the formation of the multi-droplet aggregates and chains we observed. These observations may provide a general model for MIL-bacteria interactions, but further work is needed to explore this phenomenon. First, a very high load of *S. marcescens* (~$10^7$ – $10^8$ CFU $mL^{-1}$) was used here. Additionally, we do not know if other modes of binding, such as hydrophobic interactions, also play a role in MIL-base capture of bacteria. Future FIM-based analysis of MIL-bacteria dynamics using other *Enterobacteriaceae* at various cell concentrations may shed additional light on the microscale interactions governing MIL-based capture of Gram-negative bacteria.

**Table 6** Enrichment factors for other enterobacterial strains

| Strain | Enrichment Factor |
|---|---|
| *P. eucalypti* 299R[a] | 169 |
| *K. aerogenes* ATCC 29940[b] | 71 |
| *P. carotovorum* pv. *carotovorum*[a] | 24 |
| *C. sakazakii* 01088P[b] | 12 |
| *E. amylovora* Ea935[a] | 10 |
| Y. *enterocolitica* ATCC 2371[b] | 5 |
| Y. *enterocolitica* ATCC 9160[b] | 5 |

[a] $E_F$ determined using Columbia Agar. [b] $E_F$ determined using Tryptic Soy Agar.

## Conclusion

In this work, we explored the further utility of the Ni(II) MIL as a novel, cell-friendly reagent for preanalytical sample preparation. We evaluated the extraction performance and/or physiological effects of this MIL on nine *Salmonella* serotypes, eight *E. coli* O157:H7 strains and nine additional members of the family *Enterobacteriaceae* of importance to agriculture, food safety or human health. We used differential plating on non-selective and selective agars, various MIL exposure times and an O-antigen-deficient *S.* Minnesota mutant to demonstrate that the Ni(II) MIL possesses no overt antimicrobial activities against bacteria tested. These results highlight the potential suitability of the Ni(II) MIL for integration into detection schemes involving the use of selective media screens. Additionally, we determined the key factors behind the observed antimicrobial effects of the Dy(III) MIL, knowledge of which may help design new, less toxic transition metal-based MILs having improved magnetic properties. Finally, we used Flow Imaging Microscopy (FIM) to observe the dispersion behavior of the Ni(II) MIL under various ionic conditions and to demonstrate that MIL coalescence and aggregation behaviors are dramatically different in the presence of *S. marcescens*. These later observations may suggest a general mechanism governing the capture and concentration of Gram-negative bacteria from aqueous samples. This study provides the foundation for further investigation into the capture and recovery of other notable foodborne pathogens, including viruses, and establishes MILs as a viable platform for rapid preconcentration and extraction of Gram-negative bacteria for potential use in environmental, food and clinical applications.

## Author Contributions

Stephanie A. Hice and Marcelino Varona contributed equally to this work.

**Acknowledgements**

BFBS acknowledges financial support from the Midwest Dairy Association (MDA) and Iowa Agriculture and Home Economics Experiment Station Project No. IOW03902, sponsored by Hatch Act and State of Iowa funds. JLA acknowledges funding from the Chemical Measurement and Imaging Program at the National Science Foundation (CHE-1709372). We thank Dr. Gwynn Beattie, Iowa State University Department of Plant Pathology, for supervision of work with plant pathogens and Fluid Imaging Technologies, Inc. for collecting data on MIL droplets and VisualSpreadsheet® analysis advice.

**References**

1. Octavia S, Lan R. The Family *Enterobacteriaceae*. In: Rosenberg E, DeLong EF, Lory S, Stackebrandt E, Thompson F, editors. The Prokaryotes: Gammaproteobacteria. Fourth Edition ed. Berlin: Spring-Verlag; 2014. p. 225-86.

2. Scallan E, Hoekstra RM, Angulo FJ, Tauxe RV, Widdowson MA, Roy SL, et al. Foodborne illness acquired in the United States--major pathogens. Emerg Infect Dis. 2011;17(1):7-15.

3. Hoffman S, Maculloch B, Batz M. Economic burden of major foodborne illnesses acquired in the United States. *Current Politics and Economics of the United States, Canada and Mexico*. 2015;17(4).

4. Brehm-Stecher B, Young C, Jaykus LA, Tortorello ML. Sample preparation: the forgotten beginning. J Food Prot. 2009;72(8):1774-89.

5. Bisha B, Brehm-Stecher BF. Simple adhesive-tape-based sampling of tomato surfaces combined with rapid fluorescence in situ hybridization for *Salmonella* detection. Appl Environ Microbiol. 2009;75(5):1450-5.

6. Weber C, Stephan R, Druggan P, Joosten H, Iversen C. Improving the enrichment procedure for *Enterobacteriaceae* detection. Food Microbiol. 2009;26(6):565-72.

7. Soo HS, Brehm-Stecher, B.F, Jaykus, L.A. Advances in Separation and Concentration of Microorganisms from Food Samples. In: Sofos J, editor. Cambridge, UK: Woodhead Publishing; 2013. p. 173-92.

8. Hice SA, Clark KD, Anderson JL, Brehm-Stecher BF. Capture, Concentration, and Detection of *Salmonella* in Foods Using Magnetic Ionic Liquids and Recombinase Polymerase Amplification. Anal Chem. 2019;91(1):1113-20.

9. Clark KD, Purslow JA, Pierson SA, Nacham O, Anderson JL. Rapid preconcentration of viable bacteria using magnetic ionic liquids for PCR amplification and culture-based diagnostics. Anal Bioanal Chem. 2017;409(21):4983-91.

10. Clark KD, Nacham O, Purslow JA, Pierson SA, Anderson JL. Magnetic ionic liquids in analytical chemistry: A review. Analytica Chimica Acta. 2016;934:9-21.

11. Clark KD, Varona M, Anderson JL. Ion-Tagged Oligonucleotides Coupled with a Magnetic Liquid Support for the Sequence-Specific Capture of DNA. Angew Chem Int Ed Engl. 2017;56(26):7630-3.

12. Ding X, Clark KD, Varona M, Emaus MN, Anderson JL. Magnetic ionic liquid-enhanced isothermal nucleic acid amplification and its application to rapid visual DNA analysis. Anal Chim Acta. 2019;1045:132-40.

13. Merib J, Spudeit DA, Corazza G, Carasek E, Anderson JL. Magnetic ionic liquids as versatile extraction phases for the rapid determination of estrogens in human urine by dispersive liquid-liquid microextraction coupled with high-performance liquid chromatography-diode array detection. Anal Bioanal Chem. 2018;410(19):4689-99.

14. Mester P, Wagner M, Rossmanith P. Use of ionic liquid-based extraction for recovery of *Salmonella* Typhimurium and *Listeria monocytogenes* from food matrices. J Food Prot. 2010;73(4):680-7.

15. Pierson SA, Nacham O, Clark KD, Nan H, Mudryk Y, Anderson JL. Synthesis and characterization of low viscosity hexafluoroacetylacetonate-based hydrophobic magnetic ionic liquids. New Journal of Chemistry. 2017;41(13):5498-505.

16. Jett BD, Hatter KL, Huycke MM, Gilmore MS. Simplified agar plate method for quantifying viable bacteria. Biotechniques. 1997;23(4):648-50.

17. Nikaido H. Molecular basis of bacterial outer membrane permeability revisited. Microbiol Mol Biol Rev. 2003;67(4):593-656.

18. Liao CH, Fett WF. Resuscitation of acid-injured *Salmonella* in enrichment broth, in apple juice and on the surfaces of fresh-cut cucumber and apple. Lett Appl Microbiol. 2005;41(6):487-92.

19. Tecon R, Leveau JH. Symplasmata are a clonal, conditional, and reversible type of bacterial multicellularity. Sci Rep. 2016;6:31914.

20. CDC. Outbreak of *E. coli* infections linked to Romaine lettuce 2019. Available from: https://www.cdc.gov/ecoli/2019/o157h7-11-19/index.html.

21. CDC. Antibiotic Resistance Threats in the United States, 2019. In: U.S. Department of Health and Human Services C, editor. Atlanta, GA2019.

22. Walterson AM, Stavrinides J. Pantoea: insights into a highly versatile and diverse genus within the *Enterobacteriaceae*. FEMS Microbiol Rev. 2015;39(6):968-84.

23. Mitchell AM, Srikumar T, Silhavy TJ. Cyclic Enterobacterial Common Antigen Maintains the Outer Membrane Permeability Barrier of Escherichia coli in a Manner Controlled by YhdP. MBio. 2018;9(4).

24. Kalynych S, Morona R, Cygler M. Progress in understanding the assembly process of bacterial O-antigen. FEMS Microbiol Rev. 2014;38(5):1048-65.

25. Grimont P, A.D., Weill F-X. Antigenic Formulae of the *Salmonella* Serovars. WHO Collaborating Center for Reference and Research on *Salmonella*, Institut Pasteur, Paris, France. 9th ed2007.

26. Rosenberg M. Microbial adhesion to hydrocarbons: twenty-five years of doing MATH. FEMS Microbiol Lett. 2006;262(2):129-34.

## Appendix F: Supplementary Information Chapter 7

**Table S1.** Estimated numbers of annual foodborne disease cases, hospitalizations and deaths occurring in the US attributable to four key enterobacterial genera. Data excerpted from Scallan et al., 2011

| Organism | Foodborne cases | Hospitalizations | Deaths |
|---|---|---|---|
| Nontyphoidal *Salmonella* | 1,027,561 | 19,336 | 378 |
| *Shigella* spp. | 131,254 | 1,456 | 10 |
| STEC 0157 | 63,153 | 2,138 | 20 |
| *Y. enterocolitica* | 97,656 | 533 | 29 |
| **Total** | **1,319,624** | **23,463** | **437** |

**Table S2.** Average CFU counts and precision measurements

| Time (min) | Avg. (TSA) | Avg. (BSA) | SD (TSA) | SD(BSA) | RSD(TSA) | RSD(BSA) |
|---|---|---|---|---|---|---|
| Control | 20.600 | 16.200 | 4.219 | 4.207 | 0.205 | 0.260 |
| 0 | 16.182 | 10.909 | 6.096 | 2.625 | 0.377 | 0.241 |
| 5 | 14.818 | 13.545 | 3.219 | 3.857 | 0.217 | 0.285 |
| 10 | 13.222 | 13.375 | 3.701 | 1.923 | 0.280 | 0.144 |
| 15 | 15.900 | 14.889 | 4.280 | 3.887 | 0.269 | 0.261 |

**Synthesis of MILs**

The $[P_{6,6,6,14}^{+}][Ni(II)\ (hfacac)_3^{-}]$ $[P_{6,6,6,14}^{+}][Dy(III)\ (hfacac)_4^{-}]$ MILs were synthesized following a previously reported procedure.[1] Briefly, 10 mmol of hexafluoroacetyl acetone was

added dropwise into a round bottom flask sealed with a rubber septum containing 10 mmol of ammonium hydroxide in 30 mL of ethanol. After the white vapor formed settled, 3.3 mmol of nickel (II) chloride or 2.5 mmol of dysprosium(III) chloride hexahydrate were added and stirred at room temperature for 5 h. Following evaporation under vacuum, the crude product was dissolved in diethyl ether, filtered, and washed several times with deionized water until no apparent precipitate was observed when a $AgNO_3$ test was performed. Subsequently, diethyl ether was evaporated and the purified salt dried overnight in a vacuum oven at 50 °C. The purified salt was dissolved in methanol and an equimolar amount of trihexyl(tetradecyl)phosphonium chloride was added and stirred overnight. The crude MIL product was dissolved in hexane and filtered. The product was subsequently washed with aliquots of water until no precipitate was observed during a $AgNO_3$ test. Hexane was then evaporated and the purified MIL was dried in a vacuum oven overnight at 50 °C.

1. Pierson, S.A.; Nacham, O.; Clark, K.D.; Nan, H.; Mudryk, Y.; Anderson, J.L. "Synthesis and Characterization of Low Viscosity Hexafluoroacetylacetonate-based Hydrophobic Magnetic Ionic Liquids," *New Journal of Chemistry*, **2017**, *41*, 5498-5505. DOI: 10.1039/C7NJ00206H

**Precision analysis for data reported in Figure 2 and analysis of the recovery of Salmonella Typhimurium ATCC 14028 extracted with Ni(II) MIL as a function of the exposure time (0, 5, 10 and 15 min) when plated to both TSA and BSA.**

Supplementary Table 2 reports the Average CFU counts and the associated precision measurements, which include both the standard deviations (SD (TSA) and SD (BSA)) and the relative standard deviations (RSD (TSA) and RSD (BSA), compared to the mean levels). The sample sizes of cases that were plated to TSA are 11, 11, 9 and 10 for 0, 5, 10 and 15 min timepoints, respectively. The sample sizes of cases that were plated to BSA are 11, 11, 8 and 9 for timepoint 0, 5, 10 and 15 min, respectively. For each time phase, The CFU counts related to BSA have lower averaged values, as well as smaller standard deviations and relative standard deviation

values compared to those of TSA. The one standard deviation away from the averaged value is displayed as the interval in Figure 2 (vertical lines).

In order to investigate whether the recovery of *S.* Typhimurium extracted with Ni(II) MIL varies over time, we performed a statistical analysis to compare the CFU counts recovered from the aqueous Ni(II) MIL back-extraction phase over time (5, 10 and 15 min) to the initial CFU counts at time 0. The nonparametric Wilcoxon test, which does not require the normality assumption, was used for our data with positive integer values. For cases that were plated to TSA, no statistically significant differences were shown in the CFU counts over time 5 min (11 samples), 10 min (9 samples) and 15 min (10 samples) compared to time 0 (11 samples). The respective p-values were 0.7842, 0.3570, 0.9035. For cases that were plated to BSA, there is significant evidence that the CFU counts at time 5 min (11 samples), 10 min (8 samples) and 15 min (9 samples) are statistically greater compared to time 0 (11 samples), yielding p-values of 0.0953, 0.0470 and 0.0254.

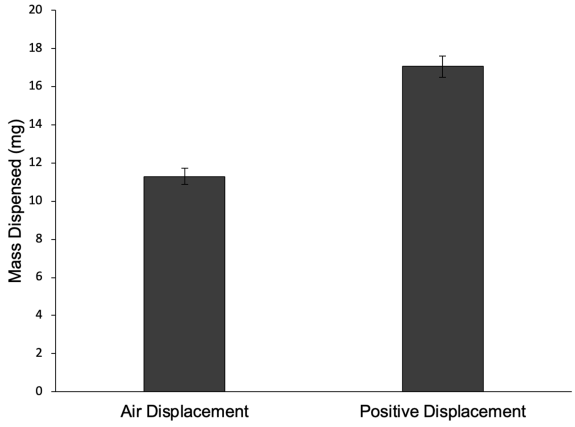


**Figure S1.** Evaluation of Ni(II) MIL delivery using air displacement (AD) and positive displacement (PD) pipettes. The average mass in mg of Ni(II) MIL dispensed using the AD and PD pipettes is reported. The PD pipette was able to deliver a substantially greater mass of Ni(II) MIL (17.1 ± 0.6 mg) compared to the AD pipette (11.3 ± 0.4 mg)

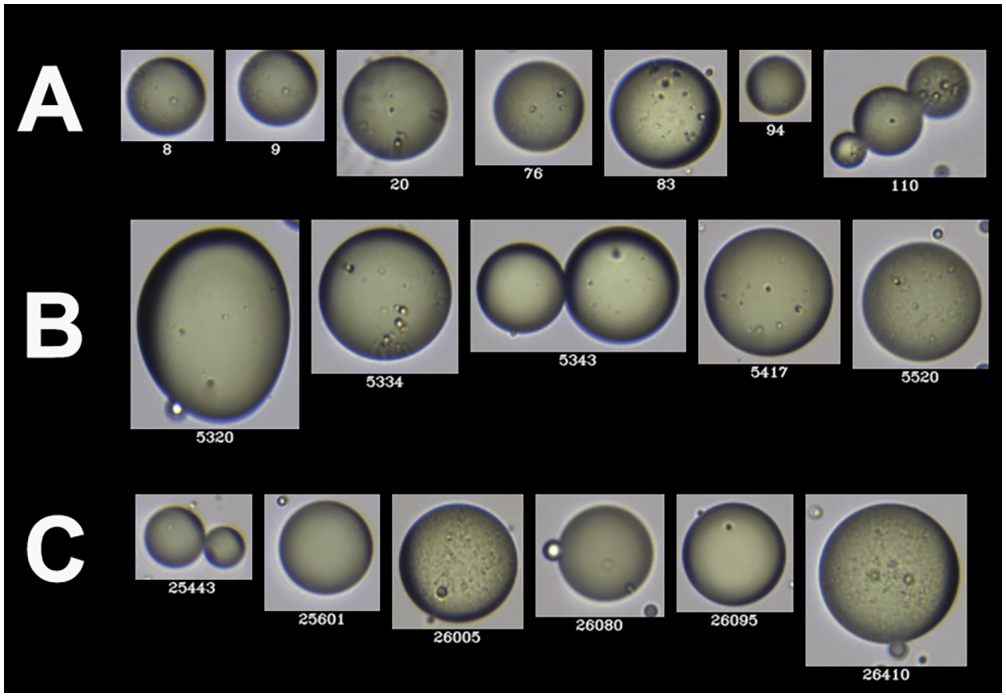


**Figure S2.** General appearance of Ni(II) MIL suspended in aqueous media of increasing ionic complexity, without added bacteria. A) 1x peptone water (PW); B) 5x PW; C) 10x PW. Apart from the size distribution data noted for each medium, these suspensions consisted generally of well-separated droplets having minimal interactions.

**Table S3.** Somatic and flagellar antigenic formulae of *Salmonella* spp. used in this study

| Strain | DNA Subgroup | Somatic (O) Antigen | Flagellar (H) Antigen | |
|---|---|---|---|---|
| | | | Phase 1 | Phase 2 |
| *S.* Typhimurium ATCC 14028 | I | 4,5,12 | i | 1,2 |
| *S. salamae* SA4406 | II | 1,9,12 | 1,w | e,n,x |
| *S. arizonae* SA4407 | IIIa | 51 | z(4),z(23) | (-) |
| *S. diarizonae* SA4408 | IIIb | 6,7 | 1,v | z(53) |
| *S. houtenae* SA4409 | IV | 45 | g,z(51) | (-) |
| *S. indica* SA4411 | VI | 1,6,14,25 | a | e,n,x |
| *S. bongori* SA4410 | V | 66 | z(41) | (-) |

Key cell surface antigens – lipopolysaccharide-based somatic (O) and flagellar (H) antigens are listed according to the Kauffmann-White scheme (Grimont and Weill, 2007). These data highlight the antigenic diversity (surface biochemical complexity) of these representatives of the seven DNA subgroups comprising the genus *Salmonella*, which all, to some degree, were captured by the Ni(II) MIL. "Diphasic" *Salmonella* are capable of expressing both Phase 1 or Phase 2 flagellar antigens in coordinate, "either/or" fashion. "Monophasic" *Salmonella* – those that only express Phase 1 flagellar antigens – are indicated by "(-)".

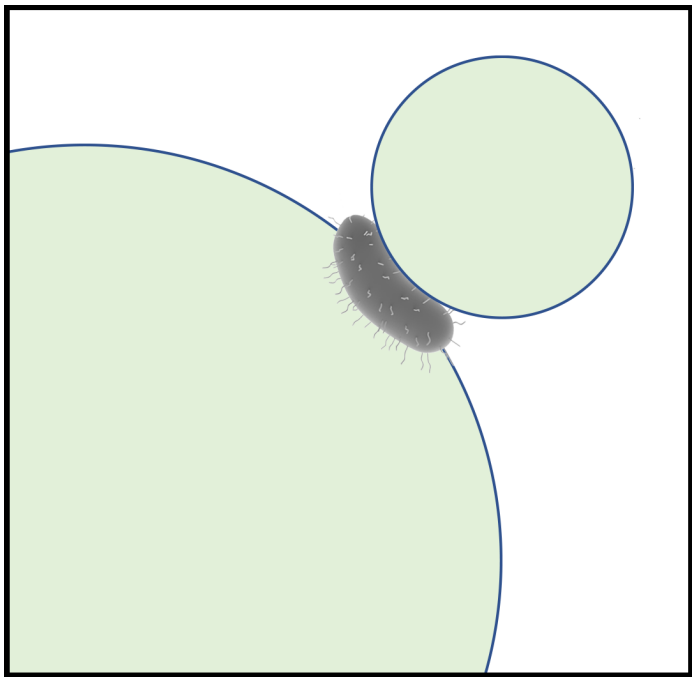

**Figure S3.** Hypothesized mechanism for cell-mediated MIL aggregation. Based on the radically different aggregation behavior of the Ni(II) MIL when *S. marcescens* is present, we hypothesize that the structures (chains and other aggregates) observed result from interfacial "sandwiching" effects, where bound bacterial cells serve to link and bridge adjacent MIL droplets, leading to cell-mediated aggregation and gravimetric deposition of MIL-cell complexes at the bottom of the sample tube after vortexing.

# CHAPTER 8. GENERAL CONCLUSIONS

This dissertation addresses previous limitations of PIL-SPME for DNA analysis and expands its use in complex biological systems. In Chapter 2, drastic reduction in the extraction time was achieved through the use of vortex agitation instead of a conventional magnetic stir-bar. Comparable extraction efficiencies were observed for a 2 min vortex extraction compared with a 30 min extraction with magnetic stirring. The developed method was successfully applied for the isolation of DNA from Mycobacterium smegmatis in artificial sputum samples. Recovered DNA was subsequently detected with isothermal multiple-self-matching-initiated amplification. A custom-buffer was also develop to allow for direct analysis of the 1 M SPME desorption solution, eliminating the need for dilution.

Chapters 3 through 5 demonstrate advancements in the sequence-specific detection of LAMP through the development of several assays incorporating molecular beacons (MBs) for detection. In Chapter 2, the dual fluorescence properties of a FAM labeled molecular beacon and HNB were exploited to develop unambiguous visual detection of LAMP. Differentiation of single-nucleotide polymorphisms could be achieved using this method, showing its high specificity. Chapter 3 shows the development of an MB-LAMP assay to detect BRAF V600E, a common mutation in melanomas. Several parameters, including reaction temperature and MBs design, were optimized to allow for optimal discrimination between the wild type and mutant sequences. The developed assay used a plate-reader for detection, eliminating the need for a real-time qPCR instrument. As a proof-of-concept, PIL-SPME was used to isolate DNA from human plasma for subsequent MB-LAMP analysis. Chapter 4 demonstrates an alternative platform for MB-LAMP detection. A FAM labeled MB was employed along with a biotinylated loop primer to enable sequence-specific detection on commercially available lateral flow immunoassay strips. To

demonstrate broad applicability, the approach was demonstrated with three distinct DNA sequences. High specificity was shown through the differentiation of wild-type and mutant BRAF V600E.

In Chapter 6, the lack of selectivity of PIL-SPME for specific sequences was addressed by developing a sequence-selective SPME sorbent through the modification of a commercially available polyacrylate (PA) fiber. Carbodiimide coupling chemistry was employed to functionalize the PA fiber with an amine-labeled oligonucleotide complementary to the target sequence. Following optimization, successful extraction of the target sequence could be achieved in the presence of interfering salmon testes DNA.

Chapter 7 investigates the interactions between magnetic ionic liquids (MILs) and Gram-negative bacteria. Selective plating is used to determine that no cellular injury occurs when Salmonella and E. coli cells are exposed to a Ni (II) based MIL. Additionally, the applicability of MIL-based capture is expanded to several enterobacterial pathogens. A proposed mechanism for bacteria-MIL interaction was also elucidated through the use of a FlowCam imaging system.